1964

Observations on the vacuum ultraviolet spectrum of atomic nitrogen emitted from the microwave-driven discharge

Henry John Hettel
Iowa State University

OBSERVATIONS ON THE VACUUM ULTRAVIOLET SPECTRUM OF ATOMIC NITROGEN EMITTED FROM THE MICROWAVE-DRIVEN DISCHARGE

by

Henry John Hettel

A Dissertation Submitted to the
Graduate Faculty in Partial Fulfillment of
The Requirements for the Degree of
DOCTOR OF PHILOSOPHY

Major Subject: Physical Chemistry

Approved:

Signature was redacted for privacy.

In Charge of Major Work

Signature was redacted for privacy.

Head of Major Department

Signature was redacted for privacy.

Dean of Graduate College

Iowa State University
Of Science and Technology
Ames, Iowa

1964

TABLE OF CONTENTS

I. INTRODUCTION

One of the best-obeyed rules of empirical spectroscopy is that intra-multiplet intensity ratios are constants whose values may be accurately predicted by both empirical and theoretical relations. This rule was observed to be violated, however, by the nitrogen doublets at 1743, 5 and 1493, 5 Å as emitted from an electrodeless discharge in a helium matrix at low pressures. Not only do these doublet ratios deviate from their theoretical value, but they vary significantly with variation in spectral source pressure. The questions then immediately arose, "What is the cause of this effect, and how can the effect be used to measure the phenomenon causing it?". The answers to these questions are the subject of this dissertation.

A. Prior Work

A search of the literature disclosed only two references dealing directly with anomalous intra-multiplet intensity ratios. Schnautz (1), in collaboration with R. Mannkopff, investigated the non-compliance of the copper doublet 3247, 3273 Å to the theoretical ratio. He concluded that line broadening effects, although quite important, were not the entire cause for the departure of the observed ratio from the theoretical value. Mannkopff (2), then proceeded to show that spectral self-absorption by copper vapor in the arc also plays a vital role in this effect.

Curiously, despite the lack of papers on this subject, it would appear to be generally known that self-absorption causes anomalous multiplet ratios. As evidence for this may be cited the remark of

Oster in the discussion following McNally's paper (3), wherein Oster points out that deviation of the multiplet ratios from their theoretical values is a very simple check on whether self-absorption effects are significant in an experimental plasma. To date, however, it appears that no use has been made of anomalous multiplet ratios as a quantitative diagnostic tool in plasma investigations.

B. The Pressure-dependent Behavior of the Doublet Ratios

The form and magnitude of the doublet ratio variation with discharge tube pressure is shown in Figures 1 to 5 for the two nitrogen doublets N 1743, 5 and 1493, 5 Å. The matrix gas for Figures 1 to 3 was helium containing 500 vpm† nitrogen, whereas Figures 4 and 5 pertain to an argon-500 vpm nitrogen matrix. Not only is there significant deviation from the theoretical doublet ratio--2. 00 for both doublets--but the dissimilarity of their behavior with pressure is especially striking.

The experimental conditions under which these data were gathered are discussed in a subsequent section.

---

† The abbreviation vpm signifies volumes per million volumes, and is thus ppm by volume.

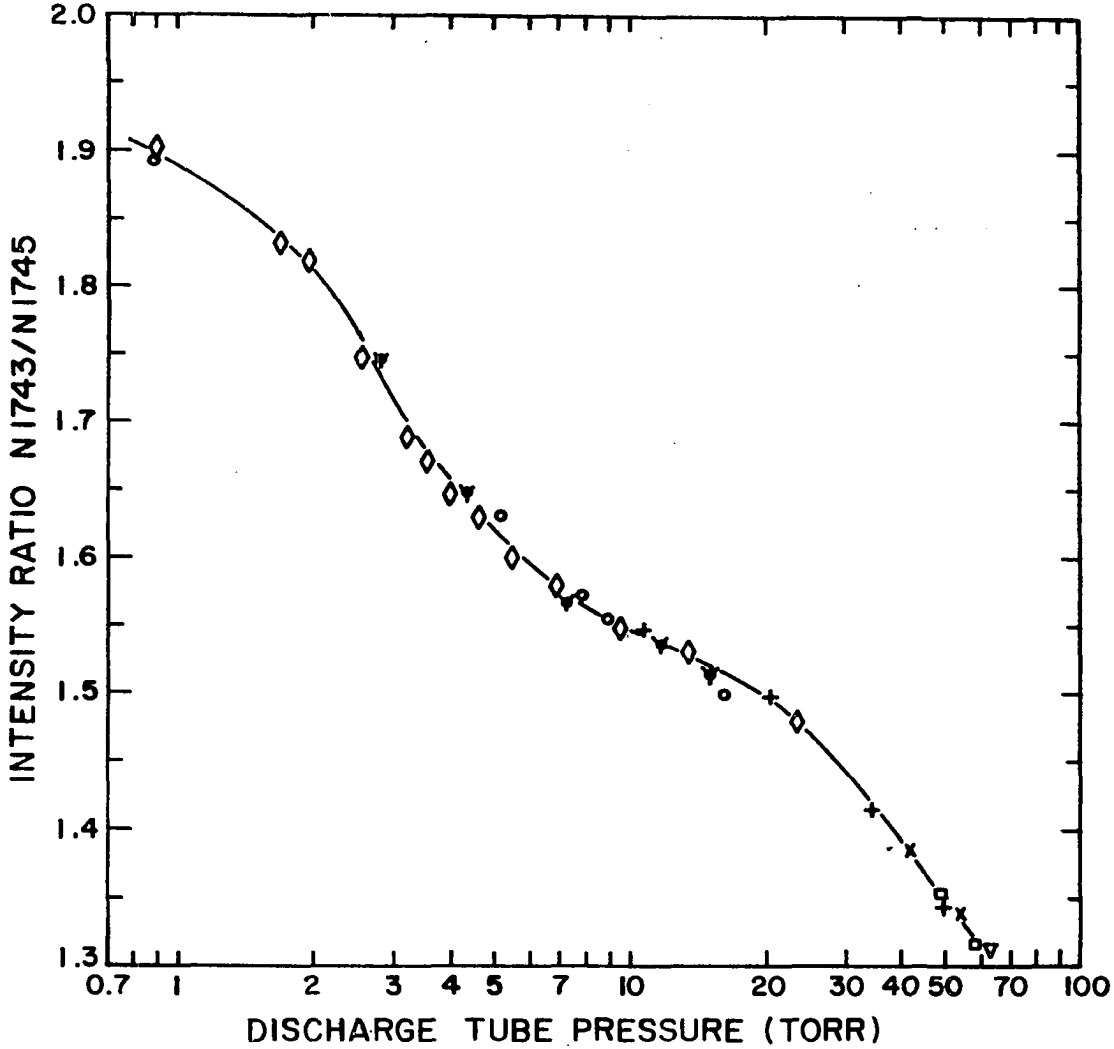

Figure 1. The N 1743/N 1745 Å doublet ratio in the helium matrix

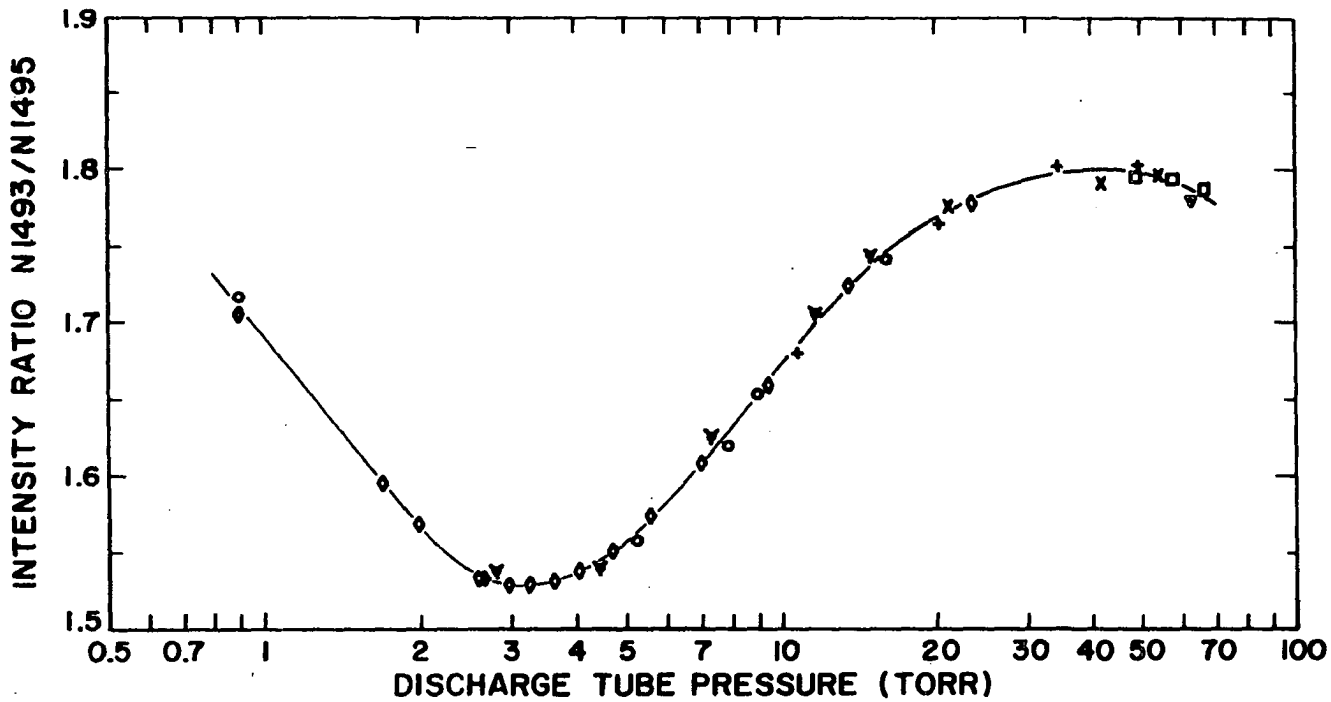

Figure 2. The N 1493/N 1495 Å doublet ratio in the helium matrix

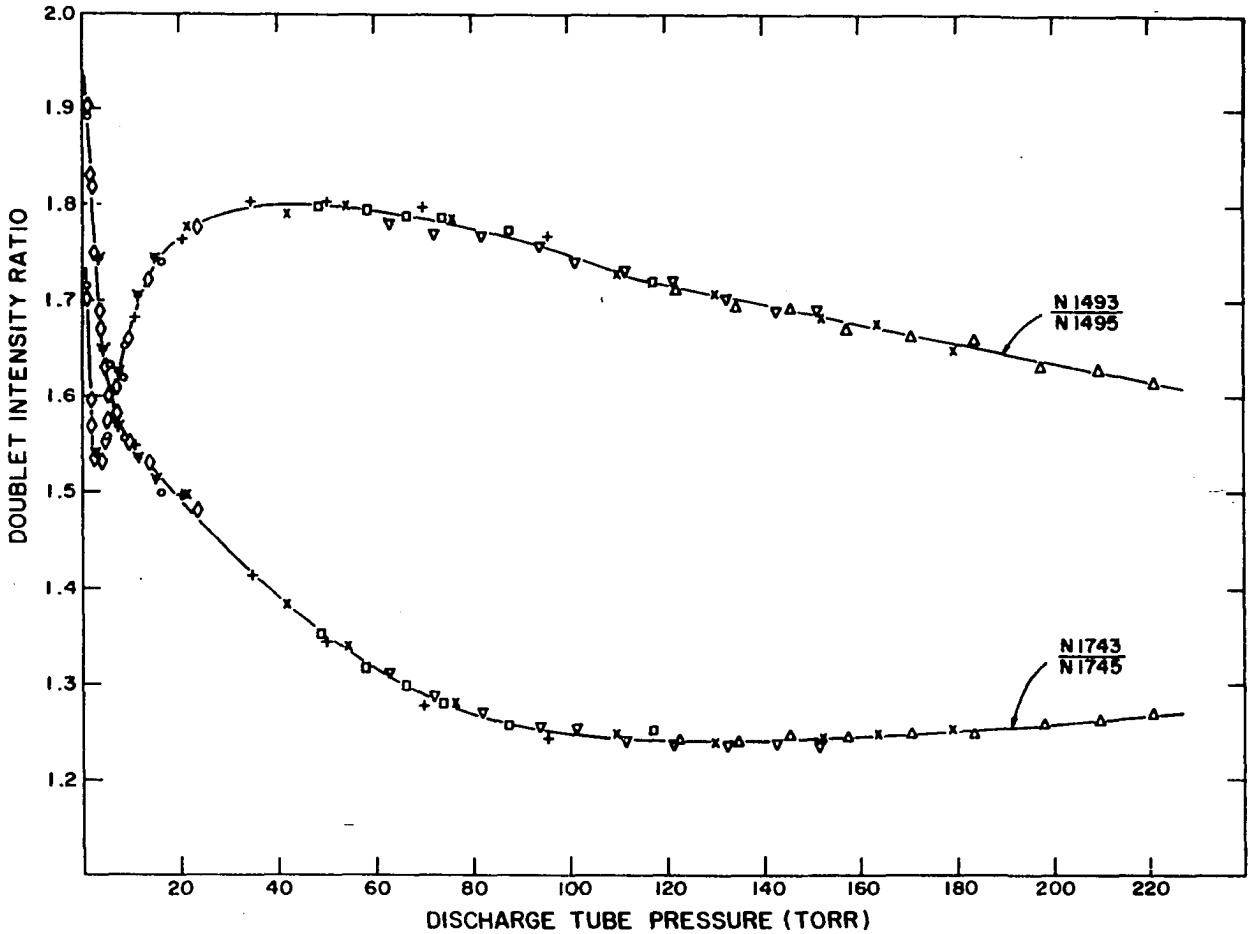

Figure 3. The behavior of both doublet ratios in the helium matrix

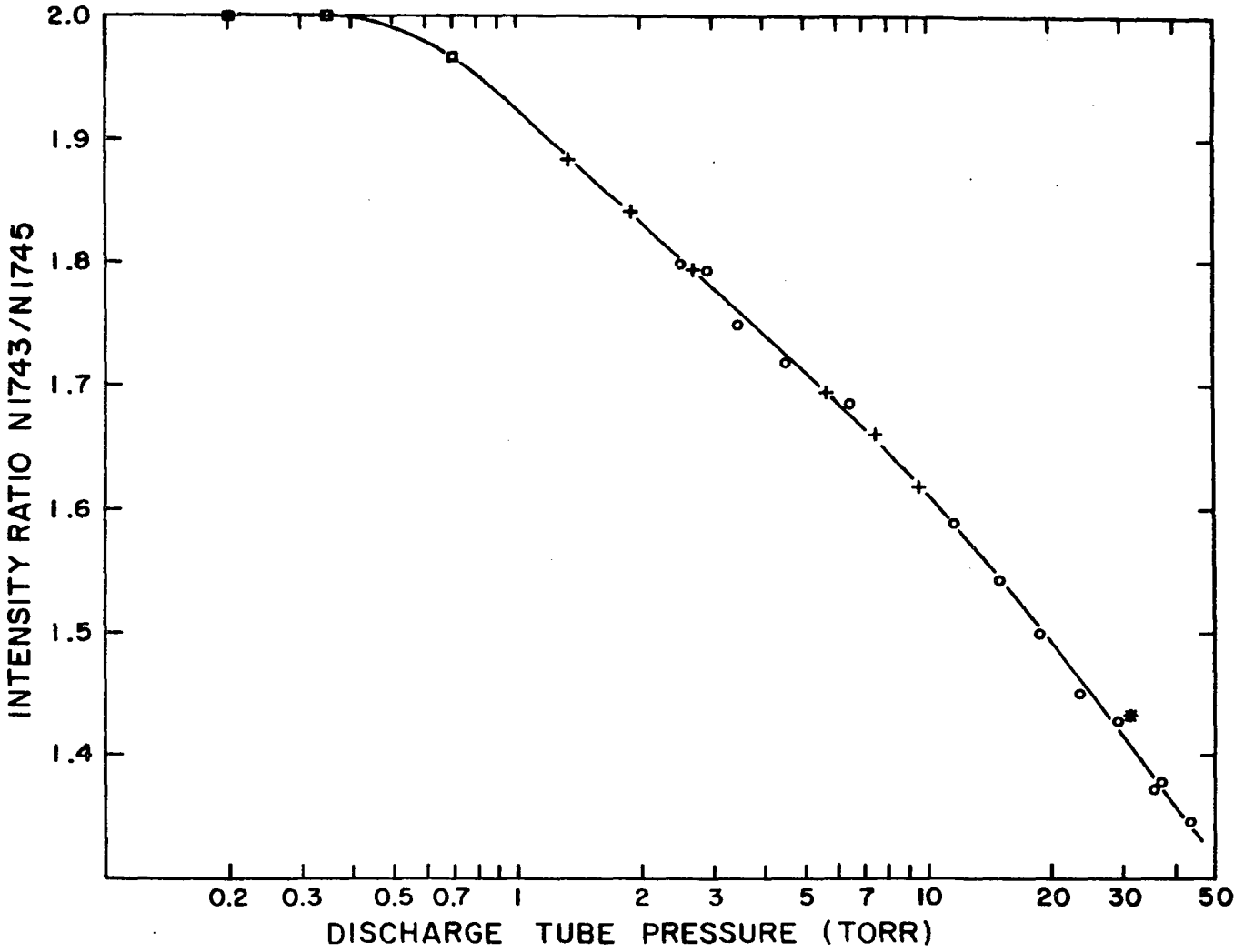

Figure 4. The N 1743/N 1745 Å doublet ratio in the argon matrix

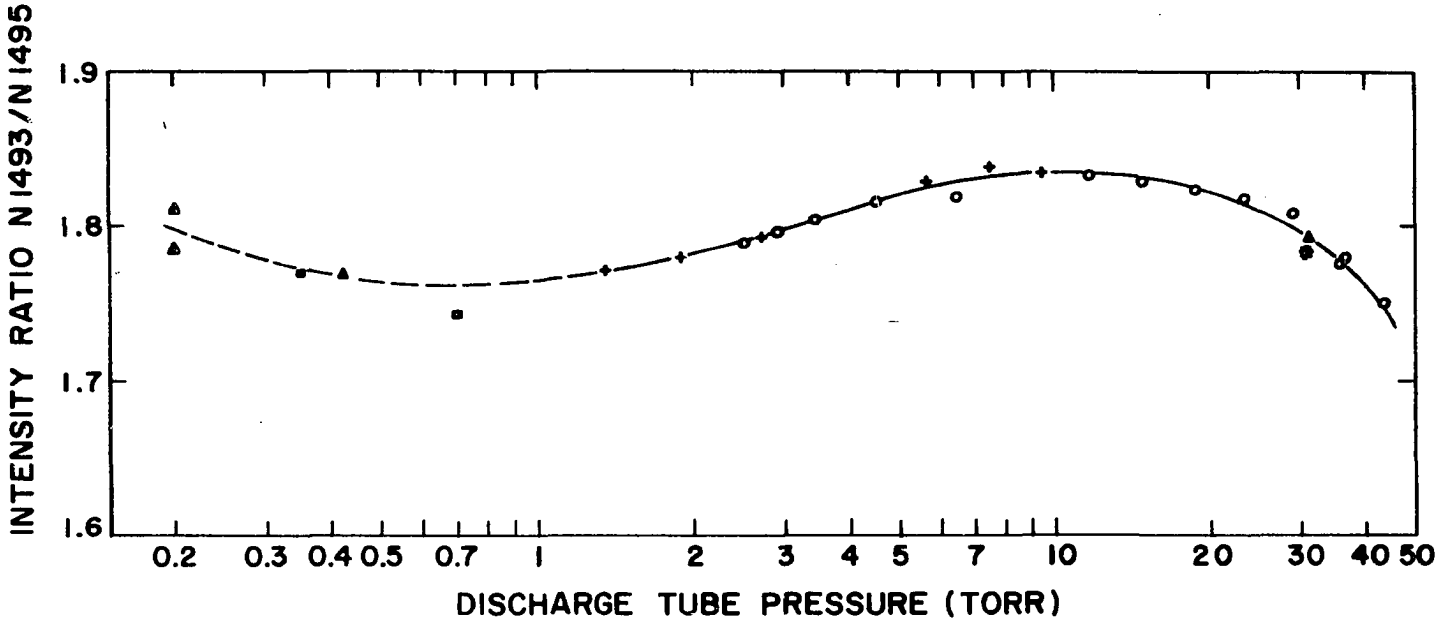

Figure 5. The N 1493/N 1495 Å doublet ratio in the argon matrix

II. APPARATUS

There is presented in Figure 6 a view of the apparatus used in this study. From left to right there appear, in order, (1) cylinders containing the following gases: commercial acetylene and oxygen (not pertinent to this investigation), argon-500 vpm nitrogen, helium-500 vpm nitrogen, commercial argon, and commercial helium, (2) gas purification and metering equipment, (3) the discharge tube with microwave resonance cavity, (4) the vacuum-ultraviolet spectrometer, and (5) the microwave frequency generator (atop the spectrometer). Figure 7 is a close-up view of the microwave-driven discharge in an argon matrix. Since the discharge is viewed axially, the spectrometer sees a source of appreciable depth.

The components comprising the spectral source, the spectrometer, and its associated electronic readout system are described in Table 1. A schematic drawing of the gas-handling system is presented in Figure 8, the components of which are also described in Table 1.

The operation of the system is most lucidly described by tracing the schematic diagram. The desired matrix gas mixture is admitted to the precision pressure regulator from the appropriate cylinder in the tank farm. With its pressure now regulated to 3.00 ± 0.01 psig, the upstream metering valve (MV) is adjusted to provide the desired flow-rate through the system, as measured by the flowmeter on the output side of the mechanical pump. The downstream metering valve may then be adjusted to provide the desired pressure in the system. Thus

Figure 6. View of the spectrometer, spectral source, and gas-handling system

Figure 7. Close-up view of spectral source

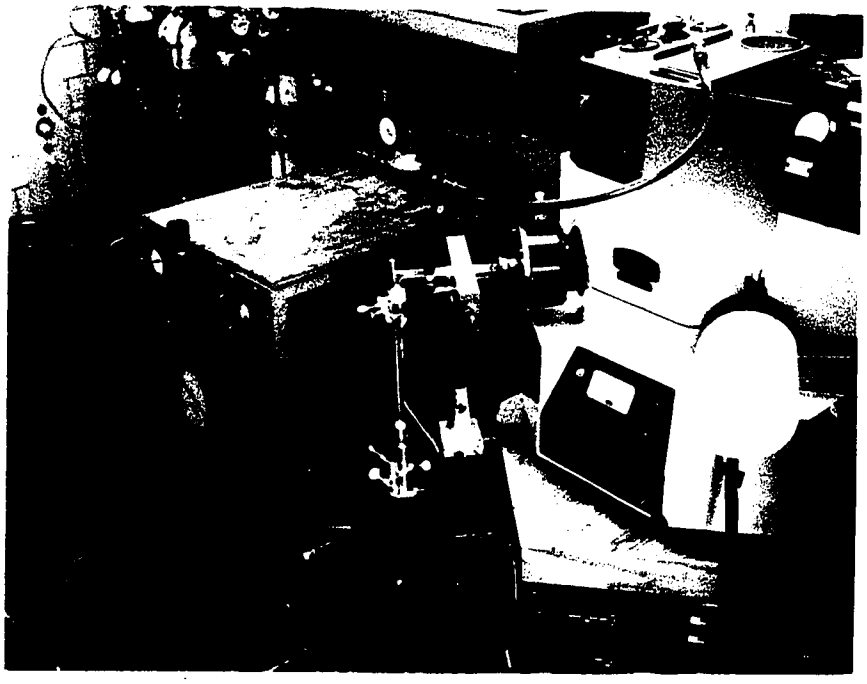

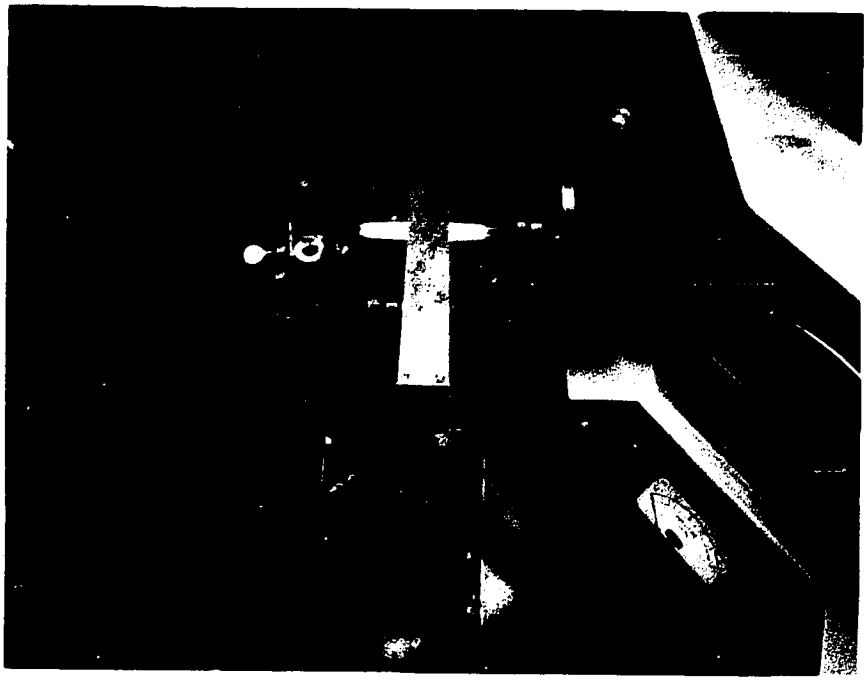

Table 1. Identification and description of apparatus components

Component	Description
Spectrometer	Jarrell-Ash Co. 0.5-meter Seya-Namioka Vacuum, 1200 gpmm grating on aluminum blank.
Photomultiplier	E. M. I. Electronics Ltd. model 6255B, 13 stages operated at 77 volts per stage.
Photomultiplier power supply	New Jersey Electronics Corp. model S-325, output continuously variable from 500 to 2500 volts dc.
Amplifier	Keithley Instruments Inc. model 410 micro-microammeter, operating range from 10×10^{-4} to 3×10^{-13} ampere full scale.
Recorder	Leeds and Northrup Co. Speedomax G, catalog no. 69809, operated on 0-10 mV scale without zero suppression.
Voltage regulator	Superior Electric Co., Stabiline series, type 1E5101.
Discharge tube	Fused quartz cylinder, 16.0 mm ID x 21 cm long, attached to spectrometer slit face via Neoprene O-ring compression seal.
Microwave cavity	Original design and construction by Douglas Microwave Co., Inc.
Microwave frequency generator	Raytheon Corp. model CMD7 diathermy generator, operating at 2450 Mc with a maximum power output of 125 watts.
Pressure gauge 0-50 torr	Wallace and Tiernan Co. model FA160, barometrically compensated aneroid manometer, 0-50 torr range in 0.5 torr divisions interpolable to 0.05 torr.

Table 1. (Continued)

Component	Description
Pressure gauge 0-800 torr	Wallace and Tiernan Co. model FA129, barometrically-compensated aneroid manometer, 0-800 torr range in 1 torr divisions interpolable to 0. 1 torr.
Flowmeter	Differential manometric using dinonylphthalate, colored with elemental iodine, as the manometric fluid. Helium sensitivity: 1 cm differential height= 4. 2 ml STP/min. Argon sensitivity: 1 cm differential height= 3. 8 ml STP/min.
Precision pressure regulator	The Matheson Co. Inc. model 71-240, low pressure corrosion-resistant, employing Teflon-faced Butyl rubber diaphragm.
Metering valves	Hoke Inc. type 2RB281, long taper micrometer screw needle.
Toggle valves	Hoke Inc. series 450, spring closing.
Diaphragm valves	Imperial Eastman Co. type 683 CS, metal diaphragm.
Cold trap	Double-wound coil containing 37 ft. of 3/8 in. OD copper tubing.
Molecular seive trap	Linde Co. molecular seive type 13-X, packed in U-tubes 3. 2 cm ID x 45 cm total length.

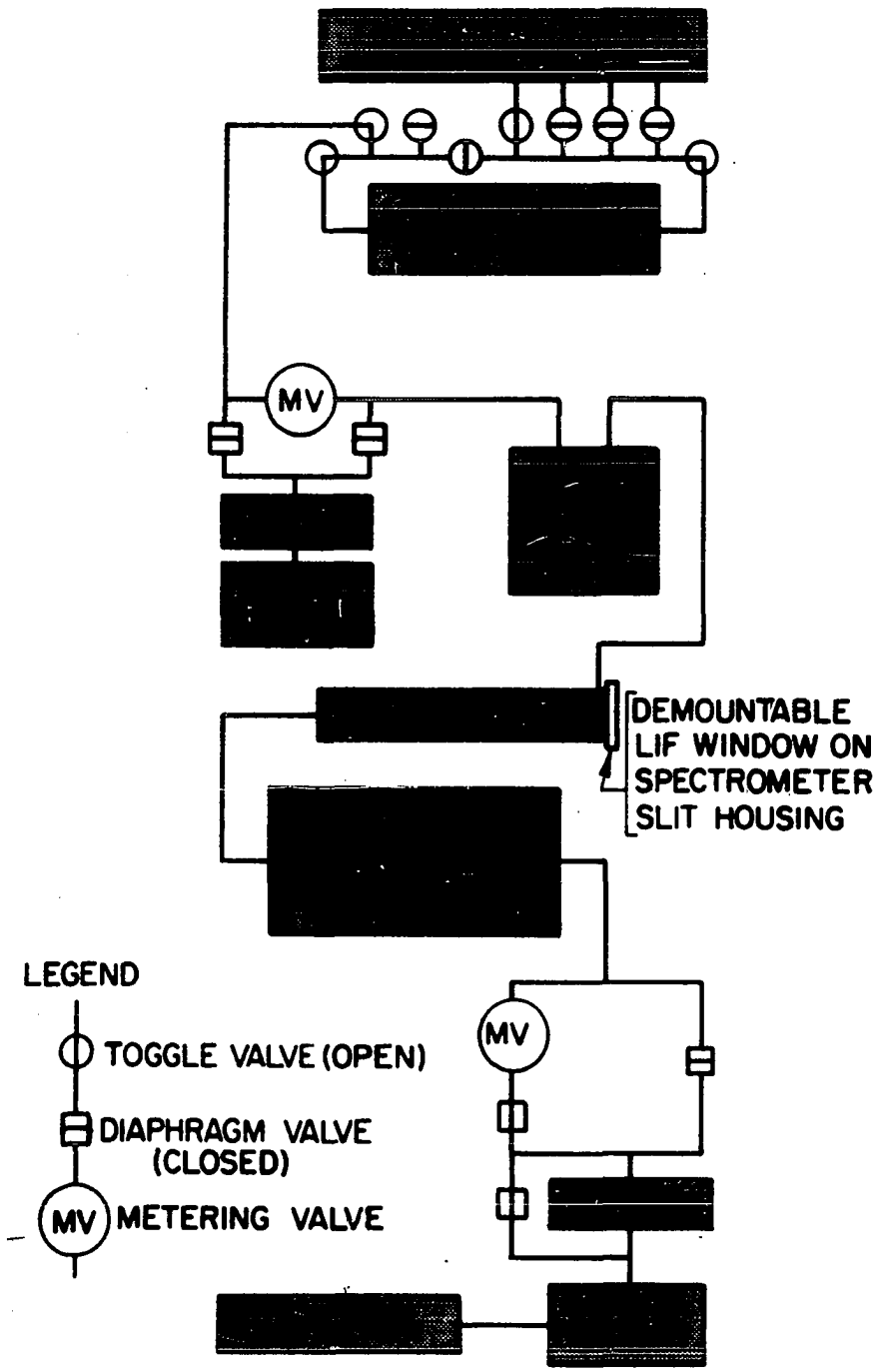

Figure 8. Flow diagram of the gas-handling system

it is seen that the discharge tube is operated with matrix gas continuously flowing through it at a specified constant flowrate and pressure.

This gas-handling system provides wide latitude for the independent selection of both pressure and flowrate. For example, a constant flowrate of 40 ml STP per minute can be maintained at all pressures between 0.8 and 500 torr with helium, and between 1.5 and 500 torr with argon. Conversely, a constant pressure of 5 torr or greater can be maintained at all flowrates between 10 and 300 ml STP per minute in both helium and argon. Outside these ranges pressure and flowrate are no longer independently variable, and the specification of one of them imposes restrictions on the selectable range of the other. Pressure regulation is excellent, short-term pressure fluctuations being controlled to $< \pm 0.05$ torr, and long-term pressure drift being controlled to < 0.01 torr per hour.

The function of the cold trap, immersed in liquid nitrogen, is to remove condensible contaminants from the matrix gas. This is necessary because the nitrogen doublet ratios are sensitive to the concentration of contaminants in the system, especially those containing carbon. It is for this same reason that the molecular sieve (MS) traps exist immediately upstream from each mechanical pump--to prevent the system from becoming contaminated with back-diffusing pump oil vapors.

III. THE CAUSE OF THE DOUBLET INTENSITY RATIO ANOMALY

Having described the nature of the phenomenon, it is now possible to proceed with its elucidation. In this section, the cause of the phenomenon will be deduced, and then proven.

A. Identification of the Transitions

There is reproduced in Figure 9 that portion of the energy level diagram (4) of the nitrogen atom which is pertinent to the N 1743, 5 and N 1493, 5 Å transitions. Before proceeding further it is desirable to establish the nomenclature of Table 2, which will be used henceforth to identify these transitions.

Table 2. Nomenclature and subscript notation for the nitrogen lines

Quantity	Symbol	Definitions
Subscript	1	N 1742.724 Å
	2	N 1745.246 Å
	3	N 1492.724 Å
	4	N 1494.673 Å
	i, j, k	Any arbitrary spectral line
	u, *l*	Upper and lower energy level of line i, j, k
Intensity	I_i	The experimentally observed intensity of the spectral line i, i = 1, 2, 3, or 4
	$I_i(0)$	The hypothetical non-absorbed intensity of the self-absorbed line i, i = 1, 2, 3, or 4
Intensity ratio	R_{12}	$R_{12} = I_1/I_2$, the observed intensity ratio of the N 1743, 5 Å doublet
	R_{34}	$R_{34} = I_3/I_4$, the observed intensity ratio of the N 1493, 5 Å doublet

Table 2. (Continued)

Quantity	Symbol	Definitions
Intensity ratio	$R_{12}(0)$	$R_{12}(0) = I_1(0)/I_2(0)$, the hypothetical doublet ratio were the 1, 2 doublet unabsorbed
	$R_{34}(0)$	$R_{34}(0) = I_3(0)/I_4(0)$, the hypothetical doublet ratio were the 3, 4 doublet unabsorbed

The energy separation of the J levels of each state has been exaggerated in Figure 9 in order to more clearly show the spectral transitions. Since the band pass of the spectrometer is considerably greater than the line fine structure resulting from the J-energy separations of the $^2P^\circ$ and $^2D^\circ$ lower states, the J levels of these latter may be considered to be degenerate in energy. It should be noted, however, that the spectral lines λ_1, λ_2, and λ_3 observed by the spectrometer actually are composite lines, being composed of the transitions a + b, c + d, and e + f, respectively. Two additional features of these nitrogen doublets should be noted, (i) that both doublets have the same upper state, and (ii) that the quartet ground state renders the lower states of the transitions metastable by the electric dipole selection rules.

B. Possible Origins of the Phenomenon

For the remainder of this chapter, the composite nature of the spectral lines denoted 1, 2, 3, and 4 will be ignored to provide a

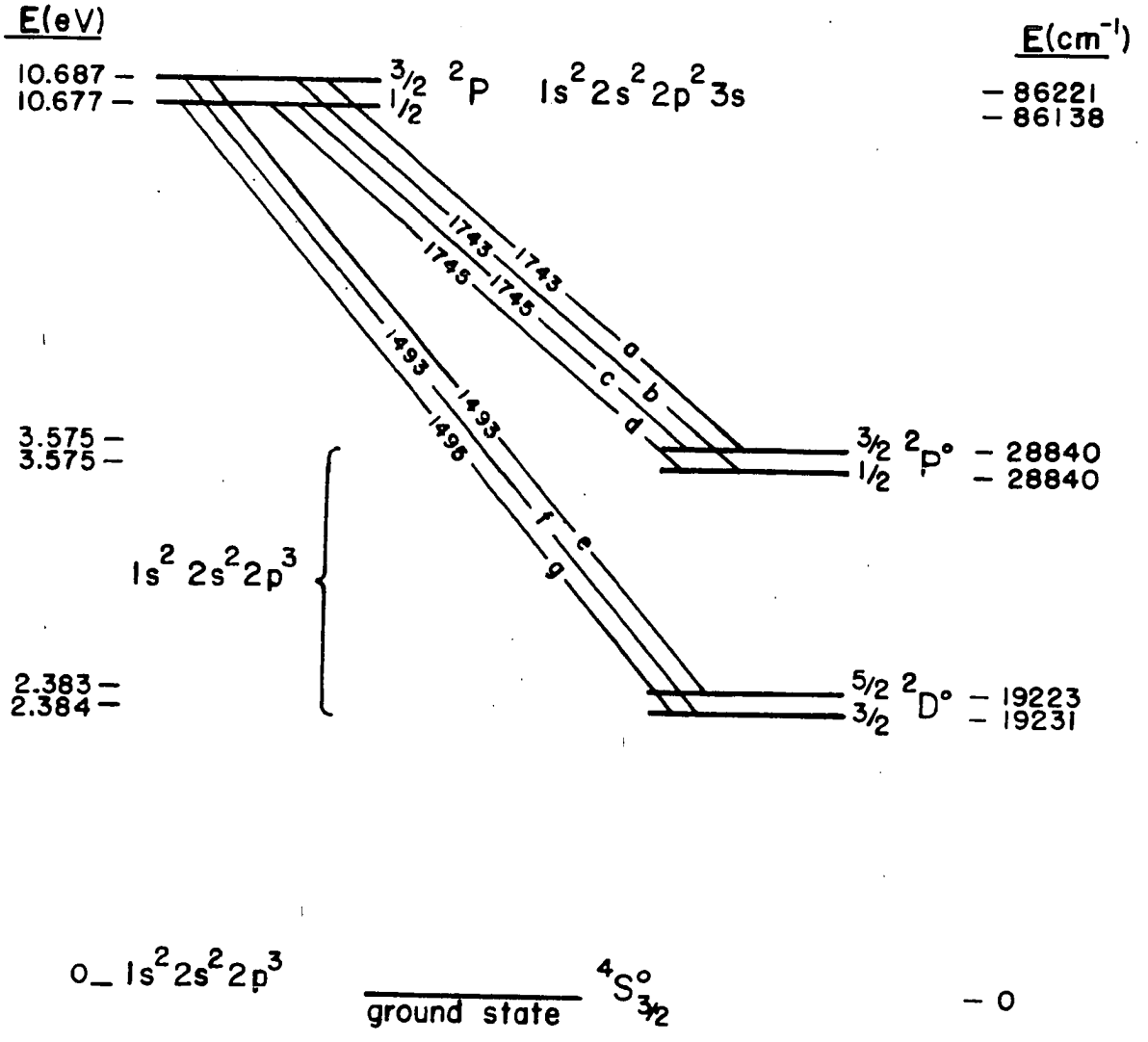

Figure 9. Pertinent transitions in the energy level diagram of the nitrogen atom

mathematically simpler treatment. It has been verified that the result is the same if the composite nature of the transitions is taken into account.

A logical and comprehensive approach to the possible origins of this phenomenon requires consideration of the following facts:

(1) N atomic spectra arise only from N atoms.

(2) The spectral lines N 1743, 5 Å arise only from population of the $1s^2, 2s^2, 2p^2, 3s\ ^2P_{1/2, 3/2}$ configuration.

(3) The anomaly can arise only from emission or absorption of radiation, or both.

(4) If it arises via emission, then by statement 2 it must come from anomalous population of the $3s\ ^2P_{1/2, 3/2}$ state.

(5) If it arises via absorption, four possibilities exist; viz., (a) instrumental absorption, (b) absorption by the helium or argon matrix, (c) absorption by molecular nitrogen species, and (d) self-absorption by the lower states of the transitions. Each possibility will be examined in turn.

(5a) Instrumental absorption cannot be the origin since (i) these are characteristically broad-band effects and should therefore affect both lines of the doublet to very nearly the same degree, and (ii) instrumental effects would be invariant with discharge tube pressure.

(5b) Absorption by the helium matrix cannot be the origin since (i) the phenomenon is also observed in an argon matrix, (ii) no states exist in helium which are capable of absorbing 7.102 and/or 7.112

eV photons, and (iii) photoionization cross-sections for absorption by the 1s2s $^1S_0$ and 1s2s $^3S_1$ helium metastables would be almost identical for photons differing in energy by only 0.01 eV, and could not therefore account for the observed magnitude of the intensity ratio shift. In addition to this, if absorption via photoionization were the cause, the pressure dependence of the N 1493/1495 Å ratio must vary in consort with that of the N 1743/1745 Å ratio, since the variation in matrix absorber concentration with pressure would be the same for both doublets. From Figures 1 - 5, however, this is observed not to be the case.

(5c) Radiative absorption by molecular nitrogen could conceivably be a cause of the anomaly since states of N_2 with energy differences of ca. 7 eV do exist. If it should then by chance happen that the N 1743 Å photon energy coincides with an allowed transition, whereas the N 1745 Å photon energy does not, the observed phenomenon could result. However, the following factors ally against this. (i) The variation of the N 1493, 5 Å ratio would require a similar coincidence of transitional and photon energies which, if it occurred, would indeed be fortuitous. (ii) If the lower state of such an absorbing transition were a molecular excited state, the following dilemma arises. It is observed experimentally that (a) in a helium matrix, the N_2 molecular band spectra decrease in intensity with increase in pressure, whereas (b) in an argon matrix, the same spectra increase in intensity

with increase in pressure. Since spectral intensity is directly related to excited state concentration, it is necessarily true that (a) in a helium matrix, $[N_2^*]$ † decreases with increase in pressure, whereas (b) in an argon matrix, $[N_2^*]$ increases with increase in pressure. But, it is also noted experimentally that the form of the doublet ratio variation is the same in argon as in helium. Hence, absorption by N_2^* states cannot cause the phenomenon since similar results in argon and helium cannot arise from absorber concentrations which, in the former case increase, and in the latter case decrease, with increase in pressure. (iii) The possibility that N_2 molecules in the ground state are absorbing the N 1743, 5 and N 1493, 5 Å photons may be ruled out experimentally by simply admitting nitrogen to the vacuum monochromator. For 500 vpm nitrogen in helium the partial pressure of nitrogen in the matrix mixture is $5 \times 10^{-4} \times P_{dt}$ ‡ which corresponds to 5×10^{-3} torr for $P_{dt} = 10$ torr. Since the radiation path in the spectrometer is about ten-fold greater than that in the discharge tube, this procedure will be a very sensitive test. It was found that the admission of air to the monochromator to a pressure of 25×10^{-3} torr produced no detectable change in the N 1743, 5 Å ratio emitted by the source at 10 torr. Hence,

---

† The notation X* signifies an excited state of the species X, and brackets are to be read "the concentration of" the quantity they enclose.

‡ P_{dt} denotes discharge tube pressure.

absorption by ground state N_2 molecules is not the cause of the doublet variation.

The conclusion is therefore inescapable that absorption by molecular nitrogen species is a highly improbable cause of the doublet ratio behavior.

(5d) Radiative self-absorption by N atoms in the metastable lower states of the transitions is the only remaining possible origin of the effect. It is a highly probable origin.

C. Specific Origin of the Effect

Barring the highly improbable molecular-N_2-absorption mechanism, there remain as causes of the N doublet ratio anomaly only the following three possibilities:

(i) anomalous population of the 3s ^2P upper state,

(ii) self-absorption by N atoms in the 2p $^2P°$ and $^2D°$ lower states,

(iii) both (i) and (ii).

Which of these is the specific cause of the anomaly can be decided experimentally. Before proceeding with this, however, it is desirable to define some terms.

1. Anomalous population vs. thermal equilibrium

A thermal population of two atomic states i and j is herein defined to be that population which is given by the Maxwell-Boltzmann energy distribution law for a system at temperature T. The statement of this law gives that

$$(3\text{-}1) \qquad N_i = \frac{N_o\, g_i \exp\left[-E_i/kT\right]}{Q},$$

wherein Q is the partition function and the other quantities have their customary significance. Hence, for two states i and j of the same atomic species, we have that

$$(3\text{-}2) \qquad N_i/N_j = (g_i/g_j) \exp\left[-(E_i-E_j)/kT\right] \cong g_i/g_j = \text{constant if } E_i \cong E_j.$$

This condition is well fulfilled by the upper and lower states of the N 1743, 5 and N 1493, 5 Å transitions, since the separation of the J levels of the common 3s $^2P_{1/2,\ 3/2}$ upper state is only 0. 01 eV, and the separations of the J levels of the $^2P^\circ_{1/2,\ 3/2}$ and $^2D^\circ_{3/2,\ 5/2}$ lower states are 0. 000 and 0. 001 eV, respectively. Hence, the specification that the upper or lower states of the N 1743, 5 or N 1493, 5 Å transitions be thermally populated indicates that the relative population of the J levels of that state is a constant independent of <u>all</u> experimental parameters, since it is independent of plasma temperature.

In contradistinction, a non-thermal -- or anomalous -- population of the J levels of these states may be defined as one wherein

$$(3\text{-}3) \qquad N_i/N_j = \text{fn}(p,\ T) \neq \text{constant},$$

wherein p is the discharge tube pressure and T is the excitation temperature of the plasma.

There remains to be considered the relation between the population densities of the $^2D^\circ$ and $^2P^\circ$ metastable states when these lower states are in thermal equilibrium. This relation is given by the Maxwell-Boltzmann distribution as

$$(3\text{-}4) \qquad \frac{N(^2P^\circ)}{N(^2D^\circ)} = \frac{g(^2P^\circ)}{g(^2D^\circ)} \exp\left[E(^2D^\circ) - E(^2P^\circ)/kT\right].$$

Since, in the microwave-driven discharge, the excitation temperature is a function of discharge tube pressure, it follows that Equation 3-4 may be expressed in the form

$$(3\text{-}5) \qquad \frac{N(^2P^\circ)}{N(^2D^\circ)} = \text{constant} \cdot Fn(p).$$

It is therefore seen that the relative population of the lower states of the N 1743, 5 and N 1493, 5 Å transitions is pressure-dependent even when the states are thermally populated. For non-thermal population, the relative concentrations will be some different function of pressure, which may be designated as

$$(3\text{-}6) \qquad \frac{N(^2P^\circ)}{N(^2D^\circ)} = \text{constant} \cdot fn(p).$$

2. Theory underlying the investigative technique

As mentioned above, the three possibilities which might account for the observed anomaly are (i) non-thermal population of the 3s ^2P

upper state, (ii) spectral self-absorption by atoms in the 2p $^2P^\circ$ and $^2D^\circ$ lower states, or (iii) both. A complete statement of all the possibilities relating to the excitation of N 1743, 5 and N 1493, 5 Å radiation is, therefore:

(i) the upper state may be either thermally (T) or non-thermally (NT) populated,

(ii) the lower states may be either T or NT,

(iii) self-absorption effects occur (+) or do not (-).

All combinations of these possibilities are tabulated in Table 3. Each of these cases will be considered in detail after deducing some general conclusions on the behavior of spectral line intensity with pressure.

3. The pressure-dependent behavior of self-absorbed spectral line intensities

No relation has, as yet, been introduced to describe the variation with pressure of the intensities of self-absorbed spectral lines. The derivation of the specific relation which accounts for the geometry of the source and spectrometer used in this study is somewhat complex, and does in fact comprise the major part of this dissertation. Fortunately, however, it is possible to prove that self-absorption is the cause of the doublet ratio anomaly by (i) merely recognizing the existence of such an equation, and (ii) recognizing one of its properties.

The equation of a self-absorbed spectral line may be defined in the form

Table 3. All cases conceivably responsible for the doublet ratio variation

Case	Upper State	Lower State	Self-absorption
I	T	T	-
II	NT	T	-
III	T	NT	-
IV	NT	NT	-
V	T	T	+
VI	NT	T	+
VII	T	NT	+
VIII	NT	NT	+

(3-7) $I = I(0)\,\zeta(K)$

wherein I is the experimental self-absorbed line intensity, I(0) is the intensity it would have if it were not self-absorbed, K is the absorption coefficient for the spectral line in question, and $\zeta(K)$ is that function of K which describes the absorption behavior of the line for the source in question under the experimental conditions in question. It is obvious from Equation 3-7 that $\zeta(K)$ must possess the property

(3-8) $\lim_{K \to 0} \zeta(K) = 1$

since, for K = 0, there is no self-absorption whereupon

(3-9) $I(K = 0) \equiv I(0),$ †

† The notation ≡ signifies "is defined as or by".

Formulating the intensity ratio of two spectral lines, denoted 1 and 2, we have from Equation 3-7 and the definitions of Table 2 that

$$(3\text{-}10) \qquad R_{12} = R_{12}(0)\,\Omega_{12}$$

wherein the additional definition has been made that

$$(3\text{-}11) \qquad \Omega_{12} \equiv \zeta(K_1)/\zeta(K_2).$$

It will prove convenient to express Equation 3-10 in logarithmic form, viz.,

$$(3\text{-}12) \qquad \ln R_{12} = \ln R_{12}(0) + \ln \Omega_{12},$$

Furthermore, from Equations 3-8 and 3-11 it follows that

$$(3\text{-}13) \qquad \lim_{\substack{K_1 \to 0 \\ K_2 \to 0}} \Omega_{12} = 1.$$

The doublet intensity anomaly is observed as a variation in R_{12} with discharge tube pressure, hence the functional form of the quantity $\partial \ln R_{12}/\partial p$ is of interest, wherein p is defined as the total gas pressure in the discharge tube. Now, although $\partial \ln R_{12}/\partial p$ is the experimental measurable, the quantity of theoretical interest is $\partial \ln R_{12}/\partial p_{N_2}$, since it is the nitrogen pressure rather than the total pressure which directly influences R_{12}. From the Chain Rule we have that

$$(3\text{-}14) \qquad \frac{\partial}{\partial p} = \frac{\partial}{\partial p_{N_2}} \frac{\partial p_{N_2}}{\partial p}.$$

However, for a fixed concentration of nitrogen in helium, we have that

$$(3\text{-}15) \qquad p = c p_{N_2}, \quad (c = \text{constant}),$$

from which it follows that

$$(3\text{-}16) \qquad \frac{\partial}{\partial p_{N_2}} = c \frac{\partial}{\partial p}.$$

Thus, the derivative of Equation 3-12 with respect to p_{N_2} yields

$$(3\text{-}17) \qquad \frac{\partial \ln R_{12}}{\partial p_{N_2}} = c \frac{\partial \ln R_{12}}{\partial p} = c \frac{\partial \ln R_{12}(0)}{\partial p} + c \frac{\partial \ln \Omega_{12}}{\partial p}.$$

Employing, for typographical convenience, the conventional notation wherein a prime signifies the first derivative, there result the following definitions,

$$(3\text{-}18) \qquad R'_{12} \equiv \frac{\partial \ln R_{12}}{\partial p}, \quad R'_{12}(0) \equiv \frac{\partial \ln R_{12}(0)}{\partial p}, \quad \Omega'_{12} \equiv \frac{\partial \ln \Omega_{12}}{\partial p},$$

whereupon Equation 3-17 becomes

$$(3\text{-}19) \qquad R'_{12} = R'_{12}(0) + \Omega'_{12}.$$

4. $R_{12}(0)$ for a non-absorbed spectral doublet

It is necessary to consider in some detail the relationship which exists between the intensity of a spectral line and the concentration of atoms in its upper state. Obviously, the intensity of a spectral transition is proportional to the number of atoms making that transition per unit time. Thus, for the transitions depicted in Figure 9,

$$(3\text{-}20) \qquad I_a(0) \sim n_a, \qquad I_b(0) \sim n_b, \qquad I_c(0) \sim n_c, \qquad \text{etc.},$$

where the n_i are the numbers of atoms making the transitions i per unit time. Now, as it happens,

$$(3\text{-}21) \qquad \lambda_a = \lambda_b, \qquad \lambda_c = \lambda_d, \qquad \lambda_e = \lambda_f$$

within the ability of the spectrometer to differentiate between them. Thus, the spectrometer sees only the transitions λ_1, λ_2, λ_3, and λ_4, whose intensities are given by

$$(3\text{-}22) \qquad I_1 = I_a + I_b, \qquad I_2 = I_c + I_d,$$
$$I_3 = I_e + I_f, \qquad I_4 = I_g.$$

It follows, then, from the proportionalities 3-20 that

$$(3\text{-}23) \qquad I_1 \sim n_a + n_b, \qquad I_2 \sim n_c + n_d,$$
$$I_3 \sim n_e + n_f, \qquad I_4 \sim n_g.$$

But the number of atoms which leave a given state radiatively by a given path is proportional to the number of atoms which are in the state

and the probability that they will leave by the given path. The latter is given by the Einstein spontaneous emission transition probability and ν^4- factor, which together yield the quantity $A\nu$. Thus,

$$(3\text{-}24) \qquad n_a + n_b \sim A_I\ \nu_1\ N_1, \qquad n_c + n_d \sim A_2\ \nu_2\ N_2$$

$$n_e + n_f \sim A_3\ \nu_3\ N_3, \qquad n_g \sim A_4\ \nu_4\ N_4\ ,$$

wherein $A_i\ \nu_i$ is the $A\nu$-factor for the transition i, and N_i is the number of atoms per unit volume in the upper state of the transition i. Insertion of the proportionalities 3-24 into the proportionalities 3-23 yields

$$(3\text{-}25) \qquad I_i(0) = C\ A_i\ \nu_i\ N_i, \quad i = 1,\ 2,\ 3,\ 4,$$

wherein C is the constant of proportionality. The intensity in this latter equation is the absolute intensity of the spectral line. In terms of the experimental measurable -- the intensity as seen by the spectrometer -- Equation 3-25 may be written

$$(3\text{-}26) \qquad I_i(0) = Z_i\ A_i\ \nu_i\ N_i\ , \qquad i = 1,\ 2,\ 3,\ 4,$$

wherein Z_i is a parameter which includes (i) the proportionality constant, (ii) the source - spectrometer geometry factor, and (iii) the wavelength - dependent intensity calibration of the instrument. Thus, the intensity ratio for a non-absorbed spectral doublet may be formulated to be

$$(3\text{-}27) \qquad R_{ij} \equiv \frac{I_i(0)}{I_j(0)} = \frac{Z_i\ A_i\ \nu_i\ N_i}{Z_j\ A_j\ \nu_j\ N_j}, \qquad i,\ j = 1, 2 \text{ or } 3, 4.$$

Since the wavelength separations of the 1, 2 and 3, 4 doublets are less than three angstroms, it follows that

$$(3\text{-}28) \qquad Z_i \cong Z_j$$

with the result that $R_{ij}(0)$ is insensitive to both the absolute and relative intensity distribution of the source - spectrometer combination.

5. $R'_{12}(0)$ for thermal population of the upper state

Specification that the upper state be thermal implies, by Equation 3-2, that N_1/N_2 is a constant. Furthermore, A and ν are atomic constants and therefore not functions of source pressure, nor are Z_1 and Z_2 functions of source pressure. Hence, the derivative of the logarithm of Equation 3-27 with respect to pressure yields

$$(3\text{-}29) \qquad R'_{12}(0) = 0$$

for thermal population of the upper state. From what has been said, it is seen that this result is true for all doublet intensity ratios arising from the N 3s ^{2}P upper state provided only that this state be thermally populated, and that this result is insensitive to all instrumental and source parameters.

6. $R'_{12}(0)$ for non-thermal population of the upper state

That the upper state be NT implies that there is a preferential population or de-population of one or the other of the J levels of the state. Any process leading to the population of that state which is

independent of J will contribute to a thermal distribution, whereas any population process which is J-dependent will lead to preferential population, and hence an NT distribution. If, then, the upper state be NT, then no matter what the nature of the population mechanism is,

$$(3\text{-}30) \qquad N_i/N_j = fn(p) \equiv F_o(p),$$

wherein $F_o(p)$ is a specific pressure function which describes the upper state for the source in question under the experimental conditions in question. Nothing is known nor need be known about the analytical form or magnitude of this function. It is identified here merely to recognize its physical existence, just as will be done for the remaining pressure functions which will be identified below.

Note that in Equation 3-30 no explicit cognizance has been taken of the possibility that N_i/N_j is a constant independent of pressure, but of a value different from the g_i/g_j of the upper state thermal case. It will be seen that this possibility is automatically handled with the upper state thermal case since in the treatment of the latter the magnitude of the constant is immaterial.

Upon insertion of Equation 3-30 into Equation 3-27, taking the indicated derivative yields

$$(3\text{-}31) \qquad R'_{12} = F'_o(p) \equiv F_1(p)$$

for non-thermal population of the upper state.

7. Consideration of cases

There were listed in Table 3 all cases conceivably responsible for the anomaly, provided that the cause of the anomaly arises from atomic nitrogen species. Each of these cases will now be considered:

Case I: (T, T, -). For upper state T, we have from Equation 3-29 that $R'_{12}(0) = 0$. Similarly, $R'_{34}(0) = 0$ since R_{34} simply corresponds to a different lower state, and the argument leading to Equation 3-29 holds irrespective of the identity of the lower state. Furthermore, since radiative self-absorption is absent in this Case,

(3-32) $\Omega'_{12} = 0.$

Hence, since all terms on the right hand side of Equation 3-19 are zero, we have that

(3-33) $R'_{12} = R'_{34} = 0,$ for (T, T, -).

Case II: (NT, T, -). For upper state NT, we have from Equation 3-31 that $R'_{12}(0) = F_1(p)$. Similarly, since the argument is independent of the identity of the lower state of the transition, we may define

(3-34) $R'_{34}(0) \equiv f_1(p).$

The question then arises whether there is a relationship between $F_1(p)$ and $f_1(p)$. Reference to Figure 9 shows that both doublet transitions considered here arise from the same upper state. Consequently, the function N_i/N_j defined by Equation 3-30 is identical for both the N 1743, 5 and N 1493, 5 Å doublets, i. e.,

(3-35) $N_1/N_2 = N_3/N_4$.

Thus,

(3-36) $F_1(p) = f_1(p)$

with the result that

(3-37) $R'_{12}(0) = R'_{34}(0) = F_1(p)$

which may be rewritten to yield

(3-38) $R'_{12}(0)/R'_{34}(0) = 1$.

It is important to note that this result is true regardless of the form or value of the function N_i/N_j of the upper state.

Since radiative self-absorption does not occur in this case, Ω'_{12} is again zero, with the result that

(3-39) $R'_{12}/R'_{34} = R'_{12}(0)/R'_{34}(0) = 1$, for (NT, T, -).

Case III: (T, NT, -). The spontaneous transition of an electron from an upper state i to a lower state ℓ is an intra-atomic reaction. If the atom be anthropomorphized, it might be said that the atom undergoing a transition is completely unconcerned with the condition of its neighbors at the time. Hence, what transition the atom decides to make depends only on what transition it feels like making and, at least to a first approximation, does not depend on what other atoms have done or are doing. Hence, in the absence of self-absorption, the J-population ratio

of the assembly of atoms in the lower state ℓ does not influence the doublet ratio emitted by the assembly of atoms in the upper state u. As a consequence, Case III is degenerate with Case I.

Case IV: (NT, NT, -). The foregoing argument applies equally well to this Case, hence Case IV is degenerate with Case II.

Case V: (T, T, +). This Case differs from Case I only in that the self-absorption mechanism is operative. Analytically, this signifies that now

$$(3\text{-}40) \qquad K_1 \neq 0, \quad K_2 \neq 0, \quad K_3 \neq 0, \text{ and } K_4 \neq 0.$$

It will be shown in a subsequent section that

$$(3\text{-}41) \qquad K_1 = \frac{\lambda_1}{8\pi} \frac{g_u}{g_\ell} A_1 \cdot f(\text{line broadening}) \cdot f(\text{concentration of state } \ell).$$

Now, since $\lambda_1 \neq \lambda_2$, and $g_u)_1 \neq g_u)_2$ for the 1, 2 doublet, and the same is true for the 3, 4 doublet it follows that

$$(3\text{-}42) \qquad K_1 \neq K_2, \quad \text{and } K_3 \neq K_4.$$

Furthermore, it will be shown in a subsequent section that line broadening is quite pressure-dependent, hence

$$(3\text{-}43) \qquad K_i = K_i(p), \quad i = 1, 2, 3, 4,$$

whereupon it is obvious that

(3-44) $\Omega'_{ij} = \Omega'_{ij}(p), \qquad ij = 12 \text{ or } 34.$

Since line broadening is known to be a non-linear function of pressure, as will also be shown in the subsequent section, it must result that

(3-45) $\Omega'_{ij} = \Omega'_{ij}(p).$

Having established this result, it is possible to proceed with the investigation of Case V. It was shown in Equation 3-19 that

(3-19) $R'_{12} = R'_{12}(0) + \Omega'_{12}.$

It was also established in Case I that for upper state T

(3-46) $R'_{12}(0) = R'_{34}(0) = 0.$

The Ω' which correspond to the lower state thermal are specific functions of pressure, and must therefore be identified as such, which requires the definitions

(3-47) Ω'_{12} (lower state thermal) $\equiv F_2(p),$

Ω'_{34} (lower state thermal) $\equiv F_3(p).$

The insertion of the relations (3-46) and (3-47) into Equation 3-19 yields

(3-48) $R'_{12} = F_2(p), \text{ and } R'_{34} = F_3(p),$

which may be ratiod to yield

(3-49) $R'_{12}/R'_{34} = F_2(p)/F_3(p)$ = function of pressure.

Case VI: (NT, T, +). For upper state NT, we have from Equation 3-37 that $R'_{12}(0) = R'_{34}(0) = F_1(p)$. For lower state T, we have from Equation 3-47 that $\Omega'_{12} = F_2(p)$ and $\Omega'_{34} = F_3(p)$. Inserting these results into Equation 3-19 yields,

(3-50) $R'_{12} = F_1(p) + F_2(p)$, and $R'_{34} = F_1(p) + F_3(p)$

which, when ratiod, yields

(3-51) $$\frac{R'_{12}}{R'_{34}} = \frac{F_1(p) + F_2(p)}{F_1(p) + F_3(p)} = \text{function of pressure}$$

Case VII: (T, NT, +). As was true for Equation 3-47, the Ω'_{ij} which correspond to lower state NT must also be certain specific functions of pressure, which are herein identified as

(3-52) Ω'_{12} (lower state NT) $\equiv F_4(p)$,
Ω'_{34} (lower state NT) $\equiv F_5(p)$.

As in Case V, for upper state T we have again that $R'_{12}(0) = R'_{34}(0) = 0$, whereupon Equation 3-19 yields

(3-53) $R'_{12} = F_4(p)$, and $R'_{34} = F_5(p)$.

Hence,

(3-54) $R'_{12}/R'_{34} = F_4(p)/F_5(p)$ = function of pressure.

Case VIII: (NT, NT, +). From Case VI we have that $R'_{12}(0) = R'_{34}(0) = F_1(p)$, and from Case VII with have that $\Omega'_{12} = F_4(p)$, and $\Omega'_{34} = F_5(p)$. Hence, as before, it results that

$$(3\text{-}55) \qquad \frac{R'_{12}}{R'_{34}} = \frac{F_1(p) + F_4(p)}{F_1(p) + F_5(p)} = \text{function of pressure}$$

8. Conclusions

The following facts have been established:

(1) the anomaly cannot arise from instrumental absorption,

(2) the anomaly cannot arise from matrix gas absorption,

(3) the anomaly cannot arise from absorption by ground state nitrogen molecules,

(4) it is highly improbable that the anomaly arises from absorption by excited nitrogen molecules,

(5) it is highly probable that the anomaly stems from atomic nitrogen species.

Concerning this latter, detailed consideration of each of the possible Cases describing all possible combinations of the T or NT character of the atomic nitrogen species permits the conclusion that (i) if radiative self-absorption is not the cause of the anomaly, then $R'_{12}/R'_{34} = 1$, whereas (ii) if radiative self-absorption is the cause, then R'_{12}/R'_{34} is a function of pressure. This result is unequivocal since no assumptions have been made concerning the nature of the pressure functions involved, and the argument is independent of excitation

mechanisms, instrument calibration, etc. Indeed the treatment is even independent of the form of the absorption equation used.

D. Experimental Form of the Quantity R'_{12}/R'_{34}

Plots of R_{12} and R_{34} vs. discharge tube pressure have been presented as Figure 1 and 2 for the helium matrix. If these be replotted in the form ln R_{12} vs. pressure, and ln R_{34} vs. pressure on linear coordinate paper, the derivatives R'_{12} and R'_{34} may be taken graphically. The ratio of these derivatives yields the quantity R'_{12}/R'_{34}, which is plotted vs. pressure in Figure 10. There can be no doubt that R'_{12}/R'_{34} is a function of pressure, and not a constant of value unity. The cause of the doublet ratio effect is therefore definitely identified to be radiative self-absorption by the atoms in the metastable lower states of the respective transitions.

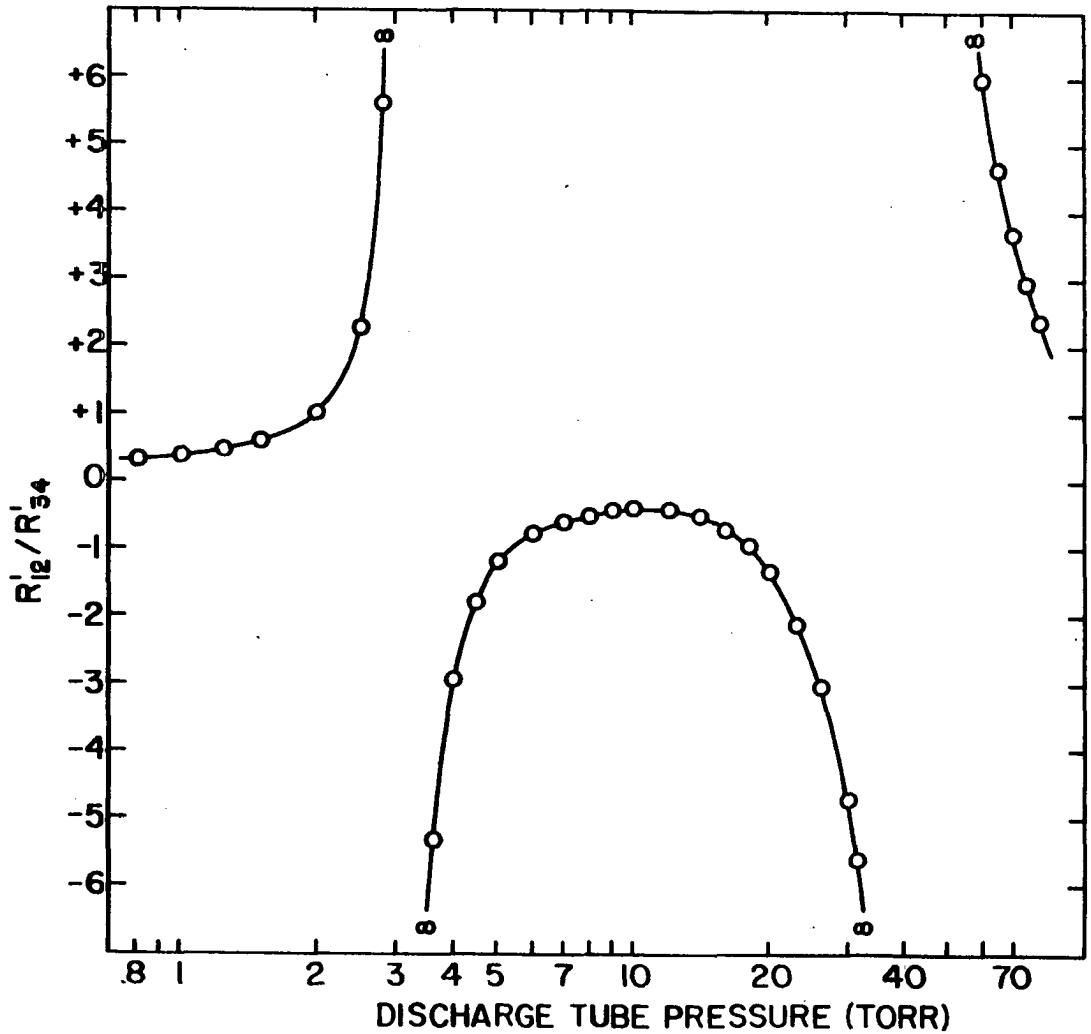

Figure 10. Establishment of the radiative self-absorption mechanism

IV. THE TOTAL INTEGRATED INTENSITY OF A SELF-ABSORBED SPECTRAL LINE

The preceding treatment served to identify the origin of the doublet ratio phenomenon, but it provided no insight into how the effect may be used as a quantitative experimental measure of this origin. In this section, a quantitative relationship will be established between the doublet ratio phenomenon and its causes.

A. Identification of the Absorption Coefficient $k(\nu)$

The following derivation of the absorption coefficient is adapted from the treatment of Cowan and Dieke (5). Consider a microvolume of a discharge plasma of unit cross-sectional area and incremental length dx, such as that of Figure 11, and suppose that collimated radiation is traversing its length parallel to the x-axis. Furthermore, let this radiation consist of a single spectral line of frequency ν_o. This spectral line does, of course, possess a certain frequency distribution which may be described by a function $\rho(\nu)$, wherein $\rho(\nu)$ is defined by

$$(4\text{-}1) \qquad \rho(\nu) = \frac{\text{ergs of radiant energy}}{\text{unit volume} \cdot \text{unit frequency interval}} .$$

The total radiant energy in the frequency interval $d\nu$ which is contained in the microvolume at any instant is therefore $\rho(\nu)\, dx d\nu$.

Let there be contained in this microvolume atoms capable of absorbing the spectral line ν_o, and let their concentration be N atoms per unit volume. Then the number of absorbers in the radiation path of the microvolume is Ndx.

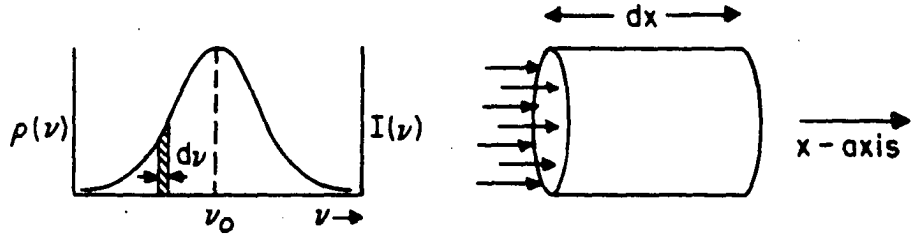

Figure 11. The irradiated plasma microelement

Not every atom is capable of absorbing every photon which comprises the spectral line. To account for this, let there be defined a function $P_a(\nu)$ which will express the probability that the atom encountered by the photon ν will be capable of absorbing it. It will later be shown that $P_a(\nu)$ is governed by the line broadening processes extant in the plasma. The function $P_a(\nu)$ will be defined as the probability of absorption per frequency interval $d\nu$ upon encounter with an atom, and will be taken to be normalized function such that

$$(4\text{-}2) \qquad \int_0^\infty P_a(\nu)\, d\nu = 1.$$

Now, the radiant energy absorbed in the frequency interval $d\nu$ within the microvolume is proportional to (i) the radiant energy present in the interval $d\nu$ within the microvolume, (ii) the number of absorbers in the radiation path within the microvolume, and (iii) the probability of absorption of a photon in the interval $d\nu$ upon encounter with an absorber. The mathematical statement of this is

$$(4\text{-}3) \qquad -d[\rho(\nu)dxd\nu] \sim \rho(\nu)dxd\nu \cdot Ndx \cdot P_a(\nu).$$

The insertion of a constant of proportionality k, followed by appropriate cancellation of the quantity dx, yields

$$(4\text{-}4) \qquad -d[\rho(\nu)d\nu\,] = k\rho(\nu)NdxP_a(\nu)d\nu$$

which, noting that $dx = cdt$ where c is the velocity of light, further

transforms to

$$(4\text{-}5) \qquad \frac{d}{dt}\left[\rho(\nu)d\nu\right] = -ckN\rho(\nu)P_a(\nu)d\nu.$$

The total spectral line energy contained in the microvolume is given by

$$(4\text{-}6) \qquad E = \int_0^\infty \rho(\nu)d\nu$$

wherein the integral over the spectral line width may be taken on the interval $[0, \infty]$ since the incident radiation has been stipulated to consist solely of the spectral line in question. In practice, this requires that neighboring spectral lines be sufficiently resolved that taking the integral over finite limits introduces negligible error.

From Equation 4-6 it follows that

$$(4\text{-}7) \qquad \frac{dE}{dt} = \frac{d}{dt}\int_0^\infty \rho(\nu)d\nu$$

which, upon identification with Equation 4-5, produces the result

$$(4\text{-}8) \qquad dE/dt = -ckN\int_0^\infty \rho(\nu)P_a(\nu)d\nu.$$

To evaluate k, it need only be noted that Equation 4-8 holds for all radiation distribution functions $\rho(\nu)$, hence it also holds for the specific function $\rho(\nu)$ = constant. This latter function corresponds to the case where the incident radiation is a black body continuum since, over the

practical width of a spectral line, its energy density is sensibly constant.

For this case, Equation 4-8 may be rewritten in the form

$$(4\text{-}9) \qquad \frac{dE(bb)}{dt} = -ckN\rho(bb) \int_0^\infty P_a(\nu)d\nu = -ckN\rho(bb)$$

wherein, being a constant with respect to ν, ρ (black body) may be removed from under the integral sign, and the integral remaining equals unity by Equation 4-2. But the definition of the Einstein coefficient of absorption, B is given (5) by

$$(4\text{-}10) \qquad \frac{dE}{dt} = NB\rho(bb)h\nu_o$$

which, when compared with Equation 4-9, establishes the result

$$(4\text{-}11) \qquad k = h\nu_o B/c.$$

Having derived the value of k from energy density considerations, the transformation of B to A -- the Einstein coefficient of spontaneous emission -- must also employ the energy density form. This is given (6) by

$$(4\text{-}12) \qquad B_{\ell u} = \frac{c^3}{8\pi h\nu_o^3} \frac{g_u}{g_\ell} A_{u\ell} = \frac{\lambda_o^3}{8\pi h} \frac{g_u}{g_\ell} A_{u\ell}$$

wherein the second equality arises from the relation $\nu\lambda_{vac} = c$, and the u, ℓ subscripts refer, respectively to the upper and lower states of the transition in question. Thus, by Equation 4-12, Equation 4-11

becomes

$$(4\text{-}13) \qquad k = \frac{\lambda_o^2}{8\pi} \frac{g_u}{g_\ell} A_{u\ell} \ .$$

This value of k is, of course, just as valid when $\rho(\nu) \neq$ constant; hence, it may be re-inserted into any of the preceding equations. With this in mind, consider again Equation 4-4, which may be rewritten in the form

$$(4\text{-}14) \qquad -\frac{d[\rho(\nu)d\nu]}{\rho(\nu)d\nu} = kP_a(\nu)Ndx.$$

The differential in Equation 4-14 refers to the variation of $\rho(\nu)$, and not to the variation in $d\nu$. Indeed, this latter quantity is an arbitrary constant with respect to $\rho(\nu)$ since, as seen from Figure 11, it may have been chosen larger or smaller at will without affecting $\rho(\nu)$ -- the latter being defined by Equation 4-1 as the energy density per <u>unit</u> frequency interval. The left hand side of Equation 4-14 is thus of the form

$$(4\text{-}15) \qquad \frac{d(au)}{au} = \frac{adu}{au} = \frac{du}{u} = d\ln u.$$

Now, there exists a relation between energy density and intensity of radiation given (7) by

$$(4\text{-}16) \qquad \rho = \frac{4\pi}{c} I \equiv bI.$$

If this substitution be made in Equation 4-15 there arises the result that

$$(4\text{-}17) \qquad \frac{d(au)}{au} = \frac{d(abv)}{abv} = \frac{abdv}{abv} = d\ln v.$$

Making the identifications $u = \rho(\nu)$ and $v = I(\nu)$, Equation 4-14 becomes

$$(4\text{-}18) \qquad d\ln I(\nu) = -kP_a(\nu)Ndx$$

which, upon employing the value of k from Equation 4-13, becomes

$$(4\text{-}19) \qquad d\ln I(\nu) = -\frac{\lambda_\circ^2}{8\pi} \frac{g_u}{g_\ell} A_{u\ell} NP_a(\nu)dx.$$

It will prove convenient to the remainder of this report to define the following nomenclature:

$$(4\text{-}20) \qquad k = \frac{\lambda_\circ^2}{8\pi} \frac{g_u}{g_\ell} A_{u\ell},$$

$$(4\text{-}21) \qquad k^\bullet = kN = \frac{\lambda_\circ^2}{8\pi} \frac{g_u}{g_\ell} A_{u\ell} N,$$

$$(4\text{-}22) \qquad k(\nu) = k^\bullet P_a(\nu) = \frac{\lambda_\circ^2}{8\pi} \frac{g_u}{g_\ell} A_{u\ell} NP_a(\nu).$$

B. The ν, x-Dependent Equation for a Self-Absorbed Spectral Line

The model depicted in Figure 11 consists of a differential thickness of absorber upon which radiation of frequency distribution $I(\nu)$ is falling. The differential equation describing the absorption in this model is given

by Equations 4-19 and 4-22 as

(4-23) $d\ln I(\nu) = -k(\nu)\, dx.$

To find the transmitted intensity through a path length x per unit frequency interval requires simply an integration on dx on the interval [0, x]. This is straight-forward, and yields the result

(4-24) $I(\nu) = I^{\circ}(\nu) \exp [-k(\nu)x],$

which is recognized as Lambert's law. $I(\nu)$ is the intensity per unit frequency interval transmitted through the absorber, and $I^{\circ}(\nu)$ is the incident intensity per unit frequency interval. For Equation 4-24 to hold rigorously, it is necessary that $k(\nu)$ be constant throughout the path [0, x]. This is practically never true in plasma sources, because every plasma source has a temperature distribution. This fact may be taken into account by replacing $k(\nu)$ by $\bar{k}(\nu, x)$--the average absorption coefficient over the path [0, x]--whereupon Equation 4-24 becomes

(4-25) $I(\nu) = I^{\circ}(\nu) \exp [-\bar{k}(\nu, x)x].$

The physical system to which Equation 4-25 will be applied is presented in Figure 12, which is a cross-sectional diagram of the source - spectrometer slit orientation. Consider the on-axis plasma microelement at x, and for the moment let this microelement emit plane waves which travel down the axis of the tube to the spectrometer slit. Let the magnitude and frequency distribution of the emitted radiation be $I^{\circ}(\nu, x)$. This radiation must traverse the on-axis path of length x

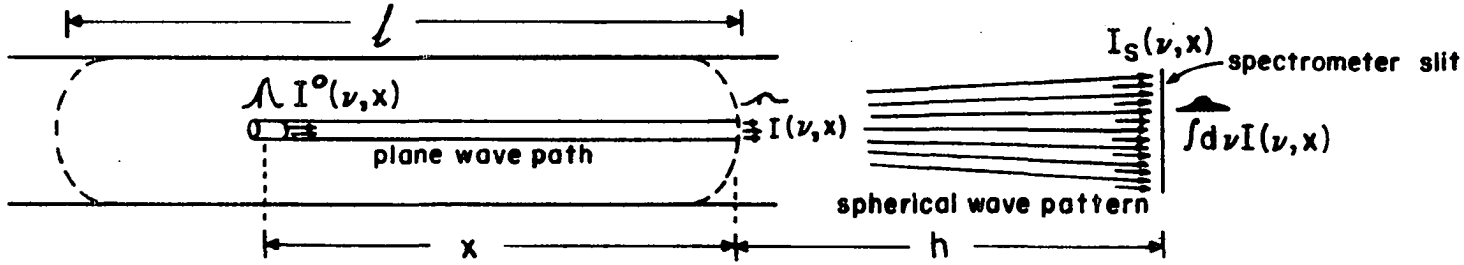

Figure 12. Radiation paths through the plasma

through the plasma. If $I(\nu, x)$ denotes the frequency distribution of the radiation transmitted through this path, then by Equation 4-25 we have that

$$(4\text{-}26) \qquad I_s(\nu, x) = I^\circ(\nu, x) \exp\left[-\bar{k}(\nu, x)x\right],$$

wherein the notation $I_s(\nu, x)$ signifies the intensity incident upon the spectrometer slit.

In actuality, however, $I^\circ(\nu, x)$ is emitted from the microelement as spherical waves, hence the intensity incident upon the slit from it decreases with increasing x according to the inverse square law. Hence $I(\nu, x)$ incident upon the slit is given by

$$(4\text{-}27) \qquad I_s(\nu, x) \sim \frac{I^\circ(\nu, x)}{(x+h)^2} \exp\left[-\bar{k}(\nu, x)x\right].$$

Now, it is not the intensity incident upon the slit which counts, but rather the intensity incident upon the photocathode of the PM tube. Not all of the radiation which passes through the slit reaches the photocathode and, what is of greater importance, the fraction of that radiation passing the slit which reaches the photocathode is dependent upon the position of the microelement in the discharge plasma. This may be seen by reference to Figures 13 and 14. To account for this, we may define a function g(x+h) such that

$$(4\text{-}28) \qquad g(x+h) \equiv \frac{I_p(\nu, x)}{I_s(\nu, x)}$$

wherein $I_p(\nu, x)$ is the intensity reaching the photocathode from the

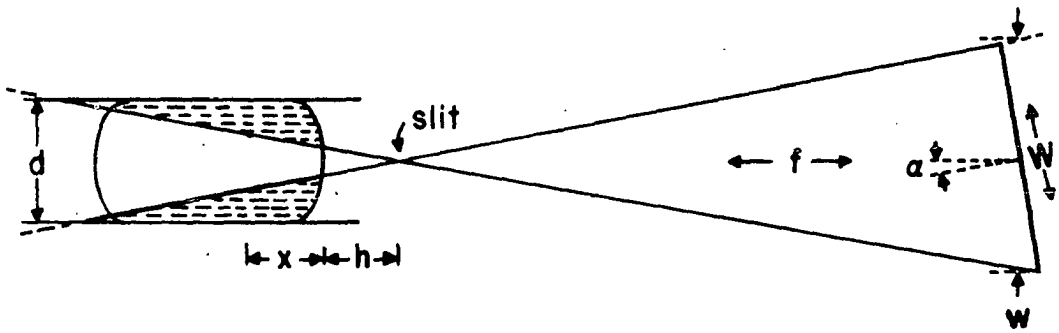

Figure 13. Light paths in the horizontal plane

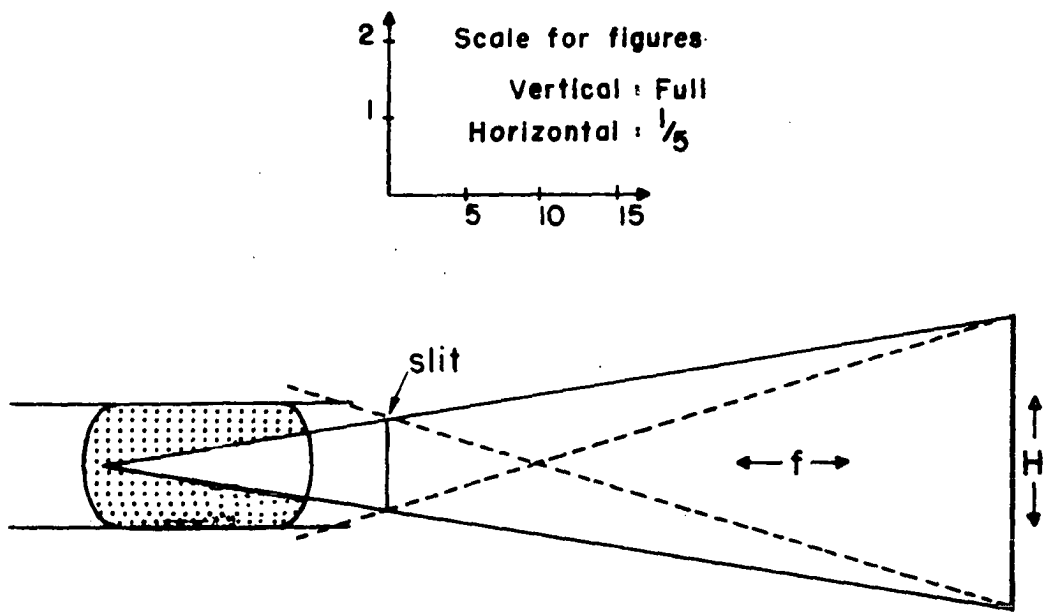

Figure 14. Light paths in the vertical plane

microelement at x, and $I_s(\nu, x)$ is the intensity passing the slit from the microelement at x. Taking this geometry factor into account, Equation 4-27 becomes

$$(4\text{-}29) \qquad I_p(\nu, x) \sim I^\circ(\nu, x) \frac{g(x+h)}{(x+h)^2} \exp\left[-\bar{k}(\nu, x)x\right].$$

It will prove convenient, now, to further define a function G(x+h) such that

$$(4\text{-}30) \qquad G(x+h) \equiv C \frac{g(x+h)}{(x+h)^2}, \qquad C = \text{constant}.$$

Why this should be done will become clear in a subsequent section wherein the quantity G(x+h) will be evaluated. The G, by the way, stands for Geometry since it arises only from the geometry of the source and spectrometer and contains no explicit ν-dependence. Incorporation of Equation 4-30 into Equation 4-29 yields

$$(4\text{-}31) \qquad I_p(\nu, x) = I^\circ(\nu, x)\, G(x+h) \exp\left[-\bar{k}(\nu, x)x\right].$$

An implicit assumption was made in the statement of Equation 4-27, and therefore also exists in the statement of Equation 4-31. The radiation path through the plasma is equal to x only for the co-axial path from the on-axis plasma element to the slit center. If z(x, s) is the path length in the plasma for a ray from the element at x to any point s on the slit length, as shown in Figure 24, then x should properly be replaced in the exponent by $z(x, \bar{s})$, which denotes the average value of z(x, s). Furthermore, since $k(\nu)$ also depends upon the specific radiation path,

it follows that $\bar{k}(\nu, x)$ should be replaced by $\bar{k}(\nu, x, \bar{s})$, whereupon Equation 4-31 becomes

$$(4\text{-}32) \qquad I_p(\nu, x) = I^\circ(\nu, x)\, G(x+h) \exp\left[-\bar{k}(\nu, x, \bar{s})\, z(x, \bar{s})\right].$$

So far, Equation 4-32 has been derived only for on-axis microelements. It may be generalized to include off-axis elements in the following way. Let cylindrical coordinates be used to describe the plasma geometry, as in Appendix A. Then the intensity of radiation per unit frequency interval arising from a plasma element at any point (x, r, θ) in the source may be denoted $I^\circ(\nu, x, r, \theta)$. Correspondingly, the intensity from the element as seen by the photocathode is $I_p(\nu, x, r, \theta)$. With this notation Equation 4-32 becomes

$$(4\text{-}33) \qquad I_p(\nu, x, r, \theta) = I^\circ(\nu, x, r, \theta)\, G(x+h, r, \theta) \exp\left[-\bar{k}(\nu, x, r, \theta, \bar{s})\, z(x, r, \theta, \bar{s})\right].$$

The experimental quantity involved in this study is I_p, which is the intensity seen by the photocathode from the entire source for that fraction of the spectral line width which is subtended by the exit slit width of the spectrometer. If the spectrometer exit slit be wide with respect to the entrance slit width, then the photocathode sees the entire spectral line width coming from all portions of the discharge. Mathematically, then, the photocathode sees the ν-integrated, x-integrated, r-integrated, and θ-integrated intensity from all microelements of the plasma. Thus,

$$(4\text{-}34) \qquad I_p = \int d\nu \int dx \int r\,dr \int d\theta \; I_p(\nu, x, r, \theta)$$

which, from Equation 4-33 yields

$$(4\text{-}35) \qquad I_p = \int d\nu \int dx \int r dr \int d\theta \; I^\circ(\nu, x, r, \theta)\, G(x+h, r, \theta) \exp$$

$$[-\bar{k}\,(\nu, x, r, \theta, \bar{s})\; z\,(x, r, \theta, \bar{s})],$$

wherein I_p is the experimental intensity seen by the spectrometer. This is a perfectly general result involving no assumptions. It will yield an exact result.

Obviously, any attempt to evaluate Equation 4-35 as it stands is patently ridiculous. If we are not to give up and go home at this point, some simplifying assumptions will have to be made.

1. Assumption A -- uniformly excited source

The first and most sweeping assumption is that the plasma is uniformly excited. This requires that all quantities such as translational temperature, electronic temperature, electric field gradient, species concentration, etc., be the same throughout the source, i.e., independent of x, r, and θ. It does not require that these quantities be invariant with experimental parameters such as power input, discharge tube pressure, or identity of the matrix gas, nor does it require that thermal equilibrium exist. It simply assumes that whatever non-equilibrium discharge conditions the experimental parameters establish at one point in the plasma they also establish at every other point in the plasma.

Edels (8) has shown that an error of less than five percent is intro-

duced into the determination of the self-absorption of certain spectral lines of the high-pressure mercury arc if this arc is assumed to be a uniformly excited source. If this be true for a source with such large thermal gradients and spatial variations, the application of the uniform excitation approximation to the glow discharges used herein appears quite justifiable.

The effect of this assumption is to average the quantities $I^\circ(\nu, x, r, \theta)$ and $\bar{k}(\nu, x, r, \theta, \bar{s})$ throughout the source, since these are the quantities in Equation 4-35 which are dependent upon the discharge conditions within the plasma. It follows, then, that the metastable state concentrations resulting from this study will also be average values over the source. With this assumption Equation 4-35 may be rewritten

$$(4\text{-}36) \qquad I_p = \int d\nu \int dx \int r dr \int d\theta \; I^\circ(\nu)\, G(x+h, r, \theta) \exp \left[-k(\nu) z\,(x, r, \theta, \bar{s})\right].$$

2. Assumption B -- equidistance of the z(s)

The approximation will be made that $z(x, r, \theta, \bar{s}) = x$. The validity of this approximation is discussed in detail in Appendix A, wherein it is shown that the error introduced by making it is quite negligible. With this assumption, Equation 4-36 may be rewritten

$$(4\text{-}37) \qquad I_p = \int d\nu \int dx \int r dr \int d\theta \; I^\circ(\nu)\, G(x+h, r, \theta) \exp \left[-k(\nu)\, x\right].$$

The terms $I^\circ(\nu)$ and $\exp[-k(\nu)x]$ possess no r, θ-dependence so they may be moved through these integral signs to yield

$$(4\text{-}38) \qquad I_p = \int d\nu \int dx \; I^\circ(\nu) \exp[-k(\nu)x] \int r\,dr \int d\theta \; G(x+h, r, \theta).$$

The evaluation of the r, θ integral will be pursued in a subsequent section. In the meantime, we shall carry this quantity along by making, for typographical convenience, the identification

$$(4\text{-}39) \qquad \Gamma \equiv \int r\,dr \int d\theta \; G(x+h, r, \theta),$$

whereupon Equation 4-38 becomes

$$(4\text{-}40) \qquad I_p = \int d\nu \int dx \; I^\circ(\nu)\, \Gamma \exp[-k(\nu)\,x].$$

This equation is amenable to integration.

C. Integration over the Variable ν

Equation 4-40 involves integration over the variables ν and x. Since these variables are independent, the order of integration is immaterial. It is expedient to integrate first over the variable ν.

Reversing the order of integration yields

$$(4\text{-}41) \qquad I_p = \int dx \; \Gamma \int d\nu \, I^\circ(\nu) \exp[-k(\nu)x].$$

It is seen from Figure 11 that $I^\circ(\nu)$ is related to the shape of the spectral line. Various line broadening processes occur in a discharge plasma which may influence the spectral line profile emitted from a microelement, but none of them affect the total intensity of emitted radiation. Put another way, the area under the spectral line profile is a constant independent of the line broadening processes occurring. It is natural, then, to define a function $P_e(\nu)$ such that

$$(4\text{-}42) \qquad P_e(\nu) \equiv \frac{I^\circ(\nu)}{I^\circ}$$

where I° is the total ν-integrated intensity of the spectral line emitted from a microelement. Thus, $P_e(\nu)$ has the physical significance of being the fraction of the total spectral line intensity which exists in the frequency interval $d\nu$. I° is, of course, not a function of ν, which permits it to be removed from under the ν-integral when inserted into Equation 4-41. Hence,

$$(4\text{-}43) \qquad I_p = \int dx \; I^\circ \; \Gamma \int d\nu \; P_e(\nu) \exp[-k(\nu)x].$$

From Equation 4-22 we have that $k(\nu) = k^\circ P_a(\nu)$, from which there results

$$(4\text{-}44) \qquad I_p = \int dx\, I^\circ\ \Gamma \int d\nu\ P_e(\nu) \exp\,[-k^\circ \times P_a(\nu)].$$

$P_e(\nu)$ describes the shape of the emission line profile, and $P_a(\nu)$ describes the shape of the absorption line profile. But by Kirchhoff's law,

$$(4\text{-}45) \qquad P_e(\nu) = P_a(\nu) \equiv P(\nu)$$

whereupon Equation 4-44 becomes

$$(4\text{-}46) \qquad I_p = \int dx\, I^\circ\ \Gamma \int d\nu\ P(\nu) \exp\,[-k^\circ \times P(\nu)].$$

Upon identifying the function $P(\nu)$, Equation 4-46 may be integrated over ν.

1. $P(\nu)$ as a description of Doppler broadening

The shape of a spectral line is influenced, in general, by five line broadening processes (6):

(1) Natural broadening due to the finite lifetimes of the atomic states.

(2) Doppler broadening due to the motion of the atoms relative to the spectrometer.

(3) Pressure broadening, which may be resolved into two types:

   (a) Lorentz broadening due to collisions with foreign gas atoms or molecules.

   (b) Holtsmark broadening due to collisions with other atoms of the

same species in the same excited state.

(4) Stark broadening due to collisions with electrons and ions.

We shall now proceed to make Assumption C -- that Natural, Lorentz, Holtsmark, and Stark broadening are negligible by comparison with Doppler broadening for the species in question under the experimental conditions of this study. This assumption is discussed in Appendix B. Although, as it happens, this assumption is quite justifiable here, a sizable amount of error can actually be tolerated from this source since in subsequent treatment line broadening effects will be cancelled out.

For Doppler broadening, $P(\nu)$ is given (5) in the form

$$(4\text{-}47) \qquad P(\nu-\nu_o) = \frac{2}{\Delta\nu}\left(\frac{\ln 2}{\pi}\right)^{1/2} \exp$$

$$\left\{-\left[\frac{2(\nu-\nu_o)}{\Delta\nu}\sqrt{\ln 2}\right]^2\right\}$$

wherein $\Delta\nu$ is the Doppler half-width--line width at half-height, and ν_o is the line center -- that ν corresponding to maximum $I(\nu)$. Considerable simplification of Equation 4-47 may be effected by defining a quantity ω such that

$$(4\text{-}48) \qquad \omega = \frac{2(\nu-\nu_o)}{\Delta\nu}\sqrt{\ln 2}$$

from which it follows that

$$(4\text{-}49) \qquad d\omega = \frac{2\sqrt{\ln 2}}{\Delta\nu}\, d(\nu-\nu_o).$$

Effecting a change of variable in Equation 4-46 from ν to $(\nu-\nu_o)$ permits the accomodation of Equation 4-47, whereupon a second change of variable from $(\nu-\nu_o)$ to ω permits the accomodation of Equations 4-48 and 4-49. The end result is

$$(4\text{-}50) \qquad I_p = \int dx\, I^\circ\ \Gamma \frac{1}{\sqrt{\pi}} \int_{-\infty}^{\infty} \exp\left[-\omega^2\right] \exp$$

$$\left\{ - \frac{2k^\circ x}{\Delta\nu} \left(\frac{\ln 2}{\pi}\right)^{1/2} \exp\left[-\omega^2\right] \right\} d\omega.$$

Making the identification

$$(4\text{-}51) \qquad \kappa = \frac{2k^\circ x}{\Delta\nu} \left(\frac{\ln 2}{\pi}\right)^{1/2}$$

we have that

$$(4\text{-}52) \qquad I_p = \int dx\, I^\circ\ \Gamma \frac{1}{\sqrt{\pi}} \int_{-\infty}^{\infty} e^{-\omega^2} \exp\left[-\kappa e^{-\omega^2} \right] d\omega.$$

D. The Turning Point--The Path to Ratios

At this point, a decision must be made on which of two possible paths to select for further development. The first path leads ultimately to the determination of absolute concentrations of the atomic nitrogen metastable states, but for reasons to become apparent later the uncertanties in these numbers will probably be large. This path requires that the ν-integral of Equation 4-52 be numerically evaluated by a

digital computer.

The second path leads ultimately to the ratio of the metastable state concentrations and, in principle at least, to the metastable/ground state ratios. These ratios will possess significantly greater accuracy since many errors will cancel. Choice of this second path would not require the evaluation of the ν-integral. This second path is more direct and precise, so it shall be pursued at this time. The former path will be discussed in a subsequent section.

1. Extraction of the absorption coefficient from the ν-integral

From Equation 4-21 it is seen that k° contains N -- the absorber concentration. In Equation 4-52, k° is buried within the ν-integral in the quantity κ. Since the ultimate goal is to solve for k° in terms of experimental quantities, it is obvious that k° must be extracted from the ν-integral in a tractable form. It would be most desirable to do this without evaluating the integral. Let us then investigate its form. Consider the quantity

$$(4\text{-}53) \qquad \frac{1}{\sqrt{\pi}} \int_{-\infty}^{\infty} e^{-\omega^2} \exp\left[-\kappa e^{-\omega^2}\right] d\omega.$$

It is interesting to note that the quantity 4-53 may be written as

$$(4\text{-}54) \qquad \frac{\int_{-\infty}^{\infty} e^{-\omega^2} \exp\left[-\kappa e^{-\omega^2}\right] d\omega}{\int_{-\infty}^{\infty} e^{-\omega^2} d\omega.}$$

since the value of the integral in the denominator = $\sqrt{\pi}$. The quantity 4-54 is suggestive of the expectation value procedure. In this context, it is pertinent that the Doppler line profile follows the Gaussian distribution, which latter is given (9) by

$$(4\text{-}55) \qquad f(x) = \frac{1}{\sigma\sqrt{2\pi}} \exp\left[-\left(\frac{x-\mu}{\sigma\sqrt{2}}\right)^2\right],$$

where f(x) is the probability density function for the Gaussian distribution. For Doppler broadening $P(\nu-\nu_o)$ was given by Equation 4-47, which is seen to correspond precisely to f(x) if

$$(4\text{-}56) \qquad \mu=0, \quad \sigma=\frac{\Delta\nu}{2\sqrt{2}\ln 2}, \quad x=\nu-\nu_o.$$

The expectation value of a function g(x) which is governed by the Gaussian distribution law is given by

$$(4\text{-}57) \qquad \langle g^n(x)\rangle = \frac{\int_{-\infty}^{\infty} g^n(x)\, f(x)\, dx}{\int_{-\infty}^{\infty} f(x)\, dx}.$$

Making the transformation of variable specified in Equation 4-48 we have that

$$(4\text{-}58) \qquad P(\omega)\, d\omega = \frac{1}{\sqrt{\pi}} \exp\left[-\omega^2\right]$$

which corresponds to f(x) dx in Equation 4-57.

To see more clearly, now, the correspondence between Equations 4-57 and 4-54, let there be defined a quantity $a(\omega)$ such that

$$(4\text{-}59) \qquad a(\omega) = \exp\left[-\omega^2\right]$$

whereupon Equation 4-54 becomes

$$(4\text{-}60) \qquad \frac{\int_{-\infty}^{\infty} e^{-\kappa a(\omega)} a(\omega)\, d\omega}{\int_{-\infty}^{\infty} a(\omega)\, d\omega} = \frac{\int_{-\infty}^{\infty} \left[e^{-a(\omega)}\right]^{\kappa} a(\omega)\, d\omega.}{\int_{-\infty}^{\infty} a(\omega)\, d\omega}$$

Comparison of the right hand side of Equation 4-60 with Equation 4-57 shows that

$$(4\text{-}61) \qquad e^{-a(\omega)} \rightarrow g(x), \qquad \kappa \rightarrow n, \qquad a(\omega)\, d\omega \rightarrow f(x)\, dx.$$

Thus, since $f(x)\, dx = a(\omega)\, d\omega$, and since $g^n(x)$ can be <u>any</u> function of x, it follows that Equation 4-60 must possess a solution of the form $\langle [e^{-a(\omega)}]^{\kappa} \rangle$ since Equation 4-57 does.

Now, $\langle [e^{-a(\omega)}]^{\kappa} \rangle$ is a number. If the κth root of this number be taken, one obtains another number which is related to the first. We may express this relation by defining a number $e^{-f(a)}$ such that

$$(4\text{-}62) \qquad e^{-f(a)} = \left\{ \langle [e^{-a(\omega)}]^{\kappa} \rangle \right\}^{1/\kappa}$$

wherein $f(a)$ may be any function of a. If this number be then raised to the κth power, it follows that

$$(4\text{-}63) \qquad e^{-\kappa f(a)} = \langle [e^{-a(\omega)}]^{\kappa} \rangle .$$

For the sake of consistency, we note that since a is a function of ω, f(a) is also a function of ω, albeit a different function, so that it is proper to write

$$(4\text{-}64) \qquad e^{-\kappa f(a)} = e^{-\kappa F(\omega)} .$$

Thus the result has been established that

$$(4\text{-}65) \qquad \frac{1}{\sqrt{\pi}} \int_{-\infty}^{\infty} e^{-\omega^2} \exp\left[-\kappa e^{-\omega^2}\right] d\omega = e^{-\kappa F(\omega)} .$$

The crucial observation may now be made that, in Equation 4-57, the n on the right hand side is identical with the n on the left hand side; consequently, in Equation 4-65 it is likewise true that the κ within the integral is identical with the κ in the solution. Hence, κ has been extracted from the integral without explicit solution of the integral.

Insertion of Equation 4-65 into Equation 4-52 yields that

$$(4\text{-}66) \qquad I_p = \int dx\, I^{\circ}\, \Gamma \exp\left[-\kappa F(\omega)\right] .$$

2. Disposition and physical significance of F(ω)

The value of $F(\omega)$ is, of course, not known since the ν-integral was not explicitly evaluated. This is inconsequential since ultimately a concentration ratio will be formed whereupon $F(\omega)$ will cancel out. In

line with this, it may be noted that any errors introduced by the assumption that only Doppler broadening is significant will also cancel out in this process.

The physical significance of $F(\omega)$ may be deduced with the help of Figure 15. We observe from Equation 4-48 that

$\omega = 1$ when $2(\nu-\nu_o) = \Delta\nu/\sqrt{\ln 2} = 1.20\ \Delta\nu$,

$\omega = 2$ when $2(\nu-\nu_o) = 2\Delta\nu/\sqrt{\ln 2} = 2.40\ \Delta\nu$, etc.

Thus, when the line broadening is such that the spectrometer exit slit jaws subtend a line width equal to $1.20\ \Delta\nu$, $\omega = 1$. As the line broadening decreases, the same exit slit width will subtend a greater fraction of line width, whence ω increases.

As the spectrometer entrance slit width is increased, the spectral line undergoes positive magnification. For the same exit slit width, then, ω decreases whence $F(\omega)$ changes also. Thus it is seen that $F(\omega)$ is related not only to the variation in line broadening as spectral source conditions are changed, but that it is also related to the spectrometer exit/entrance slit width ratio. Since the functional dependency of the latter effect is insensitive to the frequency of the line viewed, the ultimate formation of a concentration ratio will cancel not only line broadening effects arising in the source, but spectrometer slit width effects as well.

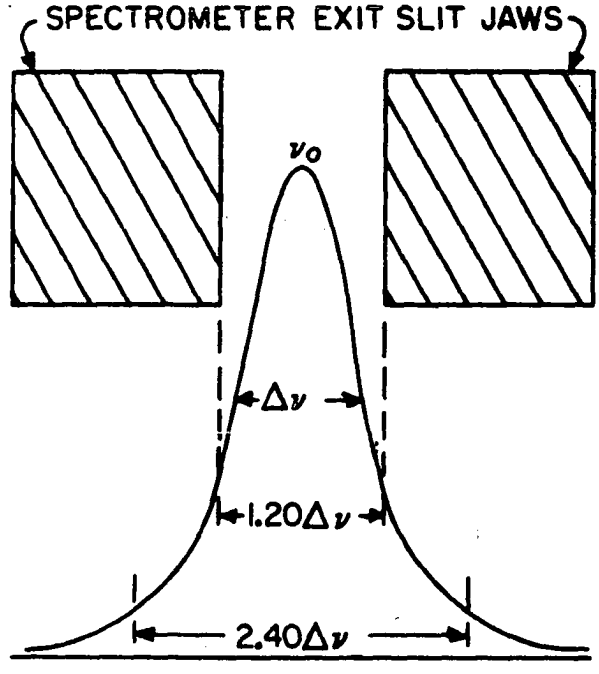

Figure 15. Physical significance of ω

E. Solution of the x-Integral

Equation 4-66 may be written in the form

$$(4\text{-}67) \qquad I_p = I^\circ \int_0^{\ell} \Gamma \exp\left[-\kappa F(\omega)\right] dx$$

by noting that $I^\circ \neq I^\circ(x)$ because of Assumption A--that the source is uniformly excited. From Equation 4-51, the defining equation for κ, we have that

$$(4\text{-}51) \qquad \kappa \equiv \frac{2k^\circ x}{\Delta\nu} \left(\frac{\ln 2}{\pi}\right)^{1/2}$$

For typographical expediency, a quantity K will be defined by

$$(4\text{-}68) \qquad K \equiv \frac{2k^\circ}{\Delta\nu} \left(\frac{\ln 2}{\pi}\right)^{1/2} F(\omega),$$

whereupon Equation 4-67 becomes

$$(4\text{-}69) \qquad I_p = I^\circ \int_0^{\ell} \Gamma \exp\left[-Kx\right] dx.$$

Following the investigation of Γ, Equation 4-69 will be integrated.

1. Elucidation of the geometry function

In Section IVB mention was made of the fact that account must be taken of light losses in the spectrometer, since the magnitude of these losses varies with position in the source. A function $G(x+h, r, \theta)$ was

defined to accomplish this. The physical necessity for this function becomes clear upon reinspection of Figures 13 and 14. The light paths in the horizontal plane are diagrammed in Figure 13, from which it is seen that microelements of the discharge occupying the hatched region contribute no intensity to the photocathode since their radiation falls off the collimating aperture. The limiting rays in the vertical plane are shown in Figure 14, which demonstrates that a large penumbra region exists. The figures are drawn to the scales shown; the slit is sealed with a plane window or left unsealed.

It is obvious that the light gathering power of the spectrometer is not constant throughout the discharge volume, and it is thus seen that $G(x+h, r, \theta)$ is actually a weighting function for the radiation emitted from any point $(x+h, r, \theta)$.

An attempt was made to calculate $G(x+H, r, \theta)$ from geometrical considerations, but it proved impractical since the occultation functions are defined for regions with variable bounds -- the bounds being functions of x+h. A better plan suggested itself, viz., to evaluate $G(x+h, r, \theta)$ empirically. The physical basis for this is the following:

(1) For a non-absorbed line, K=0 since $k^\circ = 0$, which follows from Equation 4-21 since N = 0. Hence, for a non-absorbed (na) line, Equation 4-69 becomes

$$(4\text{-}70) \qquad I_p{}^{na} = I^\circ{}_{na} \int_0^{\ell} \Gamma \, dx.$$

(2) From Figure 6 it is seen that the microwave cavity can be moved along the discharge tube axis and, as might be expected, the plasma within the tube moves with the cavity.

(3) Moving the discharge closer-to or farther-from the spectrometer slit does in no way whatever change the nature of the discharge, since the latter is quite independent of its position in the universe. Hence, I°_{na} is invariant with respect to translation of the source.

(4) $G(x+h, r, \theta)$ is a geometrical property of the point $(x+h, r, \theta)$ in space, and exists whether a plasma element envelopes this point or not.

Therefore, from Equation 4-70, if the variation in I_p^{na} be measured as a function of distance of the discharge from the slit, then since I°_{na} is a constant, the variation in $\int \Gamma \, dx$ with distance from the slit can be measured. From this it should be possible to deduce Γ. We shall now look at this procedure mathematically.

The quantity Γ is defined by

$$\Gamma \equiv \int r dr \int d\theta \; G(x+h, r, \theta). \tag{4-39}$$

We shall immediately remove the r, θ dependency by invoking Assumption B, whereupon

$$G(x+h, r, \theta) = G(x+h) \tag{4-71}$$

and Equation 4-39 thus becomes

(4-72) $\Gamma = AG(x+h)$

wherein A is the cross-sectional area of the discharge. Thus, Equation 4-70 becomes

$$(4\text{-}73) \qquad I_p^{na} = AI^{\circ}_{na} \int_0^{\ell} G(x+h)\, dx.$$

It is convenient to make the integral homogeneous in the variable x+h, to which end we shall define a quantity y such that

(4-74) $y = x+h$

whereupon Equation 4-73 becomes

$$(4\text{-}75) \qquad I_p^{na} = AI^{\circ}_{na} \int_h^{h+\ell} G(y)\, dy.$$

The physical picture of this state of affairs is presented in Figure 16. I_p^{na} is the experimental intensity of the plasma occupying the region $h \rightarrow h+\ell$, A is the cross-sectional area of a laminus of plasma of thickness dy, y is the position of this laminus which has the weighting function G(y), I°_{na} is the intensity of a non-absorbed line emitted from a microelement in the laminus, ℓ is the length of the discharge, and a is an arbitrary -- but fixed--distance from the slit. For clarity in what is to follow, let I_p^{na} be denoted I(h, $h+\ell$) to signify that it is the intensity of the plasma existing in the spatial region between h and $h+\ell$.

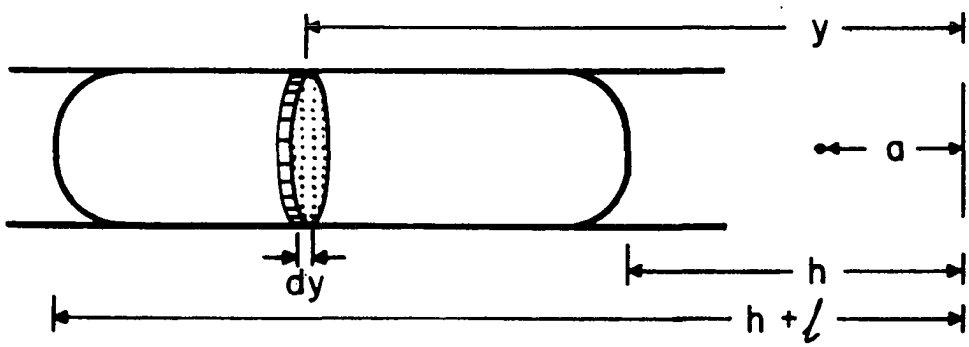

Figure 16. The plasma laminus described by G(y)

Let there now be selected some fixed point a along y such that $0<a<h$. Then, since I is a real number and real numbers are associative, it is true that

(4-76) $I(h,\ h+\ell) = I(a,\ h+\ell) - I(a,\ h).$

Furthermore, it is a property of integrals that

$$(4\text{-}77) \qquad \int_{h}^{h+\ell} G(y)\ dy = \int_{a}^{h+\ell} G(y)\ dy - \int_{a}^{h} G(y)\ dy.$$

Hence, it follows that

$$(4\text{-}78) \qquad I(a,\ h+\ell) = AI^{\circ} \int_{a}^{h+\ell} G(y)\ dy,$$

$$(4\text{-}79) \qquad I(a, h) = AI^{\circ} \int_{a}^{h} G(y)\ dy.$$

From a theorem of the calculus regarding variable limits of integration (10), we have the statement

(4-80) If $F(a, x) = \int_{a}^{x} f(t)\ dt$, f(t) continuous for all t in

$[a, x]$, then $\frac{dF}{dx} = f(x)$.

Identification of the corresponding quantities in Equations 4-78 and 4-79 with Equation 4-80 leads to

$$(4\text{-}81) \qquad \frac{dI(a,\ h+\ell)}{d(h+\ell)} = AI^{\circ}\ G(h+\ell),$$

$$(4\text{-}82) \qquad \frac{dI(a,\ h)}{dh} = AI^{\circ}\ G(h).$$

In order to combine these latter two equations, it is necessary that the variables of differentiation be made uniform. To do this, we note that if all experimental parameters be held constant save that the discharge be moved down the tube to vary h, then ℓ will be a constant. Hence, since

$$(4\text{-}83) \qquad \frac{d}{dh} = \frac{d}{d(h+\ell)} \cdot \frac{d(h+\ell)}{dh}$$

and since

$$(4\text{-}84) \qquad \frac{d(h+\ell)}{dh} = \frac{dh}{dh} + \frac{d\ell}{dh} = 1 + 0 = 1,$$

then

$$(4\text{-}85) \qquad \frac{dI(a,\ h+\ell)}{d(h+\ell)} = \frac{dI(a,\ h+\ell)}{dh}.$$

Thus, subtracting Equation 4-82 from Equation 4-81 yields, in view of Equation 4-85,

$$(4\text{-}86) \qquad \frac{d}{dh}\ [I(a,\ h+\ell) - I(a,\ h)] = AI^{\circ}\ [G(h+\ell) - G(h)].$$

But by Equation 4-76, Equation 4-86 becomes

$$(4\text{-}87) \qquad \frac{dI(h,\, h+\ell)}{dh} = AI^{\circ}\ [G(h+\ell) - G(h)].$$

Furthermore, since $[G(h+\ell) - G(h)] = [G(y)]_{h}^{h+\ell}$, we have that

$$(4\text{-}88) \qquad \frac{dI(h+\ell)}{dh} = AI^{\circ}\ [G(y)]_{h}^{h+\ell}.$$

Now, I° is an arbitrary constant with respect to the determination of G(y), since G(y) is a function of geometry only and is independent of the intensity of the non-absorbed line by which we choose to measure it. Furthermore, $I(h, h+\ell)$, h, ℓ, and A are experimental quantities. Hence, since Equation 4-88 is an equation containing one unknown, it is in principle possible to determine G(y).

2. Experimental evaluation of $AI^{\circ}G(y)$

Three studies have been made on the variation of experimental line intensities with h. Two of them used the non-absorbed lines He 4026 and He 4121; the other used the N 1743, 5 Å doublet which is, of course, self-absorbed. The details of these studies are discussed in Appendix C, wherein it is shown that for all three wavelengths the spectral line intensity varies linearly with h within experimental error. This totally unexpected result both suggests and justifies Assumption D--that for all spectral lines used in this study.

$$(4\text{-}89) \qquad I_{p}^{na} = mh+b.$$

From Equation 4-88, after taking the indicated derivative, we have that

$$(4\text{-}90) \qquad AI^{\circ}\,[G(y)]_{h}^{h+\ell} = m.$$

The only function for G(y) capable of satisfying Equation 4-90 is

$$(4\text{-}91) \qquad G(y) = \mu y + \beta,$$

i.e., a straight line. From Figure 17 it follows that

$$(4\text{-}92) \qquad \mu = \frac{m}{AI^{\circ}\ell},$$

whence

$$(4\text{-}93) \qquad G(y) = \frac{my}{AI^{\circ}\ell} + \beta.$$

The quantity β may be evaluated via Equations 4-75 and 4-89, since these establish that

$$(4\text{-}94) \qquad AI^{\circ} \int_{h}^{h+\ell} G(y)\,dy = AI^{\circ} \int_{h}^{h+\ell} \left(\frac{my}{AI^{\circ}\ell} + \beta\right) = mh+b.$$

Performing the indicated integration and equating the coefficients of corresponding powers of h provides the result

$$(4\text{-}95) \qquad AI^{\circ}\beta = \frac{b}{\ell} - \frac{m}{2}.$$

Thus, Equation 4-93 yields that

$$(4\text{-}96) \qquad AI^{\circ}G(y) = \frac{my}{\ell} + \frac{b}{\ell} - \frac{m}{2}.$$

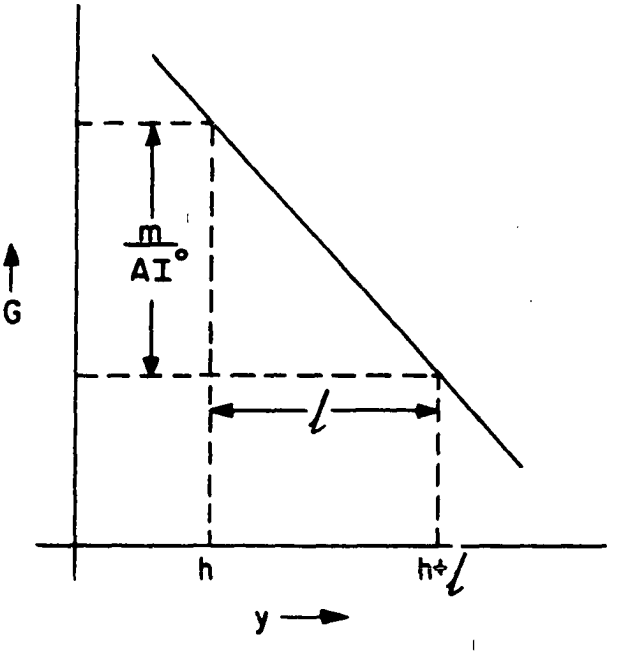

Figure 17. The slope of G(y)

3. The final x-integration

The equation for the total integrated intensity of a self-absorbed spectral line as measured by the spectrometer used in this study may now be obtained. From Equations 4-69 and 4-72 we have that

$$(4\text{-}97) \qquad I_p = \int_0^{\ell} AI^\circ G(x+h) \exp[-Kx]\, dx$$

which becomes, under the variable transformation y = x+h previously defined,

$$(4\text{-}98) \qquad I_p = \exp[Kh] \int_h^{h+\ell} AI^\circ G(y) \exp[-Ky]\, dy.$$

Inserting Equation 4-96 yields the result that

$$(4\text{-}99) \qquad I_p = \exp[Kh] \int_h^{h+\ell} \left(\frac{my}{\ell} + \frac{b}{\ell} - \frac{m}{2}\right) \exp[-Ky]\, dy.$$

Straight-forward integration produces the result

$$(4\text{-}100) \qquad I_p = \frac{1-\exp[-K\ell]}{K\ell}\left(mh + \frac{m}{K} + b - \frac{m\ell}{2}\right) - m\ell\, \frac{e^{-K\ell}}{K\ell}$$

From Equation 4-89 we note that $mh+b = I_p^{na}$. Consequently,

$$(4\text{-}101) \qquad I_p = \frac{1-\exp[-K\ell]}{K\ell}\left\{ I_p^{na} + \frac{m}{K} - \frac{m\ell}{2}\right\} - \frac{m\ell \exp[-K\ell]}{K\ell},$$

which may be rearranged to yield

$$(4\text{-}102) \qquad I = \frac{1-\exp[-K\ell]}{K\ell}\left\{I(0)+\frac{m\ell}{K\ell}-\frac{m\ell}{2}\coth\frac{K\ell}{2}\right\}.$$

A slight change in notation has been introduced in Equation 4-102. From this point on, the only intensity discussed will be I_p, hence the subscript p has been dropped. Furthermore, since I is really I(K), it follows that $I_p^{na} = I_p(K=0) \equiv I(0)$. Hence, I is the experimental self-absorbed intensity read by the spectrometer, and I(0) is the intensity the line would have had were it not self-absorbed.

It will prove convenient to define a quantity δ such that

$$(4\text{-}103) \qquad \delta = m\ell/I(0),$$

whereupon Equation 4-102 becomes

$$(4\text{-}104) \qquad I = I(0)\,\frac{1-\exp[-K\ell]}{K\ell}\left\{1+\frac{\delta}{K\ell}-\frac{\delta}{2}\coth\frac{K\ell}{2}\right\}.$$

If Equation 4-104 be correct, then it must reduce to I = I(0) when K=0, since this is the condition for a non-absorbed line. It must furthermore reduce to I = 0 when $K = \infty$, since the spectral line cannot escape from the plasma under this condition. It is shown in Appendix D that Equation 4-104 does possess these limiting behaviors.

V. THE DOUBLET RATIO EQUATION AND ABSORBER CONCENTRATIONS

Equation 4-104 holds for any spectral line emitted and observed by the specific source - spectrometer combination described herein. It therefore holds for each of the component lines of any resolved spectral multiplet. In the treatment fo follow we shall continue to use the notation of Table 2 introduced earlier. The doublet ratio equation may be formulated from Equation 4-104 to be

$$(5\text{-}1) \qquad R_{12} = R_{12}(0)\,\frac{K_2(1-\exp[-K_1\ell\,])}{K_1(1-\exp[-K_2\ell\,])}\left\{\frac{1+(\delta_1/K_1\ell)-(\delta_1/2)\coth(K_1\ell/2)}{1+(\delta_2/K_2\ell)-(\delta_2/2)\coth(K_2\ell/2)}\right\}.$$

There are four unknown quantities in Equation 5-1, viz., K_1, K_2, $I_1(0)$, and $I_2(0)$. One equation containing four unknowns cannot be solved; three additional independent equations are needed. If the spectral lines are components of the same multiplet, independent relations amongst these unknowns become available provided the following condition is fulfilled.

A. The Assumption of Thermal J-population

Prior to this point, it has not been necessary to make any assumptions concerning the existence of thermal equilibrium in the source. It now becomes necessary to make Assumption E--that thermal J-population exists amongst the nitrogen atomic states. Consider the $3s\ ^2P$ state shown in Figure 9. Thermal J-population requires that the relative populations of the J = 3/2 and J = 1/2 levels be that given by the Maxwell-Boltzmann distribution. This is stated mathematically in

Equation 3-2. Assumption E requires also that the same be true for the J-levels of all other nitrogen states, and the 2p $^2P^\circ$ and 2p $^2D^\circ$ states in particular. Thus thermal J-population requires that an intra-state thermal equilibrium exists; it does not require or assume anything at all about the inter-state population distribution, which may be -- and probably is -- distinctly non-maxwellian. Hence, the assumption of thermal J-population does not require the assumption that the discharge plasma be in thermal equilibrium.

The subject of thermal equilibrium is discussed very briefly in Appendix E, but only insofar as it relates specifically to the validity of Assumption E. This discussion demonstrates only that Assumption E is not improbable. In actuality, however, physical evidence exists, and is presented below, attesting to the fact that Assumption E is highly probable.

B. Thermal J-population and $R_{12}^t(0)$

An evaluable relationship exists between two of the unknowns in Equation 5-1. The quantities $I_1(0)$ and $I_2(0)$ are neither known nor measurable for self-absorbed spectral lines since they are hypothetical quantities -- the intensities the self-absorbed lines would exhibit were they unabsorbed. This quandry is immediately circumvented if Assumption E is valid, for then $R_{12}(0)$ is given by the theoretical doublet ratio, denoted $R_{12}^t(0)$. The values of $R_{12}^t(0)$ and $R_{34}^t(0)$ are calculated in Appendix F; the value is 2.00 in both cases to an accuracy

which exceeds the experimental accuracy of the apparatus. Hence,

$$(5\text{-}2) \qquad R_{12}(0) = R^t_{12}(0) = 2.00, \qquad R_{34}(0) = R^t_{34}(0) = 2.00,$$

if Assumption E be valid.

Consider Figure 4, wherein it is seen that as the discharge tube pressure is reduced, R_{12} approaches the value 2.000. In fact, the experimental values for R_{12} at the pressures 0.35 and 0.20 torr were 1.999_2 and 1.998_8, respectively. What more need be said? Since

$$(5\text{-}3) \qquad \lim_{p \to 0} K = 0,$$

the R_{12} behavior of Figure 4 experimentally demonstrates that

$$(5\text{-}4) \qquad \lim_{K \to 0} R_{12} \equiv R_{12}(0) = 1.999 = R^t_{12}(0)$$

within experimental error, at pressures below 0.35 torr in an argon matrix. Now, it follows from the argument of Appendix E that the discharge approaches Maxwellian behavior as the pressure is increased. Thus, if thermal J-equilibrium exists at limiting low pressure where departure from Maxwellian behavior is maximal, it is reasonable to assume that thermal J-equilibrium will exist at higher pressures as well. Thus, the validity of Assumption E appears highly probable in the argon matrix, and justifies the assignments

$$(5\text{-}5) \qquad R_{12}(0) = R^t_{12}(0) = 2.00, \qquad R_{34}(0) = R^t_{34}(0) = 2.00,$$

for all pressures greater than 0.20 torr.

Unfortunately, the discharge in the helium matrix is not operable at sufficiently low pressure to determine the limiting low pressure behavior of R_{12} in it. It is seen from Figure 1, however, that the curve appears to be approaching the theoretical value of 2.00, and would probably reach it in the vicinity of 0.1 torr. On theoretical grounds, there is no reason to expect the behavior of nitrogen excitation in helium to be qualitatively different from that in argon. Thus the assignments of Equation 5-5 will be applied to the helium matrix also, but with cognizance of the fact that Assumption E is more of an assumption in the helium matrix than it is in the argon matrix.

C. The K_1, K_2 Relation for the Nitrogen Doublet Components

Another of the independent equations required to solve Equation 5-1 results from the fact that K_1 is related to K_2 when λ_1 and λ_2 are lines of the same multiplet. To derive this relationship, one must take into account the fact that λ_1 and λ_2 are composite lines.

From Figure 9 it is seen that λ_1 is composed of two transitions, λ_a and λ_b, and λ_2 is likewise composed of λ_c and λ_d. It is a known fact that if two spectral lines have coincident wavelengths, then the observed intensity of the composite line is the sum of the intensities of the individual lines. This can be proved by considering the indistinguishability of photons of the same energy, but it is so obvious that it is quite unnecessary to do so here. Hence, considering λ_1 as a particular example,

(5-6) $I_1 = I_a + I_b$.

It was shown in Equation 4-23 that

(4-23) $dI(\nu) = - k(\nu)\, I(\nu)\, dx$.

The relation of Equation 4-23 is true for any spectral line, hence it is true for the specific lines λ_a and λ_b, thus yielding

(5-7) $dI_a(\nu) = - k_a(\nu)\, I_a(\nu)\, dx$,

(5-8) $dI_b(\nu) = - k_b(\nu)\, I_b(\nu)\, dx$.

But Equation 4-23 is true also for the composite line λ_1, hence

(5-9) $dI_1(\nu) = - k_1(\nu)\, I_1(\nu)\, dx$.

The sum of Equations 5-7 and 5-8 yields

(5-10) $dI_a(\nu) + dI_b(\nu) = - [k_a(\nu)\, I_a(\nu) + k_b(\nu)\, I_b(\nu)]\, dx$.

But the left hand sides of Equations 5-9 and 5-10 are equal from Equation 5-6. Hence,

(5-11) $$k_1(\nu) = \frac{k_a(\nu)\, I_a(\nu)}{I_a(\nu)+I_b(\nu)} + \frac{k_b(\nu)\, I_b(\nu)}{I_a(\nu)+I_b(\nu)}.$$

We shall carry the fractions $I_a/(I_a+I_b)$ and $I_b/(I_a+I_b)$ along without comment. The $k(\nu)$ in Equation 5-11 are given by Equation 4-22 as $k^\circ\, P(\nu)$. Cancellation of the $P(\nu)$ function yields

(5-12) $$k^\circ_1 = \frac{k^\circ_a\, I_a}{I_a + I_b} + \frac{k^\circ_b\, I_b}{I_a + I_b}.$$

From Equation 4-21 we have that

$$(4\text{-}21) \qquad k^\circ = \frac{\lambda^2}{8\pi} \frac{g_u}{g_\ell} A_{u\ell} N_\ell .$$

To prevent notational difficulty arising from the u, ℓ subscripts, the following property of the Einstein spontaneous emission probability is recognized -- that all lines of the same multiplet possess the same A-value (4, p. 169). Thus, for the 3s $^2P \rightarrow$ 2p $^2P^\circ$ transition,

$$(5\text{-}13) \qquad A_a = A_b = A_c = A_d = A_1 = A_2 \equiv A_{12}$$

wherein the notation A_{12} indicates that transitions 1 and 2 both have the same A-value. Similarly, for the 3s $^2P \rightarrow$ 2p $^2D^\circ$ transitions,

$$(5\text{-}14) \qquad A_e = A_f = A_g = A_3 = A_4 \equiv A_{34}.$$

Taking formal note of the fact that $\lambda_a = \lambda_b = \lambda_1$, k_a° is given by Equation 4-21 as

$$(5\text{-}15) \qquad k_a^\circ = \frac{\lambda_1^2}{8\pi} A_{12} \frac{4}{4} [^2P^\circ_{3/2}],$$

wherein 4/4 is g_u/g_ℓ for transition a, and N_ℓ is seen from Figure 9 to be $[^2P^\circ_{3/2}]$ which, as noted previously, is to be read "the concentration of atoms in the $^2P^\circ_{3/2}$ state". Similarly,

$$(5\text{-}16) \qquad k_b^\circ = \frac{\lambda_1^2}{8\pi} A_{12} \frac{4}{2} [^2P^\circ_{1/2}]$$

Thus, Equation 5-12 becomes

$$(5\text{-}17) \qquad k_1^\circ = \frac{\lambda_1^2}{8\pi} A_{12}\left\{\frac{I_a}{I_a+I_b}\,[^2P^\circ_{3/2}] + \frac{2I_b}{I_a+I_b}\,[^2P^\circ_{1/2}]\right\}.$$

If thermal J-population exists, the J-level concentrations are related by Equation 3-2 such that

$$(5\text{-}18) \qquad [^2P^\circ_{3/2}]/[^2P^\circ_{1/2}] = g(3/2)\,/\,g(1/2) = 2,$$

and this relation is given with excellent accuracy since these levels are energy degenerate. Noting furthermore that

$$(5\text{-}19) \qquad [^2P^\circ] = [^2P^\circ_{3/2}] + [^2P^\circ_{1/2}]$$

wherein the left hand side is the total concentration of atoms in all J-levels of the $2p\ ^2P^\circ$ state, it follows that

$$(5\text{-}20) \qquad [^2P^\circ_{1/2}] = (1/3)\,[^2P^\circ]; \qquad [^2P^\circ_{3/2}] = (2/3)\,[^2P^\circ].$$

Thus, Equation 5-17 becomes

$$(5\text{-}21) \qquad k_1^\circ = \frac{\lambda_1^2}{8\pi} A_{12}\,[^2P^\circ]\left\{\frac{2}{3}\,\frac{I_a}{I_a+I_b} + \frac{1}{3}\,\frac{2I_b}{I_a+I_b}\right\},$$

which, upon factoring the 2/3 and noting that the sum of the fractions remaining is unity, becomes

$$(5\text{-}22a) \qquad k_1^\circ = \frac{2}{3} \frac{\lambda_1^2}{8\pi} A_{12} [^2P^\circ].$$

Repeating this process for the transitions $\lambda_2 = \lambda_c + \lambda_d$, $\lambda_3 = \lambda_e + \lambda_f$, and $\lambda_4 = \lambda_g$, one derives the results

$$(5\text{-}22b) \qquad k_2^\circ = \frac{1}{3} \frac{\lambda_2^2}{8\pi} A_{12} [^2P^\circ],$$

$$(5\text{-}22c) \qquad k_3^\circ = \frac{2}{5} \frac{\lambda_3^2}{8\pi} A_{34} [^2D^\circ]$$

$$(5\text{-}22d) \qquad k_4^\circ = \frac{1}{5} \frac{\lambda_4^2}{8\pi} A_{34} [^2D^\circ].$$

The quantity K was defined by Equation 4-68. Thus, for λ_1 and λ_2,

$$(5\text{-}23) \qquad K_1 = \frac{2k_1^\circ}{(\Delta\nu)_1} \left(\frac{\ln 2}{\pi}\right)^{1/2} [F(\omega)]_1, \quad K_2 = \frac{2k_2^\circ}{(\Delta\nu)_2} \left(\frac{\ln 2}{\pi}\right)^{1/2} [F(\omega)]_2,$$

whereupon K_1/K_2 is

$$(5\text{-}24) \qquad \frac{K_1}{K_2} = \frac{k_1^\circ}{k_2^\circ} \frac{(\Delta\nu)_2}{(\Delta\nu)_1} \frac{[F(\omega)]_1}{[F(\omega)]_2}.$$

Assuredly, line broadening effects will be the same for both lines of a spectral doublet, and hence the $\Delta\nu$ and $F(\omega)$ terms cancel. Hence, upon insertion of Equations 5-22a and 5-22b, one obtains the result

$$(5\text{-}25) \qquad \frac{K_1}{K_2} = 2 \frac{\lambda_1^2}{\lambda_2^2} = 1.994\,224 \equiv \alpha.$$

Similarly,

$$(5\text{-}26) \qquad \frac{K_3}{K_4} = 2\,\frac{\lambda_3^{\,2}}{\lambda_4^{\,2}} = 1.994\,788 \equiv \beta.$$

Thus it is seen that K_1/K_2 and K_3/K_4, defined α and β respectively, are quite accurately known quantities.

D. The Physical Significance and Magnitude of δ.

The quantity δ was defined by Equation 4-103 as

$$(4\text{-}103) \qquad \delta = m(0)\, \ell / I(0).$$

It is thus seen to be a dimensionless quantity which accounts for the spectrometer geometry through m(0), and for the physical characteristics of the plasma through ℓ and I(0). It possess the feature that the ratio $m(0)/I(0)$ is invariant with respect to I(0) at any given wavelength, which conclusion follows directly from Equation 4-89 since any change in I(0) must be accompanied by an identical change in m(0).

The magnitude of $m(0)/I(0)$ at λ 1743 Å would be directly calculable if a non-absorbed line existed in this wavelength region. Since as discussed in Appendix C, this is not the case, it is necessary to infer its value from the self-absorbed N 1743, 5 Å lines. This is accomplished in Appendix H, yielding the result

(5-27) $m(0)/I(0) = -0.02547 \pm 0.00153$ at $\lambda 1743,5$ Å.

This will be assumed to be the value at $\lambda 1493,5$ Å also. The error introduced by this assumption is quite small. In fact, from Equation 5-1 for $K_2\ell = 0.2860$, a 50% error in $\delta(1743,5)$ produces an error of only 0.15% in R_{12}.

E. Solution of the Doublet Ratio Equation for $K_2\ell$.

Sufficient relations and evaluations have now been established to permit Equation 5-1 to be solved for the quantity of interest, $K_2\ell$. From Equations 5-25 and 5-26 we have that

(5-28) $K_1\ell = \alpha K_2\ell, \qquad K_3\ell = \beta K_4\ell.$

From Equation 5-5 we have that

(5-5) $R_{12}(0) = R^t_{12}(0) = 2.00, \qquad R_{34}(0) = R^t_{34}(0) = 2.00$

assuming thermal J-population, and from Equation 5-27 we have that

(5-27) $m(0)/I(0) = -0.02547$

for both λ 1743,5 and λ 1493,5 Å. Hence Equation 5-1 may be re-written as

$$(5\text{-}29) \qquad R_{12} = \frac{R_{12}(0)}{\alpha}\,\frac{(1-\exp[-\alpha K_2\ell\,])}{(1-\exp[-K_2\ell\,])}\left\{\frac{1+(\delta/\alpha K_2\ell)-(\delta/2)\coth(\alpha K_2\ell/2)}{1+(\delta/K_2\ell)-(\delta/2)\coth(K_2\ell/2)}\right\}$$

wherein $K_2\ell$ is the only unknown. Obviously, it is necessary to solve for $K_2\ell$ by iteration.

The program written to accomplish this via an IBM 7074 computer is presented in Tables 4 and 5. To permit data for both the 1743, 5 and 1 493, 5 Å doublets to be processed at the same time, the values of α and β in Equation 5-28 were replaced by γ, their average. The error in R_{ij} introduced by this is 0.014%, which is insignificant.

A word concerning the use of the quantity $K_2\ell$ seems desirable. This is a more meaningful variable than is K_2 alone for the following reasons: (1) both K and ℓ are functions of pressure, and it is therefore logical to consider them together, (2) the product $K_2\ell$ can be determined with greater precision than can either K or ℓ alone, since ℓ is the least precise of the experimental measurables of this study, and (3) for the determination of concentration ratios, to be treated below, ℓ will be cancelled out anyway.

F. Extraction of the Metastable State Concentration Ratio

The iterative solution of Equation 5-29 provides experimental values of the quantities $K_2\ell$ and $K_4\ell$. From Equations 5-23 and 5-22b we observe that

$$(5\text{-}30) \qquad K_2\ell = \frac{2}{3}\,\frac{\lambda_2^{\,2}}{8\pi}\,\frac{[F(\omega)]_2}{[\Delta\nu]_2}\left(\frac{1n2}{\pi}\right)^{1/2}\ell\, A_{12}\,[^2P^\circ],$$

and similarly that

Table 4. Fortran program for iterative solution of the doublet ratio equation

Statement Number	Fortran Statement
1	READ 100, NUMCAR, ITMAX
2	READ 101, GAMMA, ROVGAM, EM, DELTA, EK2LS, DELS
3	PRINT 102
4	PRINT 103, GAMMA, ROVGAM, EM, DELTA, EK2LS, DELS
5	PRINT 104
6	DO 25 I=1, NUMCAR
7	ITNO=1
8	EK2L=EK2LS
9	DEL=DELS
10	READ 105, REX, EL
11	EK2L=EK2L-DEL
12	U=(1. 0-EXPF(-GAMMA*EK2L))/(1. 0-EXPF(-EK2L))
13	V=1. 0/(GAMMA*EK2L)-1. 0/(2. 0*TANHF(GAMMA*EK2L/2. 0))
14	W=1. 0/EK2L-1. 0/(2. 0*TANHF(EK2L/2. 0))
15	RCALC=ROVGAM*U*(1. 0+EM*EL*V)/(1. 0+EM*EL*W)
16	IF (ITNO-ITMAX) 17, 17, 27
17	ITNO=ITNO+1
18	IF (RCALC) 21, 19, 19
19	IF (ABSF(RCALC-REX)-DELTA) 24, 24, 20

Table 4. (Continued)

Statement Number	Fortran Statement
20	IF (RCALC-REX) 11, 24, 21
21	EK2L=EK2L+DEL
22	DEL=DEL/10. 0
23	GO TO 11
24	PRINT 106, REX, EK2L, RCALC, EL
25	CONTINUE
26	STOP 89
27	PRINT 107, ITMAX
28	GO TO 25
100	FORMAT (2I5)
101	FORMAT (6F10. 7)
102	FORMAT (11X46HSOLUTION OF THE DOUBLET RATIO EQUATION FOR K2L/19X30HGIVEN THE FOLLOWING PARAMETERS//)
103	FORMAT (7X6HGAMMA=F10. 7, 4X7HROVGAM=F10. 7, 4X3HEM=F8. 5/7X6H DELTA=F10. 7, 4X11HK2L(START)=F10. 6, 4X11HDEL(START)=F5. 1)
104	FORMAT (9X3HREX, 13X3HK2L, 13X5HRCALC, 12X2HEL//)
105	FORMAT (F10. 5, F10. 3)
106	FORMAT (F14. 4, 2F17. 7, F13. 2)
107	FORMAT (8X38HDATA REJECTED-ITNO HAS EXCEEDED ITMAX=I4)
108	END

Table 5. Identification of terms used in the program

Equation 5-29	Program	Comment
R_{12}	REX	The EXperimental value of R_{12}
	RCALC	The value of R_{12} CALCulated by the computer
ℓ	EL	The discharge length
	NUMCAR	The NUMber of CARds to be read by statement 10, each containing one REX, EL data set
γ	GAMMA	1.994 506
$R_{12}(0)/\gamma$	ROVGAM	R-OVer-GAMma = 1.002 755
	DELTA	The acceptance tolerance for congruence of RCALC with REX, taken = 0.0001
m(0)/I(0)	EM	-0.02547
$K_2\ell$	EK2L	
	EK2LS	The starting value for the iteration, taken = 50.00001 wherein the decimal is crucial to prevent computer hang-up
	DEL	The iteration interval for EK2L
	DELS	The starting value of DEL, taken = 10.00000
	ITNO	The number of iterations required to satisfy statement 19
	ITMAX	Infinite loop control, taken = 100

$$(5\text{-}31) \qquad K_4\ell = \frac{2}{5}\,\frac{\lambda_4^2}{8\pi}\,\frac{[F(\omega)]_4}{(\Delta\nu)_4}\left(\frac{\ln 2}{\pi}\right)^{\frac{1}{2}}\ell\, A_{34}\,[^2D^\circ].$$

For the two major line broadening processes, Doppler and Lorentz,

$$(5\text{-}32) \qquad [F(\omega)]_2 = [F(\omega)]_4 \qquad \text{and } (\Delta\nu)_2 = (\Delta\nu)_4$$

since neither is dependent upon the nature of the atomic excited state. Furthermore, for the particular case of the atomic nitrogen transitions under study here, Equation 5-32 is true also for all other broadening processes since transitions 2 and 4 have the same upper state. Consequently, the ratio of Equations 5-30 and 5-31 yields

$$(5\text{-}33) \qquad \frac{K_2\ell}{K_4\ell} = \frac{5}{3}\,\left(\frac{\lambda_2^2}{\lambda_4^2}\right)\,\frac{A_{12}}{A_{34}}\,\frac{[^2P^\circ]}{[^2D^\circ]}\,,$$

wherein line broadening effects have been cancelled out exactly.

G. A_{12}/A_{34} from Related Multiplet Considerations

Of the quantities in Equation 5-33, only A_{12}/A_{34} remains to be determined. It is, of course, possible to calculate the relative values of the spontaneous emission transition probabilities by such means as the Bates-Damgaard approximation (11). Also, a report (12) has recently appeared in which absolute values of A_{12} and A_{34} have been estimated. The use of such methods for the determination of A_{12}/A_{34}

would introduce a sizable uncertainty into Equation 5-33.

As it happens, however, a special relationship exists between the N 1743, 5 and N 1493, 5 Å doublets--they are related multiplets. This happy accident permits the calculation of a precise value for A_{12}/A_{34}. It is shown in Appendix G that

$$A_{12}/A_{34} = 0.376\ 895 \tag{5-34}$$

and that this value is valid independent of whether equilibrium of any kind does or does not exist in the experimental plasma.

With this value, Equation 5-33 may be numerically evaluated to yield

$$\frac{[^2P^\circ]}{[^2D^\circ]} = 1.167\ 644 \frac{K_2\ell}{K_4\ell} \ . \tag{5-35}$$

Therefore, the elucidation of $[^2P^\circ]/[^2D^\circ]$ from experimental values of R_{12} and R_{34} is straight-forward, provided thermal J-population exists. Values of $K_2\ell$ and $K_4\ell$ corresponding to R_{12} and R_{34} may be obtained from Equation 5-29, and the ratio of these values yields the desired concentration ratio by Equation 5-35.

VI. EXPERIMENTAL CONCENTRATION RATIOS

A. Data Collection and Reduction

The operation of the gas-handling system has been described in Section II. The operation of the photomultiplier readout console is entirely conventional and requires no discussion. However, the mechanics of the data collection technique are pertinent to statistical sampling and source equilibration considerations.

The latter consideration concerns the ability to establish a discharge whose spectral line emission is constant with time, and reproducible from day to day, for given conditions of pressure and flowrate. Experience has demonstrated that this may be achieved by the following procedure:

(1) The cold trap is immersed in liquid nitrogen prior to admission of the test gas into the system.

(2) The test gas is admitted and the metering valves adjusted to yield the desired pressure and flowrate, as described in Section II.

(3) The discharge is established, and its position varied along the discharge tube axis at ten minute intervals so as to outgas the entire tube.

(4) After positioning the microwave cavity to yield the desired value of s -- the slit-to-discharge-center distance, thirty additional minutes of discharge operation time are provided to

condition the inside surface of the tube walls and permit the establishment of a thermal steady state between the walls and the plasma. During this time, the spectrometer should be peaked on the N 1743 Å line, (i) to fatigue the photomultiplier, and (ii) to provide a visual record of the approach of the source to constancy of spectral line emission.

(5) When there has been no perceptible change in the N 1743 Å intensity and the pressure has remained constant to within ±0.5% over a period of at least five minutes, the spectrometer is set at λ 1730 Å and scanned at 10 Å/minute (i) forward to 1746 Å, (ii) back to 1741 Å, (iii) forward to 1746 Å, and (iv) back to 1741 Å. This provides a base line "zero" level followed by four scans alternately back and forth across the doublet.

(6) The spectrometer is then quick-scanned at 2500 Å/minute to λ 1480 Å, where the 10 Å/minute scan procedure is repeated (i) up to 1496 Å, (ii) back to 1491 Å, (iii) forward to 1496 Å, and (iv) again back to 1491 Å. Thus, the same pattern of base line "zero" level followed by four scans of the doublet is obtained for the N 1493, 5 Å doublet.

(7) Following immediate quick-scan up to λ 1730 Å, steps 5 and 6 are alternately repeated until four sets, each containing four scans, of both the N 1743, 5 and N 1493, 5 Å doublets are obtained.

(8) Readings of pressure, flowrate, and plasma length are recorded both prior to step 5 and subsequent to step 7.

(9) The downstream metering valve is adjusted to provide the next desired pressure setting, and the spectrometer is again peaked on the N 1743 Å line. Prosecution of steps 5 through 8 will then provide another piece of data relating doublet ratio to discharge parameters.

The pattern derived from step 5, consisting of four scans of the doublet preceded by a base line, is termed a four-scan. Step 7 prescribes that four such four-scans of the 1, 2 doublet be made alternately with four such four-scans of the 3, 4 doublet. That this is necessary becomes clear when it is realized that twenty minutes is required to prosecute the thirty-two doublet scans. Ideally, both doublets should be scanned simultaneously, but this is obviously impossible with a single spectrometer. Alternate scanning of the two doublets is the next best thing, but this is impractical from a time standpoint since a base line would have to be provided for each doublet scan. Thus there was evolved the compromise of alternate fours, each four-scan possessing a common base line.

The intensities of the spectral lines viewed were measured in units of mm peak height above the base line. The peak heights were readily measurable to ±0. 1 mm. A direct proportionality exists between the peak height of the recorder tracing and spectral line intensity

provided the response of the photomultiplier readout console is linear. The latter was checked and found to be true. Thus, the ratio of the peak heights of the doublet component tracings gives directly the doublet intensity ratio.

Sixteen replicate scans of each doublet were found to be necessary to produce a mean value for the doublet ratio such that the average deviation of the sixteen individual ratios from this mean is less than one percent. This is demonstrated in Appendix I.

B. The Experimental Doublet Ratios

The observed pressure dependence of the nitrogen doublet ratios is presented in Figures 1 to 3 for the helium-500 vpm nitrogen matrix, and in Figures 4 and 5 for the argon-500 vpm nitrogen matrix. Except for Figure 3, the discharge tube pressure is plotted logarithmically to permit expansion of scale in the lower range where interesting behavior is observed.

The data used to construct Figures 1 to 5 are presented in Appendix J. It is seen that each point plotted is the arithmetic average of 16 or more scans of the doublet in question. As was pointed out above, 16 scans of each of the two doublets required 20 minutes to accomplish. When equilibration time of approximately 20 minutes per measurement is added, together with start-up and shut-down time, it becomes understandable that the curves could be constructed at the

rate of only one point per hour. Of necessity, therefore each curve is a composite of data collected on different days, and the symbols used to identify the points refer to the latter. There is presented in Table 6 the legend which identifies these symbols in terms of days elapsed from an arbitrarily selected D-day. Accompanying this legend are the pertinent experimental parameters characterizing each day's run.

Regarding these parameters, it is pertinent to note that some variation exists among them. This occurred sometimes by accident, sometimes by design, and sometimes because the experimenter was uncertain which were the best parameters to use. Brief comment seems called for regarding the choice of spectrometer slit widths and the use of a window to isolate the discharge tube from the spectrometer.

The single piece of data denoted Run No. D+20 was actually the result of a study designed to determine the influence on the doublet ratio of the spectrometer exit/entrance slit width ratio. This study is reported in Appendix K, where it is seen that for any entrance slit width between 3 and 10 microns, any exit slit width between 10 and 50 microns may be used without significantly affecting the measured value of either doublet ratio.

A plane lithium fluoride window was used to seal the spectrometer entrance slit in the early experiments. As is well known to investigators working the vacuum ultraviolet spectral region, the transmissivity of lithium fluoride decreases upon exposure of the surface to

Table 6. Figure legend and experimental parameters for the doublet ratio measurements

Matrix Gas	Run[a] No.	Symbol[b]	Flowrate ($\frac{\text{ml STP}}{\text{minute}}$)	s[c] (cm)	Slit width (microns) Entrance	Exit	Window Used
Helium	D	o	35.2	12.00	5.5	50	yes
Helium	D+35	□	35.1	13.00	5.5	30	no
Helium	D+36	△	33.5	13.00	3.2	30	no
Helium	D+39	▽	34.3	13.00	6.5	30	no
Helium	D+41	x	34.5	13.00	5.5	30	no
Helium	D+43	+	34.3	13.00	5.5	30	no
Helium	D+46	☿	34.4	13.00	5.5	30	no
Helium	D+49	◇	35.0	13.00	5.5	30	no
Argon	D+14	□	varied	15.50	5.5	50	yes
Argon	D+19	△	varied	14.50	3.2	varied	no
Argon	D+20	*	28.3	14.50	varied	varied	no
Argon	D+54	o	37.0	16.50	5.5	30	no
Argon	D+55	+	36.8	16.15	5.5	30	no

[a]Units are days elapsed from D-day.

[b]Refers to Figures 1 to 3 for the helium matrix, and Figures 4 and 5 for the argon matrix.

[c]The slit-to-discharge-center distance.

both radiation and certain molecular species, notably water and organic compounds. Since the transmissivity of the window in use was rapidly degenerating, it was decided to remove it, which resulted in a 50-fold increase in the light level to the photomultiplier. It is seen in Figure 1 that the doublet ratios measured with and without the window agree quite well. The circles are with the window; all other points are without it. This demonstrates the lack of dependence of doublet ratio measurements on the absolute intensities of the doublet components.

Regarding the removal of the plane window, the latter was used to isolate the vacuum in the spectrometer tank from the matrix gas in the discharge tube. Its removal thus admits the matrix gas to the spectrometer. To permit the establishment of constant pressures and measurement of gas flowrates, the spectrometer's pumping port was sealed with a large bore vacuum valve. Thus, for the bulk of the measurements made in this study, the optical path of the spectrometer was immersed in discharge matrix gas at the same pressure as in the discharge tube. Since the matrix gas input is on the slit end of the discharge tube, the gas in the spectrometer tank contained no discharge reaction products.

The gas flowrates for most of the experiments may be seen from Table 6 to fall within the range of 35 ± 2 ml STP per minute. The significant exception was Run No. D+14. As mentioned in Section II,

pressures below 1.5 torr in argon could be achieved only with concomitant reduction in gas flowrate. For Run No. D + 14, the pressure - flowrate combinations used, in the units torr-ml STP per minute, were (i) 0.70 - 26.3, (ii) 0.35 - 15.8, and (iii) 0.20 - 8.3. The doublet ratio was not observed to be sensitively dependent on gas flowrate.

It will be noted that the curve of Figure 5 is broken at pressures below about one torr. It is suspected that a band of carbon monoxide underlies the N 1495 Å line. At pressures below one torr the CO band intensity begins to increase rapidly. Hence, the validity of R_{34} measurements below one torr is questionable.

The upper pressure limit for the helium matrix -- 220 torr -- is set by the inability of the microwave generator to maintain a stable discharge at higher pressures. Generators capable of delivering higher power outputs are commercially available, the use of which would probably permit the study of higher pressure ranges. The upper pressure limit for the argon matrix -- 45 torr -- is set by the change in the character of the discharge above this pressure. The diffuse and geometrically stable glow discharge constricts into numerous localized streamers which rotate and vacillate at a rapid rate. The equations derived herein are not applicable to this latter discharge configuration.

C. The Experimental Discharge Lengths

One of the experimental quantities required for the solution of Equation 5-29 is the discharge length, ℓ. Plots of ℓ vs. pressure are

given in Figures 18 and 19 for the helium-500 vpm nitrogen matrix, and in Figure 20 for the argon-500 vpm nitrogen matrix. These measurements were made during the course of the preceding experiments. The following comments are noteworthy.

The quantity ℓ is the least precise of the experimental measurables in this study. This lack of precision arises primarily from the inability to view the discharge in λ1493,5 and λ1743,5 Å light. Despite the fact that the plasma was assumed to be uniformly excited, the discharge in helium contained two zones -- an inner dense zone and an outer transparent zone. The effective discharge length should be an average of the lengths of these two zones weighted in proportion to the amount of N-doublet radiation each emits. But the latter weighting factor cannot be determined because absorption of these wavelengths by the discharge tube walls precludes viewing the discharge from the side. The weighting factors were therefore blithely assumed to be unity, and the discharge lengths reported for the helium matrix are thus the arithmetic averages of the lengths of the two zones.

The question then arises, "What effect has this uncertainty in ℓ on the calculated values of the absorption indices $K_2\ell$ and $K_4\ell$?". The quantity ℓ enters Equation 5-29 only through the parameter δ, which is seen by Equations 4-103 and 5-27 to have the magnitude $-0.02547\,\ell$. A numerical investigation of Equation 5-29 discloses that the quantity in braces exerts only a second order effect on the value of $K_2\ell$ calculated for a given value of R_{12}. In fact, a 50% error in ℓ introduces

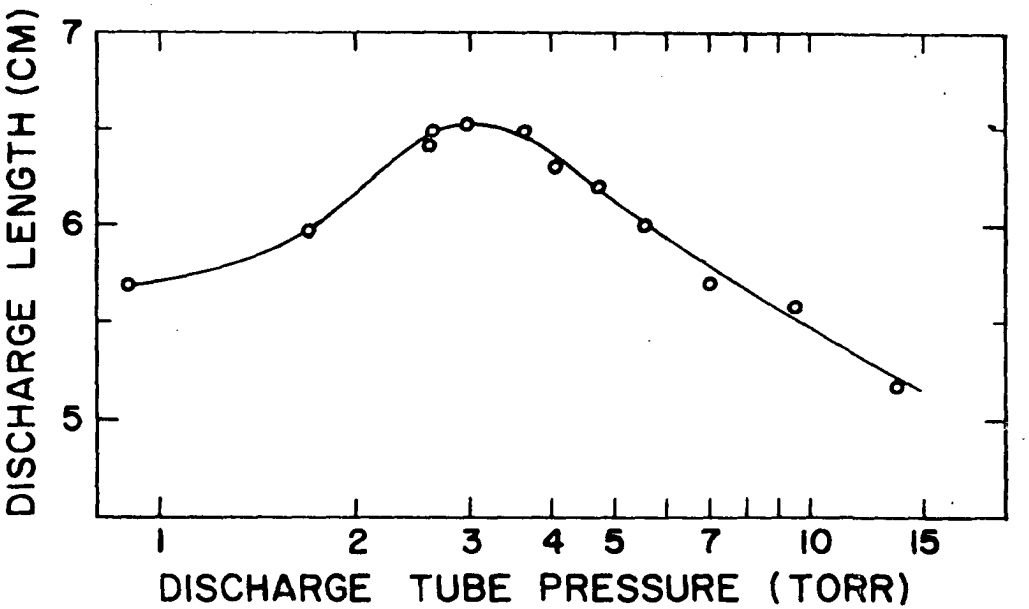

Figure 18. Discharge length in the low pressure helium matrix

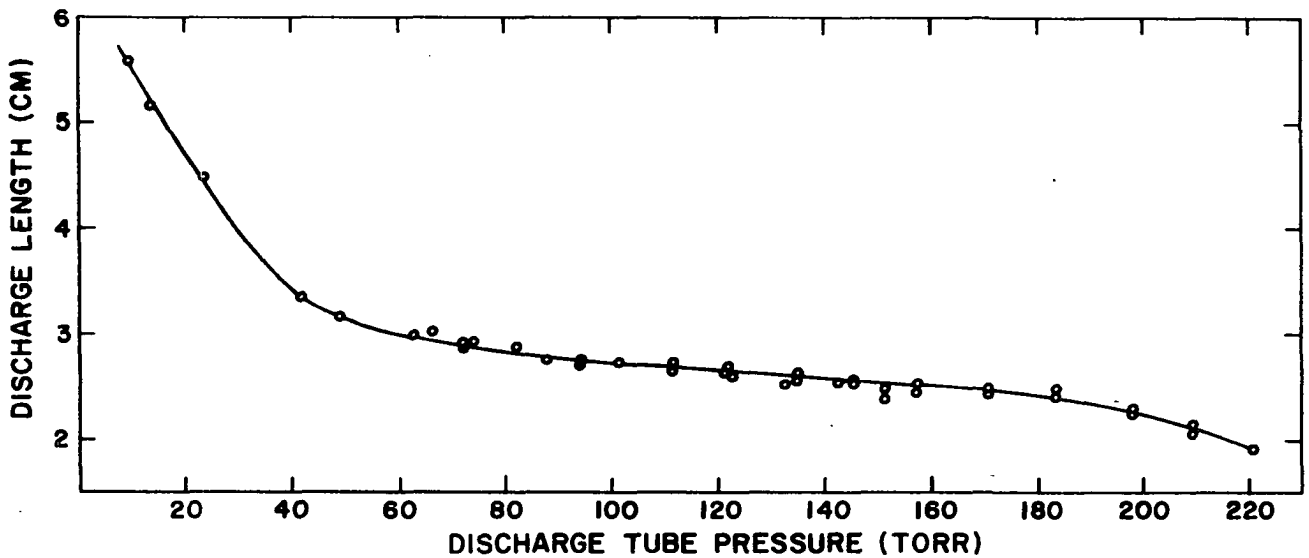

Figure 19. Discharge length in the helium matrix in the upper pressure range

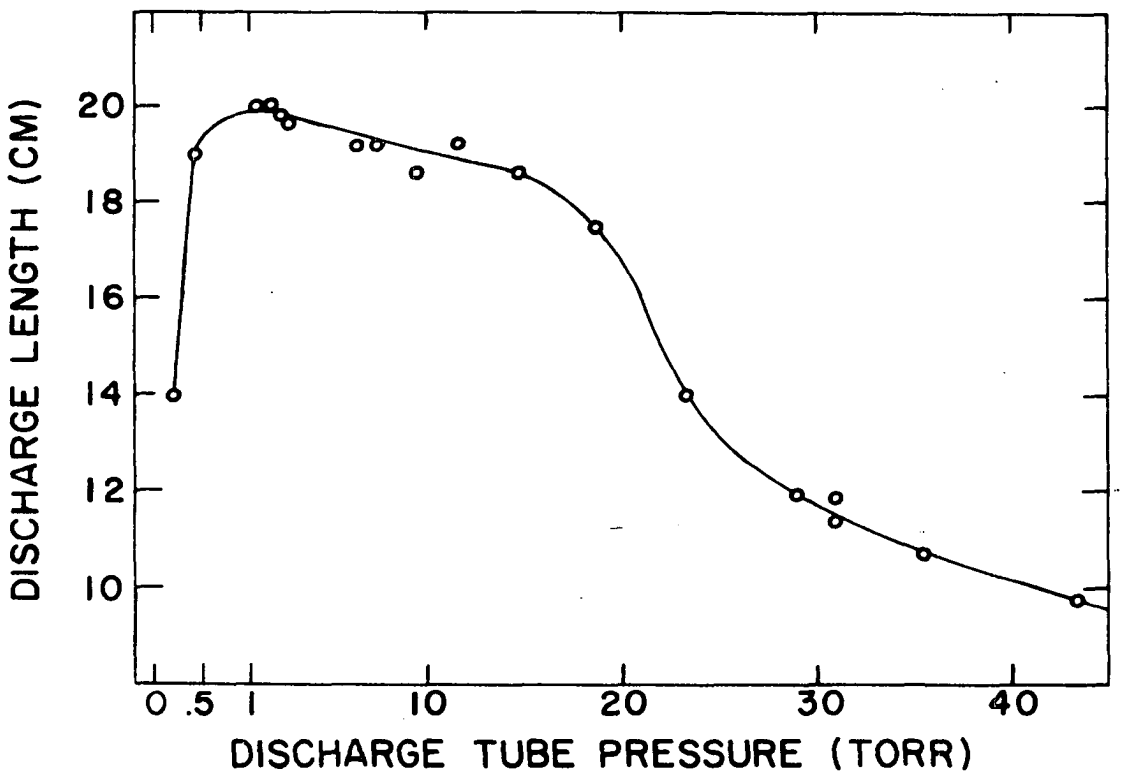

Figure 20. Discharge length in the argon matrix

an error of less than 0.5% in the value of $K_2\ell$, which is inconsequential.

The discharge in argon does not exhibit the two-zone behavior. Rather, to the naked eye at least, it appears quite uniform.

A word of caution is advisable here. The measurement of discharge lengths obviously requires looking directly at the discharge. Not only does a considerable amount of ultraviolet radiation emanate from this source, but it is highly probable that microwave radiation does too. The latter is more injurious to the eyes than the former. For this reason it is desirable to look at the discharge through a water filter, such as a water-filled spectrophotometric absorption cell with plane parallel faces.

D. Computation of the Concentration Ratios

As was described in Section VG, the calculation of the metastable state concentration ratio -- $[^2P^\circ]/[^2D^\circ]$ -- of atomic nitrogen involves merely (i) solution of Equation 5-29 for values of $K_2\ell$ and $K_4\ell$ via a digital computer, followed by (ii) calculation of the ratio via Equation 5-35. Table 7 contains, for the helium matrix, (i) the values of R_{12}, R_{34}, and ℓ which were fed to the computer, (ii) the values of $K_2\ell$ and $K_4\ell$ which it calculated, and (iii) the resultant metastable state concentration ratios. The values of R_{12}, R_{34}, and ℓ were derived from the original plots of which Figures 1-3 and 18-19 are tracings. Table 8 presents the analogous information for the argon matrix, the data being derived from the analogous sources.

Table 7. Concentration ratio calculations for the helium matrix

P[a] (torr)	R_{12}	R_{34}	ℓ (cm)	$K_2\ell$	$K_4\ell$	$\frac{^2P^\circ}{^2D^\circ}$
0.80	1.906	1.731	5.66	0.102	0.324	0.367
1.00	1.891	1.691	5.71	0.119	0.383	0.363
1.50	1.852	1.617	5.88	0.165	0.502	0.384
2.00	1.814	1.567	6.16	0.213	0.592	0.421
2.50	1.767	1.538	6.42	0.275	0.648	0.496
3.00	1.721	1.529	6.52	0.340	0.666	0.596
3.50	1.685	1.530	6.49	0.394	0.664	0.692
4.00	1.659	1.536	6.37	0.434	0.652	0.778
5.00	1.624	1.556	6.13	0.491	0.613	0.935
6.00	1.597	1.583	5.94	0.537	0.562	1.116
7.00	1.578	1.608	5.79	0.569	0.517	1.285
8.00	1.566	1.632	5.67	0.592	0.475	1.454
9.00	1.556	1.654	5.56	0.611	0.441	1.618
10.00	1.548	1.672	5.48	0.625	0.411	1.776
12.00	1.536	1.704	5.34	0.649	0.362	2.09
14.00	1.525	1.729	5.18	0.669	0.326	2.39
16.00	1.516	1.746	5.03	0.686	0.302	2.65
18.00	1.507	1.759	4.88	0.704	0.284	2.89
20.00	1.498	1.768	4.72	0.723	0.272	3.10
23.00	1.482	1.778	4.48	0.755	0.258	3.42

[a]Discharge tube pressure.

Table 7. (Continued)

P^a (torr)	R_{12}	R_{34}	ℓ (cm)	$K_2\ell$	$K_4\ell$	$\frac{^2P^\circ}{^2D^\circ}$
26.00	1.465	1.786	4.26	0.792	0.247	3.74
30.00	1.444	1.794	3.98	0.840	0.237	4.14
35.00	1.416	1.799	3.68	0.905	0.230	4.60
40.00	1.392	1.800	3.44	0.966	0.228	4.94
50.00	1.350	1.798	3.16	1.082	0.230	5.48
60.0	1.316	1.794	3.02	1.188	0.236	5.88
70.0	1.289	1.786	2.92	1.281	0.246	6.09
80.0	1.268	1.776	2.86	1.360	0.259	6.14
90.0	1.255	1.764	2.80	1.411	0.275	5.99
100.0	1.248	1.748	2.75	1.440	0.296	5.68
110.0	1.243	1.730	2.70	1.461	0.321	5.32
120.0	1.241	1.716	2.66	1.469	0.341	5.02
130.0	1.240	1.706	2.62	1.473	0.356	4.84
140.0	1.241	1.696	2.58	1.470	0.370	4.64
150.0	1.242	1.686	2.54	1.463	0.385	4.44
160.0	1.244	1.676	2.51	1.452	0.400	4.24
170.0	1.247	1.666	2.47	1.441	0.414	4.06
180.0	1.251	1.656	2.42	1.425	0.430	3.87
190.0	1.254	1.646	2.34	1.410	0.444	3.70
200.0	1.258	1.636	2.23	1.390	0.460	3.53
210.0	1.263	1.626	2.10	1.371	0.476	3.36
220.0	1.268	1.616	1.92	1.349	0.492	3.20

Table 8. Concentration ratio calculations for the argon matrix

P^a (torr)	R_{12}	R_{34}	ℓ (cm)	$K_2\ell$	$K_4\ell$	$\frac{^2P^\circ}{^2D^\circ}$
0.20	1.999	1.798	14.0	0.0008	0.244	0.004
0.50	1.992	1.764	19.4	0.010	0.299	0.037
0.60	1.980	1.762	19.6	0.023	0.301	0.089
0.80	1.952	1.762	19.8	0.054	0.302	0.210
1.00	1.924	1.764	19.8	0.087	0.299	0.340
1.50	1.870	1.772	19.9	0.154	0.287	0.627
2.00	1.832	1.782	19.8	0.204	0.273	0.871
3.00	1.779	1.797	19.7	0.277	0.252	1.286
4.00	1.741	1.811	19.6	0.334	0.232	1.678
5.00	1.711	1.820	19.5	0.380	0.219	2.03
6.00	1.687	1.826	19.4	0.419	0.211	2.32
8.00	1.646	1.832	19.2	0.488	0.202	2.81
10.00	1.612	1.834	19.0	0.550	0.200	3.21
15.00	1.544	1.831	18.5	0.684	0.204	3.92
20.00	1.493	1.822	16.8	0.791	0.213	4.33
25.00	1.451	1.810	13.0	0.873	0.226	4.50
30.00	1.416	1.796	11.8	0.956	0.244	4.58
35.00	1.385	1.780	10.9	1.038	0.263	4.61
40.00	1.358	1.763	10.2	1.116	0.286	4.55

[a]Discharge tube pressure.

The metastable state concentration ratios are plotted versus pressure in Figure 21 for the helium matrix, and in Figure 22 for the argon matrix. To provide suitable resolution for both the high and low pressure ranges, a mixed pressure scale was employed for Figure 21. The low pressure scale is logarithmic, whereas the high pressure scale is linear, with cross-over at 60 torr where the dispersion of the two scales is identical.

E. Magnitude of the Experimental Error in the Concentration Ratio

Precise values for the $[^2P^\circ]/[^2D^\circ]$ concentration ratio can be calculated provided precise values for R_{12} and R_{34} are available. But the doublet intensity ratios are measured quantities and are therefore subject to experimental error. The question therefore arises, "What error will be reflected in the concentration ratio by a given error in the doublet intensity ratios?". With the equipment available, it is shown in appendix J that doublet ratios can be measured within an average deviation of ± 1% relative for quadruplicate four-scans of the doublet.

The effect of this error on the measured concentration ratio can be assessed by solving Equation 5-29 for values of $K\ell$ corresponding to values of R which are in error by +1 and -1 percent. Denoting these $K\ell+$ and $K\ell-$, respectively, the maximum effect on the concentration ratio will arise when the combination $K_2\ell+/K_4\ell-$ and $K_2\ell-/K_4\ell+$ are inserted into Equation 5-35. By this technique the lower and upper limits of uncertainty were calculated for the concentration ratio in the

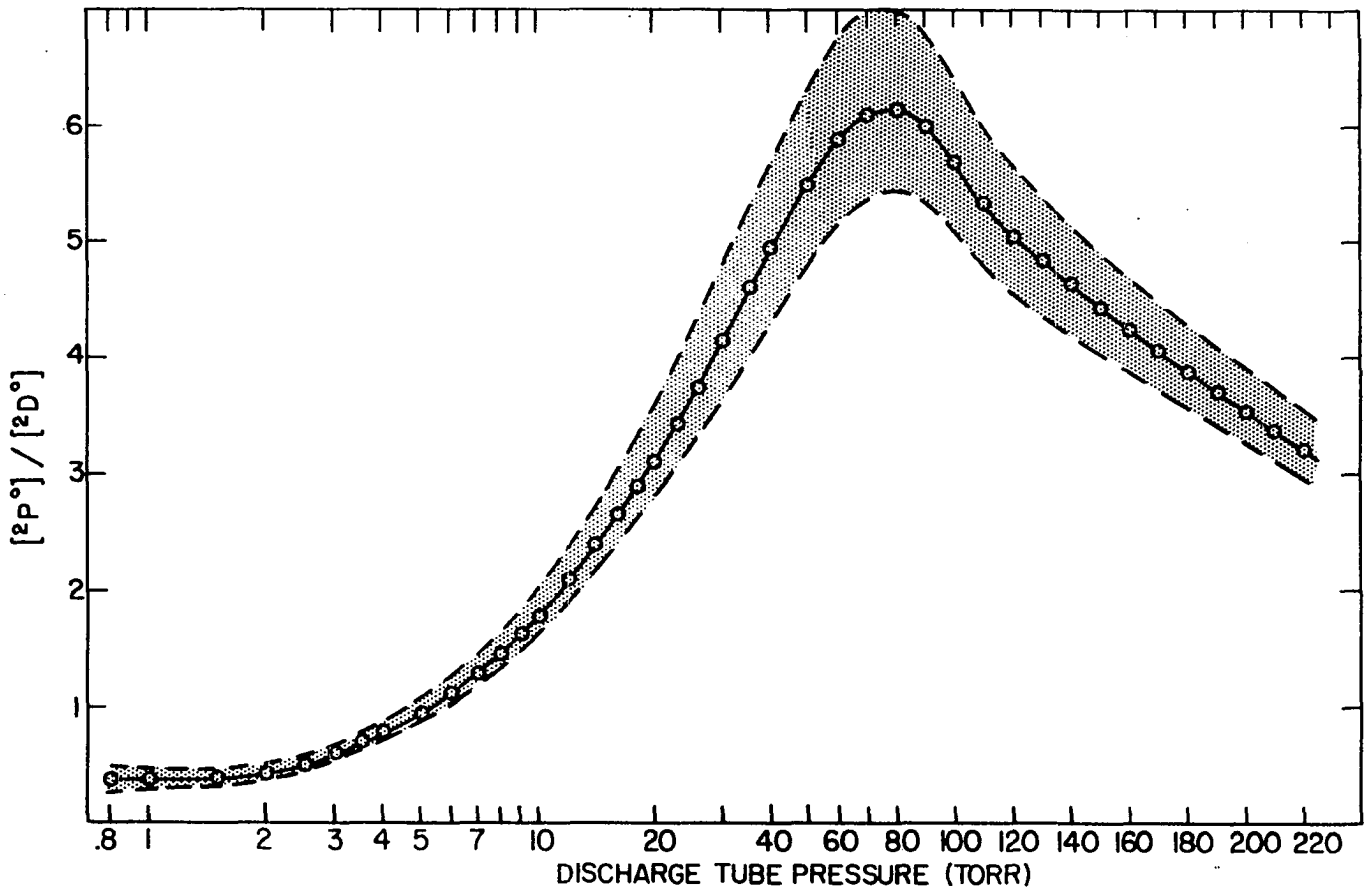

Figure 21. The metastable state concentration ratio in the helium matrix

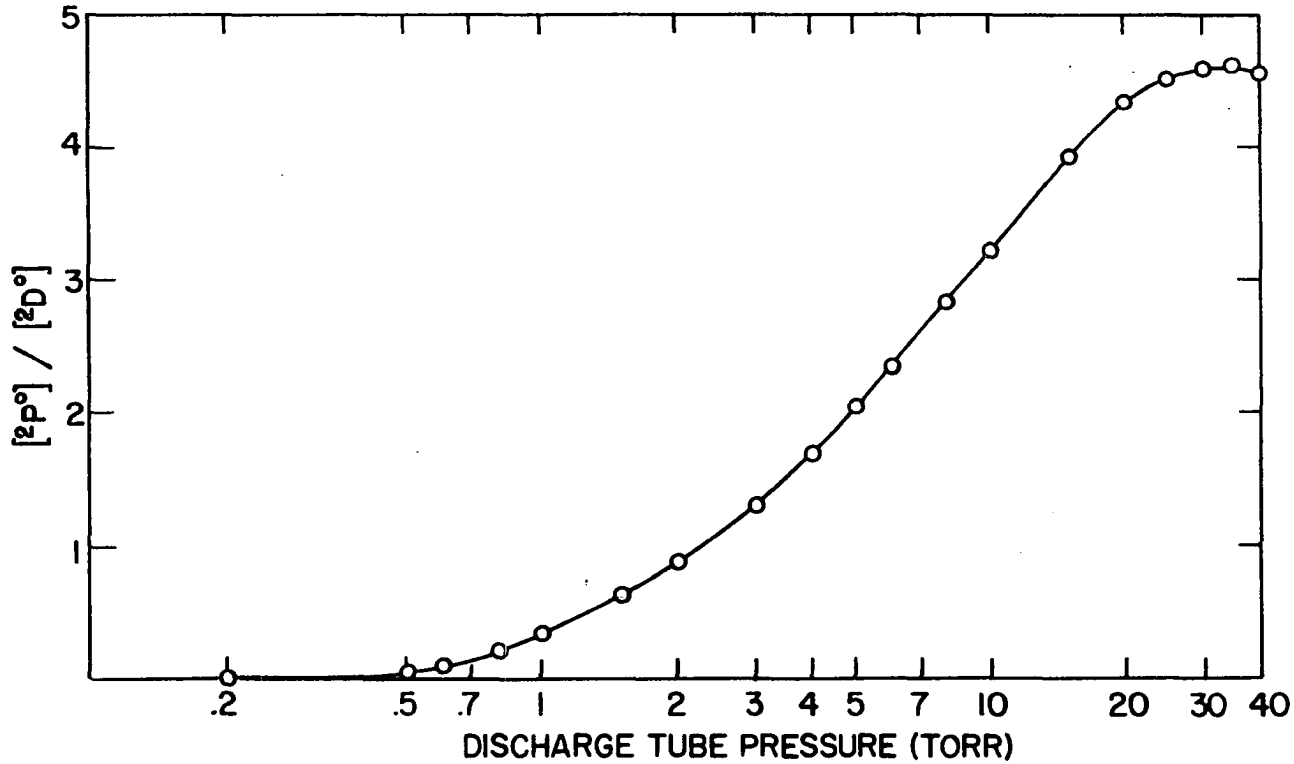

Figure 22. The metastable state concentration ratio in the argon matrix

helium matrix shown in Figure 21. The data for these curves are presented in Table 9.

It is unfortunate that the error in the doublet ratios is magnified in the concentration ratio, but it is not surprising since the doublet ratio range from 1.0 to 2.0 encompasses the absorber concentration range from infinity to zero.

F. Observations

As has been pointed out previously, the calculation of concentration ratios permits the cancellation of line broadening effects. How well these have been cancelled may be observed by comparison of Figures 1, 2, and 21. The behavior of R_{12} in helium in the vicinity of five torr was, when first observed, quite unexpected and thought-provoking. Upon calculation of the concentration ratio of Figure 21, however, no corresponding dip was observed. The most probable explanation of this result is that this R_{12} behavior is the result of line broadening effects, that the same effects exist in the R_{34} curve superimposed upon the $^2D^\circ$ concentration variation effects, and that the line broadening effects cancel exactly in the formation of the concentration ratio. It is interesting to note that the line broadening effects responsible for the R_{12} behavior in helium do not appear to be operative in the argon matrix, there being no corresponding dip in the curve of Figure 4.

The magnitude of the experimental concentration ratios in both

Table 9. Concentration ratio calculations for the doublet ratio combinations R_{12}^{+}, R_{34}^{-} and R_{12}^{-}, R_{34}^{+}

P (torr)	$K_2\ell+$	$K_4\ell-$	$\frac{^2P°+}{^2D°-}$	$K_2\ell-$	$K_4\ell+$	$\frac{^2P°-}{^2D°+}$
0.8	0.0804	0.3493	0.269	0.1239	0.3000	0.482
1.0	0.0975	0.4089	0.278	0.1414	0.3578	0.462
1.5	0.1427	0.5297	0.315	0.1878	0.4747	0.462
2.0	0.1903	0.6210	0.358	0.2366	0.5628	0.491
3.0	0.3155	0.6970	0.528	0.3655	0.6360	0.671
4.0	0.4080	0.6825	0.698	0.4608	0.6218	0.865
6.0	0.5089	0.5905	1.006	0.5650	0.5334	1.237
8.0	0.5630	0.5027	1.308	0.6210	0.4487	1.616
10.0	0.5957	0.4370	1.592	0.6550	0.3853	1.985
14.0	0.6388	0.3513	2.12	0.6998	0.3020	2.71
18.0	0.6735	0.3084	2.55	0.7359	0.2605	3.30
23.0	0.7237	0.2820	3.00	0.7880	0.2348	3.92
30.0	0.8065	0.2607	3.61	0.8746	0.2142	4.77
40.0	0.9290	0.2515	4.31	1.0036	0.2054	5.70
60.0	1.1450	0.2595	5.15	1.2329	0.2132	6.75
80.0	1.3110	0.2824	5.42	1.4110	0.2356	6.99
100.0	1.3880	0.3203	5.06	1.4950	0.2725	6.41
120.0	1.4160	0.3660	4.52	1.5250	0.3170	5.62
140.0	1.4170	0.3955	4.18	1.5260	0.3456	5.16
160.0	1.4000	0.4256	3.84	1.5070	0.3749	4.69
180.0	1.3740	0.4558	3.52	1.4790	0.4040	4.27
200.0	1.3400	0.4867	3.21	1.4420	0.4340	3.88

helium and argon indicate that a population inversion exists for the nitrogen metastable states. Since it is difficult to explain this on the basis of the conceivable mechanisms responsible for populating these states, it follows that the depopulation mechanisms must exert considerable influence on the metastable state concentrations. Furthermore, if the depopulation mechanisms for both states are the same, then they must be more efficient for the $^2D^\circ$ than for the $^2P^\circ$ atoms, in which case it would appear necessary that the efficiency of the mechanism be dependent upon the energy of the metastable state. It is also interesting to speculate whether there might exist a depopulation mechanism unique to the $^2D^\circ$ atoms. Such a mechanism must be related to the angular momentum of the metastable state.

VII. ATTRIBUTES OF THE METHOD

The intra-multiplet intensity ratio technique as developed herein for the measurement of the nitrogen metastable state concentration ratio possesses some desirable characteristics. Chief amongst these is its applicability to non-equilibrium plasma systems. The only equilibrium required is thermal J-population, which has been demonstrated to exist in this plasma under otherwise severe non-equilibrium conditions, and is likely to exist in other non-thermal plasmas as well. A necessary corollary of this characteristic is that the method requires nowhere that an "excitation temperature" be specified for the species under consideration, since the concept of excitation temperature is as difficult to define as it is to measure in non-thermal plasmas.

From a practical point of view, an inviting feature is that the measurements are simple and direct. Since the components of spectral multiplets are generally of proximate wavelengths, no independent calibration of the spectral response of the source-spectrometer combination is necessary, as is the case for absolute intensity measurements. Indeed, for work in the vacuum ultraviolet, this latter feature is not just inviting, but actually decisive. Since the black body continuum emitted from conventional radiators is quite weak in this spectral region, the calibration of the spectral response of a vacuum ultraviolet spectrometer is subject to considerable error.

The procedure developed to calibrate the source-spectrometer combination for the effect of spectral source depth is, to the author's

best knowledge, original. In the past, workers have positioned the source sufficiently far from the slit to enable the assumption to be made that only plane waves from the source enter the spectrometer. This procedure wastes light, a luxury which cannot be indulged in the vacuum ultraviolet region where the working light level is as much as two orders of magnitude less than in the longer wavelength regions. In the few cases where account has been taken of the reduction of intensity with distance from the slit, the method used has been similar to that of Edels (8) wherein compensation terms are calculated from geometrical considerations. Unquestionably, direct calibration of the effect of spectral source depth is inherently superior since this procedure automatically takes into account all occultation effects operative between the source and photocathode to exactly the degree to which they are operative.

A further advantage of the use of intra-multiplet intensity ratios over the measurement of absolute spectral line intensities for self-absorption studies is that the former have been demonstrated to be insensitive within wide limits to the values of entrance and exit slit widths chosen.

The fact that the intra-multiplet intensity ratio procedure described herein compensates internally for a wide variety of instrumental factors whose magnitudes are difficult to assess with accuracy bestows a high degree of reliability on the results. If, in addition, recourse is taken to the calculation of concentration ratios, such experimental imponderables as discharge length and line

broadening effects may be cancelled as well.

A serious limitation of the method in its present form is that it is applicable only to uniformly excited sources. It remains to be seen whether multiplet ratios may be applied to stratified sources with equal utility.

VIII. OTHER APPLICATIONS

A. Excited to Ground State Ratios

Information of greater value could have been extracted from this study on the behavior of nitrogen in the microwave-driven discharge had it been possible to resolve the ground state multiplet with the spectrometer available. The $3s\ ^4P_{5/2,\ 3/2,\ 1/2} \rightarrow 2p^3\ ^4S^o_{3/2}$ resonance transition is a triplet, two of whose components could have been ratiod precisely as were the doublet transitions treated herein, with the result that $K_g\ell$ for the ground state could have been determined. The ratio $K_2\ell/K_g\ell$ would then have provided the excited/ground state concentration ratio combined with a multiplicative constant -- the ratio of the Einstein spontaneous emission probabilities for the two transitions. Line broadening effects would, however, still have cancelled since Doppler broadening is the major process, and this type of broadening is not a function of the nature of the upper or lower states of the transition.

B. Absolute Concentrations

The problem encountered in the measurement of absolute concentrations by spectrometric methods is that one commonly measures a quantity which is related to the triple product

(transition probability)(line broadening effects)(concentration).

The intra-multiplet intensity ratio technique does not solve this problem. It merely permits the value of the triple product to be specified with greater ease and reliability than has been heretofore possible.

IX. LITERATURE CITED

1. Schnautz, H. Linienabsorption und Gesamtabsorption der Kupferresonanzlinien sowie Bestimmung der Strahlungstemperatur in der Gassäule des Kupferlichtbogens. Spectrochim. Acta 1: 173-196. 1939.

2. Mannkopff, R. Über die Intensität der Resonanzlinien eines Elements im Lichtbogen in Abhängigkeit von seiner Konzentration. Spectrochim. Acta 1: 197-206. 1939.

3. McNally, J. R., Jr. The DCX and high temperature measurement in the carbon arc. In Dickerman, P. J., ed. Optical spectrometric measurements of high temperatures. pp. 95-98. Chicago, Ill., University of Chicago Press. 1961.

4. Kuhn, H. G. Atomic spectra. New York, N. Y., Academic Press Inc. 1962.

5. Cowan, R. D. and G. H. Dieke. Self-absorption of spectrum lines. Revs. Modern Phys. 20: 418-455. 1948.

6. Mitchell, A. C. G. and M. W. Zemansky. Resonance radiation and excited atoms. New York, N. Y., Cambridge University Press. 1934.

7. Aller, L. H. Astrophysics, the atmospheres of the sun and stars. New York, N. Y., The Ronald Press Co. c1953.

8. Edels, H. Self-absorption in arc sources in thermal equilibrium. Proc. Phys. Soc. (London) 65B: 794-800. 1952.

9. Sokolnikoff, I. S. and R. M. Redheffer. Mathematics of physics and modern engineering. New York, N. Y., McGraw-Hill Book Co., Inc. 1958.

10. Taylor, A. E. Advanced calculus. Palo Alto, Calif., Ginn and Company. c1955.

11. Bates, D. R. and A. Damgaard. The calculation of the absolute strengths of spectral lines. Phil. Trans. Roy. Soc. London A242: 101-122. 1949.

12. Fairchild, C. E. and K. C. Clark. Some oscillator strength measurements for atomic nitrogen and a study of nitrogen afterglows by resonance absorption in the extreme ultraviolet. (University of Washington, Seattle) Armed Services Technical Information Agency Report AD 283753. 1962.

13. Shand, E. B. Glass engineering handbook. 2nd ed. New York, N. Y., McGraw-Hill Book Co., Inc. 1958.

14. Namioka, T. Theory of the concave grating. III. Seya-Namioka monochromator. J. Opt. Soc. Am. 49: 951-961. 1959.

15. White, H. E. Introduction to atomic spectra. New York, N. Y., McGraw-Hill Book Co., Inc. 1934.

X. ACKNOWLEDGEMENTS

The author wishes to thank Dr. Velmer A. Fassel for his support and interest in this work, and Messrs. Robert B. Myers and Richard N. Kniseley together with Dr. Fassel for checking the mathematics and logic underlying the investigative technique. But thanks are due in greatest measure to my wife who has labored long over the manuscript of this dissertation, and aided much in the acquisition of the experimental data.

XI. APPENDIX A

A. Validity of the Equidistance Approximation

The approximation is made for Equation 4-37 that

(A-1) $z(x, r, \theta, \bar{s}) = x$

for all r, θ, and s. The quantities z, x, r, and θ are identified in Figure 23, which is a cross-sectional view of the discharge in the horizontal plane containing the plasma axis. Hence the spectrometer slit is perpendicular to this plane, and this is thus the $\theta = \pi/4$ plane thru the plasma axis.

The spectrometer geometry comes into play here because it defines the maximum value of r as a function of x. The quantity $w(\lambda)$ is the width of the grating aperture, the λ-dependence of which is discussed in the vicinity of Equation 4-89; f is the grating focal distance which is a constant of value 41.0 cm; and $z(x, r, \theta)$ is the absorption path length in the plasma between any point (x, r, θ) and the slit center.

The maximum error engendered by Equation A-1 will be calculated for the plane of Figure 23. It is obvious that, for any x, the maximum error will arise when $r = r_{max} \equiv R$. For mathematical convenience, we shall assume for the moment that the plasma front is planar and perpendicular to the discharge axis. Let the absorption path length from the point (x, r, θ) to this hypothetical front be denoted Z, whereupon it is seen from Figure 23 that $Z > z$. The plasma axis is colinear with the spectrometer optic axis. From similar triangles one observes that

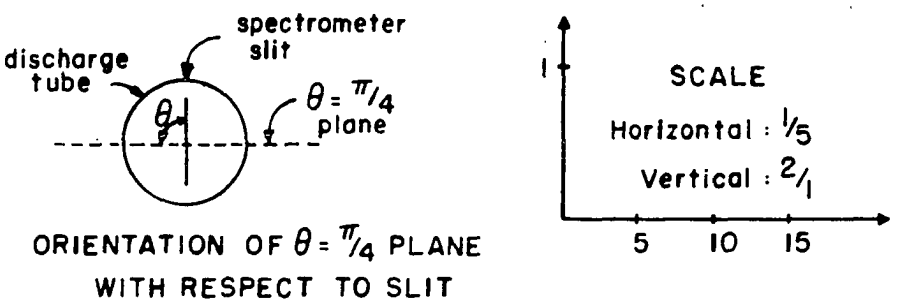

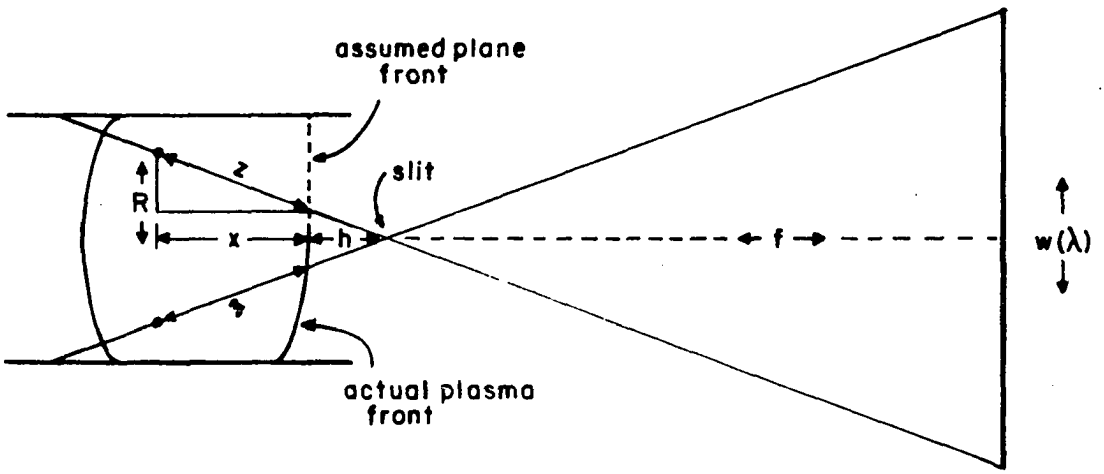

Figure 23. Plasma-spectrometer geometry in the $\theta = \pi/4$ plane through the plasma axis

$$(A\text{-}2) \qquad R = \frac{w\,(x+h)}{2f} \quad .$$

Constructing a line parallel to the plasma axis through the intersection of Z with the plane front yields a second set of similar triangles, from which it follows that

$$(A\text{-}3) \qquad Z = \frac{x}{x+h} \quad [(x+h)^2 + R^2]^{1/2} \quad .$$

Insertion of Equation A-2 yields, upon appropriate cancellation of terms,

$$(A\text{-}4) \qquad Z = x\,(1 + \frac{w^2}{4f^2})^{1/2} \quad .$$

The error in the approximation $Z \cong x$ is given by

$$(A\text{-}5) \qquad \% \text{ error} = 100\,\frac{Z - x}{Z} \quad .$$

It will follow from Equation 4-89 that, for the spectral lines used in this study, $w(\lambda)$ is a maximum for $\lambda = 1493$ Å, and it may be shown that $w(1493) = 3.0$ cm. Inserting f and $w(1493)$ into Equation A-5 yields a value of +2.68%, which is the maximum error for the plane front case since it is calculated for r_{max} and w_{max}.

Now $z < Z$ since the actual plasma front is convex rather than planar, and furthermore $\bar{z} < z$ since $\bar{r} < R$; hence, the average actual error engendered by Equation A-1 for the $\theta = \pi/4$ plane is significantly < 2.68%. For every other horizontal plane through the plasma,

$R < R(\theta = \pi/4)$, and so the actual error averaged over all horizontal planes is still less. Hence it follows that Approximation B introduces no serious error with regard to the horizontal plasma planes.

The situation with respect to the vertical plane $\theta = 0$ is shown in Figures 24 and 25, wherein the symbols used previously retain their significance, s denotes the distance along the slit from the slit center to the point under consideration, and H is the aperture height which is a constant of value 3.6 cm. The slit height = 1.2 cm.

Consider Figure 24, which illustrates the case for on-axis (r=0) emitters. Assuming again a plane plasma front, we have from similar triangles that

$$(A\text{-}6) \qquad Z = \frac{x}{f+h+x} \left[(f+h+x)^2 + (H/2)^2\right]^{1/2}.$$

Formulating the error, E, yields after manipulation

$$(A\text{-}7) \qquad E(x) = \frac{Z(x) - x}{Z(x)} = 1 - \frac{(f+h+x)}{\left[(f+h+x)^2 + (H/2)^2\right]^{1/2}}.$$

Now $E(x) \rightarrow E_{max}$ as $x \rightarrow 0$, hence

$$(A\text{-}8) \qquad E_{max} = \lim_{x \rightarrow 0} E(x) = 1 - \frac{(f+h)}{\left[(f+h)^2 + (H/2)^2\right]^{1/2}}.$$

Upon insertion of the respective values of f, h, and H, one finds that the maximum error for on-axis points = 1.21%. Thus the value of the error averaged along all on-axis points x is such that

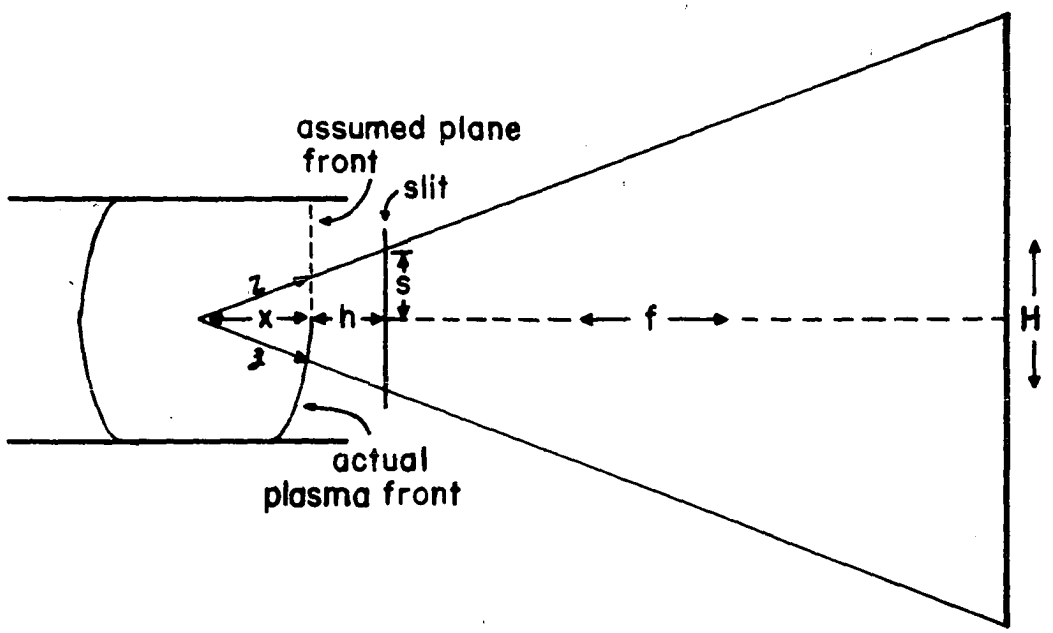

Figure 24. Plasma-spectrometer geometry for on-axis points in the $\theta = 0$ plane through the plasma axis

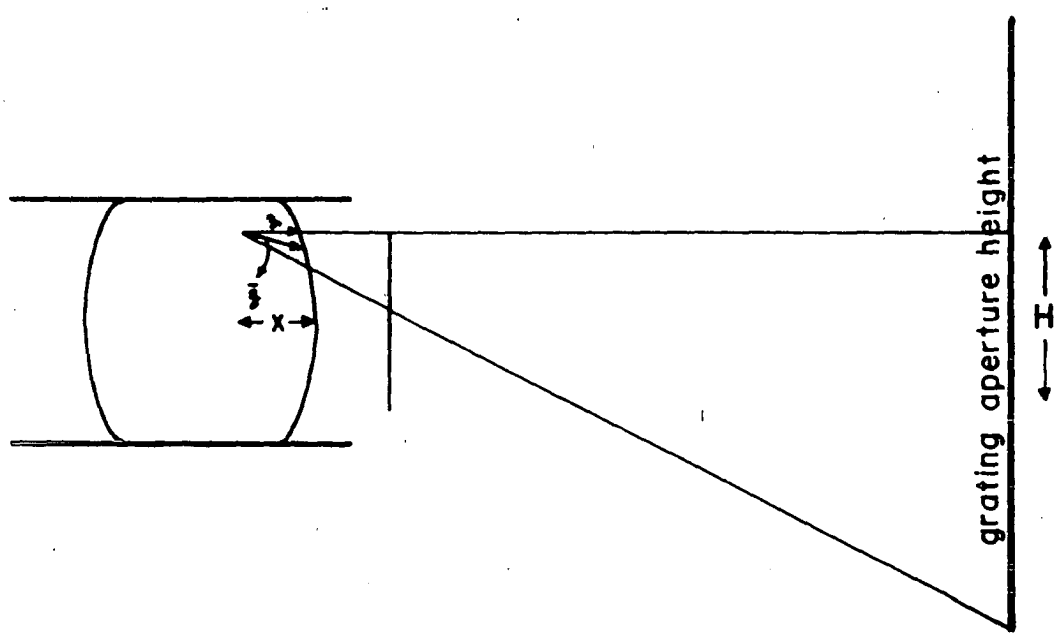

Figure 25. Plasma-spectrometer geometry for off-axis points in the $\theta = 0$ plane through the plasma axis

(A-9) $\bar{E}(x) < 1.21\%$,

and the inequality is of greater order when account is taken of the fact that $\bar{z} < z < Z$.

Consider now Figure 25, which displays the off-axis case. Simply from the geometry of this figure it can be seen that, because of the curvature of the discharge front, $z(r)$ is sometimes $< x$, hence it is safe to say that

(A-12) $\bar{E}(x, r) << + 1.21\%$

and may in fact be negative. Thus the average error engendered by Equation A-1 in the vertical planes is either a small positive number, zero, or a very small negative number.

The conclusion is therefore inescapable that Assumption B introduces very little error into the derivation.

XII. APPENDIX B

A. Justification for the Neglect of Natural, Pressure and Stark Broadening Effects

Line broadening effects enter into self-absorption phenomena via the function $P(\nu)$ in Equation 4-46, and the form and magnitude of $P(\nu)$ is different for each of the five broadening processes described in Section IV C1. It is possible to assess the relative contribution of each mechanism to the total broadening effect by calculating the magnitude of the half-width, $\Delta\nu$, for each process under the experimental discharge conditions. The experimental parameters required for these calculations are pressure and gas kinetic temperature of the plasma. Of these quantities, the latter is not known.

1. Limiting value of the gas kinetic temperature

An upper limit for the translational gas temperature may be deduced from the following observations:

(1) A Pyrex discharge tube will reach annealing temperature after exposure to the plasma for periods in excess of 30 minutes at pressures in excess of 50 torr.

(2) External cooling of the Pyrex tube with a moderate air flow eliminates tube deformation.

(3) Fused quartz discharge tubes have never been observed to soften, even after 6 hours of continuous operation at pressures in the vicinity of 200 torr.

(4) The transmission coefficient of Pyrex for high frequency electromagnetic radiation is about ten-fold less than that for fused quartz.

The annealing temperature of Pyrex is in the vicinity of 500 °C. Hence, the combined action of plasma heating plus microwave absorption is sufficient to raise the Pyrex tube walls to at least 600 °C. The translational plasma temperature cannot greatly exceed this value, however, for if it did the tube would not require such long exposure to the plasma before deformation would result. Keep in mind in this respect that the deformation is slight and slow, and that the force exerted by the atmosphere on the tube walls is sizable when the internal pressure is only 100 torr.

The strain point of fused quartz is 1070 °C, and its devitrification temperature is ca. 1000 °C (13), and 6 hours of continuous operation is certainly sufficient to establish a steady state between the plasma and the tube walls. It is therefore highly unlikely that the translational plasma termperature exceeds 1000 °C.

In view of this evidence, it seems quite safe to specify 1300 °K as the upper limit of the translational plasma temperature for discharge pressures below 200 torr.

2. Lorentz broadening

For Lorentz broadening, $\Delta\nu$ is given (6) by

$$\text{(B-1)} \qquad \Delta\nu_L = \frac{2\sigma^2 N}{\pi} \left[2\pi RT \left(\frac{1}{M_1} + \frac{1}{M_2}\right)\right]^{1/2}$$

wherein σ^2 is the effective cross-section for Lorentz broadening, N is the number of foreign gas molecules per cm^3, M_1 is the molar weight of the emitting species, and M_2 is the molar weight of the foreign gas species. The values of σ^2 for sodium in helium and mercury in helium are (6), respectively, 31.4×10^{-16} and 15.0×10^{-16} cm^2. Since these differ by only a factor of 2, it should not be totally invalidating to apply the sodium in helium value to the nitrogen in helium case.

Using the ideal gas law to evaluate N, and the appropriate constants for the nitrogen in helium case, Equation B-1 is found to yield

$$(B\text{-}2) \qquad \Delta\nu_L = 2.7 \times 10^8 \frac{p}{\sqrt{T}}$$

wherein $\Delta\nu_L$ is in cycles per second, p is the pressure in torr, and T is the translational temperature in °K.

3. Doppler broadening

For Doppler broadening, $\Delta\nu$ is given (6) by

$$(B\text{-}3) \qquad \Delta\nu_D = \frac{2}{\lambda}\left[(21n2)\, RT/M\right]^{1/2}$$

wherein M is the molar weight of the emitting species, and λ is the wavelength of the emitted spectral line. For N 1743 Å, Equation B-3 becomes

$$(B\text{-}4) \qquad \Delta\nu_D = 4.65 \times 10^8 \sqrt{T}$$

4. Relative contribution of Doppler and Lorentz broadening

From Equations B-2 and B-4 it follows directly that

$$\text{(B-5)} \qquad \frac{\Delta \nu_D}{\Delta \nu_L} = 1.74\ T/p.$$

At T = 1300 °K and p=200 torr, $\Delta\nu_D/\Delta\nu_L = 11.6$. Now, T = T(p) such that T decreases as p decreases. It is obvious, however, that T decreases more slowly than p, since for p = 1 torr a discharge exists whose translational temperature must be greater than room temperature. Hence, as p suffers a 200-fold decrease from 200 to 1 torr, the maximum decrease in T is 1300 to 300 °K -- a 4.3-fold decrease. Hence, $\Delta\nu_D/\Delta\nu_L$ must increase with decrease in p, and it must do so at a sizable rate, too. Thus, for the pressure range below 2 torr, it is probable that neglecting Lorentz broadening with respect to Doppler broadening will result in an absolute error not exceeding a few percent.

5. Holtsmark broadening

Authority for neglecting Holtsmark broadening is derived from Mitchell and Zemansky (6) who imply that it may be neglected when the partial pressure of the ground state atoms of the emitting species is < 0.01 torr. This limit is reached in helium containing 500 vpm nitrogen when the discharge tube pressure is 200 torr and the degree of dissociation is 10%.

6. Natural broadening

For Natural broadening $\Delta\nu$ is given (6) by

(B-6) $$\Delta\nu_N = \frac{A}{2\pi}$$

where A is the Einstein spontaneous emission probability. In collaboration with Equation B-4, Equation B-6 becomes

(B-7) $$\frac{\Delta\nu_D}{\Delta\nu_N} = (4.65 \times 10^8 \sqrt{T}) \frac{2\pi}{A} .$$

Now A is certainly less than 10^9 sec $^{-1}$ for the N 1743 Å transition, and T is certainly greater than 300 °K, whence it follows that $\Delta\nu_D/\Delta\nu_N$ must always be greater than 50.

7. Stark broadening

Stark broadening is not neglected; it is ignored. No data exists on ion and electron concentrations in the microwave-driven discharge, and Stark broadening therefore cannot even be estimated.

XIII. APPENDIX C

A. Variation of Non-absorbed Spectral Line Intensity with Slit-to-Discharge Distance

1. Experimental procedure

For the studies reported herein, the experimental procedure was as follows:

(1) Following adjustment of the gas-handling system to provide the gas pressure and flowrate desired, thirty minutes delay was provided to permit the system to approach dynamic equilibrium.

(2) The discharge was established, and its position was varied at five minute intervals so as to outgas the entire discharge tube.

(3) The optimum spectral scanning speed was selected, which is a function of the time constant of the photomultiplier readout console. As the scan speed is reduced stepwise, the peak height intensity increases to a maximum value which remains constant for further decrease in scan speed. The optimum scan speed is then that maximum scan speed which yields the constant, maximum peak height intensity.

(4) The microwave cavity was positioned to yield the desired value of h -- the slit-to-discharge-front distance -- and, following a five minute delay to permit the plasma and discharge tube to achieve a steady state, replicate scans of the spectral line were made.

(5) Step 4 was repeated for every subsequent cavity position and spectral line measurement.

2. Precision of measurement of h

It is pertinent to inquire into the precision of measurement of h. To permit accurate re-establishment of cavity position for replicate measurements a millimeter scale, visible in Figure 7, was attached to the optical bench. The position of the cavity mount relative to this scale may be measured to within ± 0.1 mm. Thus, the change in h per measurement is known to within ± 0.2 mm. Now, the precision of measurement of h is at least ± 1 mm because the plasma front is not better defined than this. But, as will be seen in a subsequent section , it is the relative value of h which is of importance, rather than the absolute value, since it is desired to determine the quantity dI/dh.

3. Variation of spectral line intensity with h

The relation between h and spectral line intensity is shown in Figure 26 for He 4026 and He 4121 Å. Three observations are pertinent:

(1) the relation is quite well approximated by a straight line,

(2) the straight line has a surprisingly small slope,

(3) the slope appears to be λ-dependent.

Some causes and consequences of these observations require mention.

4. Precision of the experimental intensity measurements

The precision of the experimental intensity measurements is relevant to the first observation. The raw data for the He 4121 and He 4026 Å studies are presented in Tables 10 and 11, respectively. For the He 4121 Å study, the maximum percent average deviation for

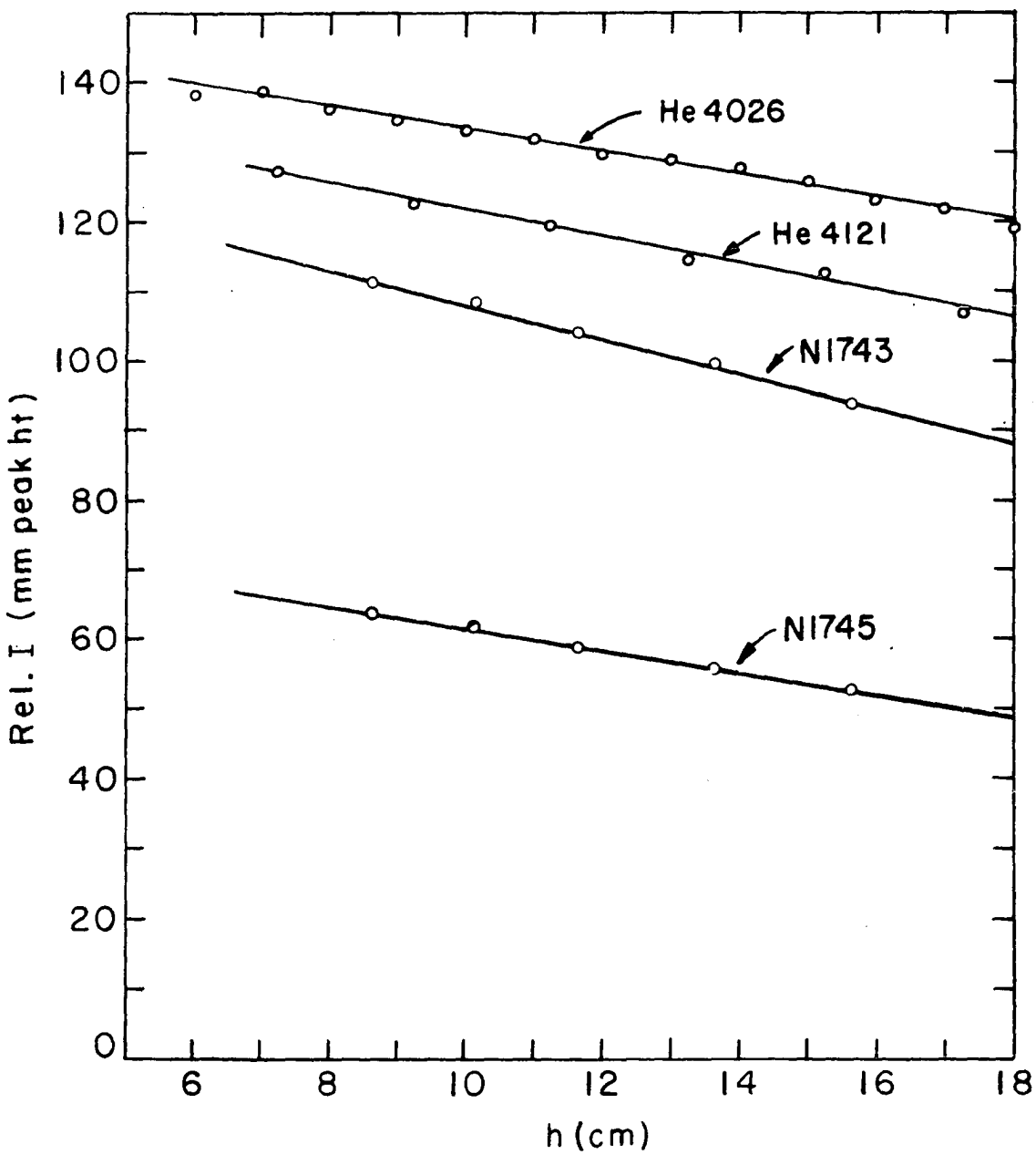

Figure 26. The variation of spectral line intensity with slit-to-discharge-front distance

Table 10. Intensity variation of helium 4121 Å with slit-to-plasma distance

Run No.	h (cm)	Time[a] Scale	Intensity[b]	Averaged Intensity	% Ave. Deviation
1	7.25	0	123.9 126.8 126.8 125.1 127.2	126.0	0.92
	9.25	6	120.9 122.9 120.2 122.2 123.8	122.0	0.95
	11.25	12	118.7 117.9 117.8 118.3 117.3	118.0	0.34
	13.25	19	114.1 114.9 112.2 110.8 112.7	112.9	1.10
	15.25	26	112.1 111.9 110.4 111.0 111.6	111.4	0.50
	17.25	34	107.8 107.2 105.4 106.8 105.8	106.6	0.75

[a]Units of minutes.

[b]Millimeters peak height above background.

Table 10. (Continued)

Run No.	h (cm)	Time Scale	Intensity	Averaged Intensity	% Ave. Deviation
2	7.25	42	130.2 127.9 127.8 129.2 126.6	128.3	0.84
	9.25	49	123.9 124.8 122.7 122.9 123.4	123.5	0.52
	11.25	56	120.8 117.7 118.3 121.1 122.4	120.1	1.37
	13.25	62	117.1 117.1 113.1 114.5 115.3	115.4	1.16
	15.25	69	112.1 113.8 111.9 114.1 114.0	113.2	0.81
	17.25	76	105.6 107.9 107.8 108.2 108.0	107.5	0.71

quintuplicate consecutive scans was 1.37%, whereas the value averaged over all the scans was 0.83%. For quadruplicate scans of He 4026 Å, the same quantities were 1.10% and 0.36%, respectively. The points of Figure 26 are therefore given with acceptable precision, especially for the He 4026 Å plot.

5. Intensity drift compensation

The time scale of Table 11 shows that the latter study required five hours of continuous operation of the discharge. It is not surprising that during this period a slight drift in spectral intensity might occur. To detect and compensate for this, the location h=9.00 cm was arbitrarily selected as a control which was measured alternately with all other discharge positions. The magnitude of the intensity drift over five hours may be found by scanning Table 12. The compensation factor for the location h=9.00 was derived by relating the measured intensity at time t to the average intensity for h =9.00, which was 134.39 mm peak height. Plotting these factors vs. time provided the compensation factors for the alternate locations h = i.

It is pertinent to note that the intensity drift is not the result of a drift in either gas flowrate or pressure. These quantities were checked at approximately twenty-minute intervals throughout the entire five hour period, without detectable deviation from the values listed in Table 13. The source of the drift has not been otherwise investigated since (1) it is small, and (2) it does not affect the doublet ratio values.

Table 11. Intensity variation of helium 4026 Å with slit-to-plasma distance

Time (min.)	h (cm)	Intensity	Average Intensity	% Ave. Deviation
0	7.00	140.8 141.9 141.1 142.4	141.6	0.42
7.5	9.00	135.4 137.0 136.9 136.2	136.4	0.42
15	11.00	134.9 134.1 134.9 133.9	134.5	0.34
20	9.00	138.0 137.9 136.8 136.5	137.3	0.47
26	13.00	131.1 131.2 129.9 129.3	130.4	0.60
30.5	9.00	137.1 137.5 135.7 137.0	136.8	0.42
36	15.00	128.3 126.8 127.0 125.7	127.0	0.55
41	9.00	136.8 136.2 136.1 136.2	136.3	0.17

Table 11. (Continued)

Time (min.)	h (cm)	Intensity	Average Intensity	%-Ave. Deviation
47	17.00	123.4 123.1 123.6 122.5	123.2	0.29
51.5	9.00	135.6 135.8 135.0 137.4	136.0	0.55
57.5	7.00	140.6 140.0 139.9 140.2	140.2	0.20
62.5	9.00	137.5 136.8 137.4 136.3	137.0	0.33
70.5	6.00	140.0 140.4 139.7 138.5	139.7	0.39
76.5	9.00	135.1 135.9 137.1 135.0	135.8	0.54
82	7.00	139.9 139.5 139.9 139.2	139.6	0.20
87.5	9.00	134.8 135.3 136.8 135.3	135.6	0.48
93.5	8.00	137.6 137.0	137.4	0.35

Table 11. (Continued)

Time (min.)	h (cm)	Intensity	Average Intensity	% Ave. Deviation
		136.9		
		138.2		
98	9.00	135.2	135.7	0.22
		135.9		
		135.5		
		136.0		
103	11.00	133.3	132.2	0.42
		132.2		
		132.0		
		131.3		
108.5	9.00	132.9	134.3	0.62
		135.0		
		135.4		
		134.2		
114.5	13.00	128.6	128.9	0.14
		128.8		
		129.2		
		128.9		
120.5	9.00	133.1	134.2	0.84
		134.9		
		135.9		
		133.0		
126.5	15.00	124.5	125.5	0.40
		125.9		
		125.5		
		126.1		
134	9.00	134.8	134.2	0.52
		133.8		
		135.1		
		133.3		
140	17.00	123.3	121.8	0.27
		121.1		
		121.8		
		121.9		

Table 11. (Continued)

Time (min.)	h (cm)	Intensity	Average Intensity	% Ave. Deviation
146	9.00	134.9 133.8 134.4 133.3	134.1	0.41
152.5	18.00	118.6 119.3 118.1 118.9	118.7	0.32
158.5	9.00	134.8 134.1 134.0 134.2	134.3	0.21
164.5	16.00	122.0 123.0 122.4 122.8	122.6	0.29
171	9.00	133.0 133.0 132.0 133.4	132.9	0.30
178	14.00	125.6 125.6 125.4 125.5	125.5	0.06
185	9.00	133.2 133.8 133.0 132.5	133.1	0.28
191	12.00	128.8 129.3 129.2 128.6	129.0	0.21
197	9.00	134.0 132.9	133.8	0.45

Table 11. (Continued)

Time (min.)	h (cm)	Intensity	Average Intensity	% Ave. Deviation
		134.8		
		133.5		
203.5	13.00	127.0	127.5	0.24
		127.9		
		127.7		
		127.4		
209.5	9.00	131.0	131.3	0.27
		131.2		
		131.9		
		130.9		
216	15.00	123.8	124.2	0.38
		123.7		
		125.1		
		124.1		
222	9.00	132.1	132.3	0.25
		131.8		
		132.9		
		132.2		
228.5	16.00	121.4	121.6	0.23
		121.2		
		121.8		
		121.9		
235	9.00	133.2	133.2	0.17
		132.8		
		133.7		
		133.2		
241.5	14.00	126.0	127.0	1.10
		125.6		
		126.5		
		129.7		
248	9.00	132.3	132.2	0.13
		132.1		
		132.5		
		132.0		

Table 11. (Continued)

Time (min.)	h (cm)	Intensity	Average Intensity	% Ave. Deviation
254	12.00	128.9 129.0 128.0 127.4	128.3	0.49
260.5	9.00	132.5 134.0 132.5 134.0	133.3	0.56
266	10.00	133.3 133.0 133.0 133.0	133.1	0.10
271.5	9.00	134.6 134.5 134.0 133.6	134.2	0.28
280.5	6.00	136.5 135.8 137.5 136.3	136.5	0.35
286.5	9.00	133.1 132.1 132.0 131.7	132.2	0.32
293	7.50	135.8 136.3 136.5 136.0	136.2	0.18
298.5	9.00	133.4 133.8 132.9 132.6	133.2	0.36

Table 12. Helium 4026 Å intensity drift compensation

h (cm)	Intensity[a]	Compensation Factor h = 9.00	Compensation Factor h = i	Compensated Intensity
7.00	141.6		0.9853	139.5
9.00	136.4	0.9853		
11.00	134.5		0.9821	132.1
9.00	137.3	0.9788		
13.00	130.4		0.9806	127.9
9.00	136.8	0.9823		
15.00	127.0		0.9842	125.0
9.00	136.3	0.9860		
17.00	123.2		0.9871	121.6
9.00	136.0	0.9882		
7.00	140.2		0.9846	138.0
9.00	137.0	0.9809		
6.00	139.7		0.9853	137.6
9.00	135.8	0.9896		
7.00	139.6		0.9903	138.2
9.00	135.6	0.9911		
8.00	137.4		0.9907	136.1
9.00	135.7	0.9903		
11.00	132.2		0.9952	131.6
9.00	134.3	1.0007		
13.00	128.9		1.0011	129.0
9.00	134.2	1.0014		
15.00	125.5		1.0014	125.7
9.00	134.2	1.0014		

[a]Millimeters peak height above background.

Table 12. (Continued)

h (cm)	Intensity	Compensation Factor h = 9.00	Compensation Factor h = i	Compensated Intensity
17.00	121.8		1.0018	122.0
9.00	134.1	1.0022		
18.00	118.7		1.0015	118.9
9.00	134.3	1.0007		
16.00	122.6		1.0060	123.3
9.00	132.9	1.0112		
14.00	125.5		1.0105	126.8
9.00	133.1	1.0097		
12.00	129.0		1.0071	129.9
9.00	133.8	1.0044		
13.00	127.5		1.0140	129.3
9.00	131.3	1.0235		
15.00	124.2		1.0197	126.6
9.00	132.3	1.0158		
16.00	121.6		1.0124	123.1
9.00	133.2	1.0089		
14.00	127.0		1.0128	128.6
9.00	132.2	1.0166		
12.00	128.3		1.0124	129.9
9.00	133.3	1.0082		
10.00	133.1		1.0048	133.7
9.00	134.2	1.0014		
6.00	136.5		1.0090	137.7
9.00	132.2	1.0166		
7.50	136.2		1.0128	137.9
9.00	133.2	1.0089		

Table 13. Experimental parameters for the h-variation studies

Parameter	He 4121 Å	He 4026 Å	N 1743, 5 Å
Matrix gas	helium, commercial	helium, purified	helium-500 vpm N_2
Discharge tube pressure			
start (torr)	14.75 ± 0.01	14.00 ± 0.01	3.25 ± 0.01
finish (torr)	14.75 ± 0.01	14.00 ± 0.01	3.25 ± 0.01
Gas flowrate (ml STP/min)			
start	69.0 ± 0.15	67.5 ± 0.15	37.9 ± 0.15
finish	69.0 ± 0.15	67.5 ± 0.15	37.9 ± 0.15
Plasma length (cm)	3.9 ± 0.2	3.5 ± 0.2	6.5 ± 0.2
Spectrometer slit widths			
entrance (microns)	5	5	5
exit (microns)	50	50	50
Scan speed (Å/min)	5	10	10
Amplifier scale (amps/full scale)	10×10^{-10}	10×10^{-9}	3×10^{-9}
Microwave power input (watts)	80	80	80
Recorder sensitivity (mv./full scale)	10	10	10

6. Correspondence of experimental intensities to a linear plot

The He 4026 Å plot of Figure 26 is derived from the compensated intensity data of Table 14. Except for the h = 6 and h = 18 values, all experimental points are within 0.54% of the straight line drawn through them. Since this is the magnitude of the precision of measurement of the points, the assumption of a linear relationship is well justified provided values of h < 7 and > 17 cm are prohibited. The latter are extreme values not normally encountered in helium discharges anyway.

7. The λ-dependence of the slope

The spectrometer used in this study employs the Seya-Namioka mounting (14). This is basically a Paschen-Runge mount with the special feature that the sum of the angle of incidence, α, and the angle of diffraction, β, is kept constant at 70.25°. Wavelength scanning is accomplished by rotation of the grating in the usual way.

Consider again Figure 8. The grating aperture is rectangular of width W and height H. Since the effective aperture width w is given by

(C-1) $w \cong W \cos \alpha$,

it is seen that w increases as α decreases, which corresponds to scanning to lower wavelengths. But as w increases, the occultation of the source in the horizontal plane decreases, so that the spectrometer accepts more light from regions of the discharge tube near the slit, whereas the occultation in the slit plane remains constant. As a result, one would expect the slope of the relation I vs. h to increase negatively as one proceeds to lower wavelengths. This is precisely

Table 14. Correspondence of experimental intensities to a linear approximation

h (cm)	I(h)	$\tilde{I}$(h)	mh+b	% Ave. Deviation
6.00	137.6 137.7	137.65	139.80	1.56
7.00	139.5 138.0 138.2	138.57	138.21	0.26
8.00	136.1	136.1	136.62	0.38
9.00	136.4 137.3 136.8 136.3 136.0 137.0 135.8 135.6 135.7 134.3 134.2 134.2 134.1 134.3 132.9 133.1 133.8 131.3 132.3 133.2 132.2 133.3 134.2 132.2 133.2	134.39	135.02	0.47
10.00	133.7	133.7	133.43	0.20
11.00	132.1 131.6	131.85	131.84	0.01

Table 14. (Continued)

h (cm)	I(h)	$\bar{I}$(h)	mh+b	% Ave. Deviation
12.00	129.9 129.9	129.9	130.24	0.26
13.00	127.9 129.0 129.3	128.73	128.65	0.06
14.00	126.8 128.6	127.70	127.06	0.50
15.00	125.0 125.7 126.6	125.77	125.46	0.25
16.00	123.3 123.1	123.2	123.87	0.54
17.00	121.6 122.0	121.8	122.28	0.43
18.00	118.9	118.9	120.69	1.51

what is observed for λ1743 Å. However, this conclusion appears to be contradicted by the λ 4121 Å study. It is probable that the greater negative slope of λ 4121 Å over λ4026 Å resulted from uncompensated intensity drift. Indeed, it was the λ4121 Å study which demonstrated the need to drift-correct the λ4026 Å study which followed it. A drift-corrected λ4121 Å study was not prosecuted since the important observation from Figure 26 is not the magnitude of the slope, but rather that I vs. h is a linear relation.

8. Intensity variation study at λ 1743, 5 Å

It would be desirable to determine the relation I(1743) vs. h in the same direct fashion that I(4026) vs. h was determined. This however requires the use of a non-absorbed spectral transition in the λ1700 Å region, but no transitions exist. By the very nature of the electronic structure of atoms, spectral transitions with energies sufficiently great to lie in the vacuum ultraviolet region arise, without discoverable exception, from transitions to atomic ground states or low-lying metastable states, and all such transitions are subject to self-absorption. No alternative exists, therefore, save to use self-absorbed spectral lines to deduce non-absorbed behavior in the λ1700 Å region.

The results of the h-variation study using the self-absorbed lines N 1743, 5 Å are presented in Figure 26. This study followed identically the procedure outlined for He 4026 Å , and the data are presented in Tables 15 and 16. The essential observation is that the experimental points also fit a linear plot even though the lines are self-absorbed. Thus, it is experimentally found that

(C-2) $I(K, h) = m(K)\, h + b(K)$

wherein the K, h notation indicates that, being self-absorbed, I is a function not only of h but also of the absorption coefficient K. It is crucial to note that neither m nor b are functions of h. Now, since a non-absorbed line is by definition one for which the absorption coefficient K is zero, we have that

Table 15. Intensity variation of nitrogen 1743 and 1745 Å with slit-to-plasma distance

Time (min.)	h (cm)	Average[a] Intensity N 1743 Å	% Ave.[b] Deviation N 1743 Å	Average[a] Intensity N 1745 Å	% Ave.[b] Deviation N 1745 Å
0	15.60	110.9	0.99	62.5	0.24
11	11.60	118.7	0.57	67.1	0.89
22.5	8.60	123.8	0.53	70.2	0.64
33	11.60	112.3	0.51	63.2	0.71
43.5	15.60	100.0	0.40	56.9	1.49
56	11.60	109.1	0.41	61.6	1.34
67	8.60	115.0	0.78	66.5	1.13
77.5	11.60	105.9	1.16	60.9	1.11
88	15.60	94.7	0.98	53.3	1.27
97.5	11.60	104.8	0.74	58.7	0.51
107.5	8.60	110.5	0.43	63.0	1.31
117	11.60	102.3	0.83	58.4	0.98
127.5	15.60	92.5	1.11	51.1	1.71
138	11.60	100.1	0.45	57.1	0.31
148.5	8.60	107.2	0.33	61.1	0.20
158	11.60	99.2	1.03	56.5	1.06
168	13.60	94.2	0.29	52.8	1.28
178	11.60	98.2	0.69	54.3	0.32
189	10.10	100.9	0.77	57.7	0.65
198.5	11.60	96.4	1.06	54.7	1.05
208	15.60	87.0	0.40	49.3	0.66
218	11.60	97.1	0.62	55.2	0.23

[a]Average of four replicate scans of the line.

[b]Percent average deviation from the mean of the four replicate scans.

Table 16. Nitrogen 1743 and 1745 Å intensity drift compensation

h (cm)	Average Intensity N 1743 Å	N 1745 Å	Compensation Factor h = 11.60	h = i	Compensated Intensity N 1743 Å	N 1745 Å
11.60	118.7	67.1	0.8768			
8.60	123.8	70.2		0.9135	113.1	64.1
11.60	112.3	63.2	0.9289			
15.60	100.0	56.9		0.9413	94.1	53.6
11.60	109.1	61.6	0.9545			
8.60	115.0	66.5		0.9647	110.9	64.2
11.60	105.9	60.9	0.9745			
15.60	94.7	53.3		0.9867	93.4	52.6
11.60	104.8	58.7	0.9977			
8.60	110.5	63.0		1.0052	111.1	63.3
11.60	102.3	58.4	1.0124			
15.60	92.5	51.1		1.0238	94.7	52.3
11.60	100.1	57.1	1.0351			
8.60	107.2	61.1		1.0403	111.5	63.6
11.60	99.2	56.5	1.0452			
13.60	94.2	52.8		1.0584	99.7	55.9
11.60	98.2	54.3	1.0717			
10.10	100.9	57.7		1.0749	108.5	62.0
11.60	96.4	54.7	1.0776			
15.60	87.0	49.3		1.0732	93.4	52.9
11.60	97.1	55.2	1.0689			

$$\text{(C-3)} \qquad \lim_{K \to 0} I(K, h) = I(0, h).$$

Thus, the behavior that N 1743 Å would exhibit were it unabsorbed may be directly deduced from Equation C-2 by

$$\text{(C-4)} \qquad \lim_{K \to 0} I(K, h) = \lim_{K \to 0} [\, m(K)\, h + b(K)\,] = m(0)\, h + b(0),$$

which is seen to be also a linear function of h. Thus, I(0) vs. h follows a linear relation also in the λ1700 Å spectral region.

XIV. APPENDIX D

A. Limit Behavior of Self-absorbed Intensity Equation

The equation for the total integrated intensity of a self-absorbed spectral line applicable to the source and spectrometer used in this study is given by Equation 4-104.

1. Limit as $K \rightarrow 0$

Inspection of Equation 4-104 reveals that its limit as $K \rightarrow 0$ contains undefined numbers arising from division by zero. To take its limit, it is therefore necessary to convert it so that its terms become indeterminate forms. Equation 4-101, which is equivalent to Equation 4-104, may be transformed by algebra to yield

$$(D\text{-}1) \qquad I = \left[I(0) + \frac{m\ell}{2} \right] \frac{1 - e^{-K\ell}}{K\ell} + m\left\{ \frac{1 - K\ell - e^{-K\ell}}{K^2\ell} \right\}$$

whereupon it is observed that

$$(D\text{-}2) \qquad \lim_{K \rightarrow 0} I = \left[I(0) + \frac{m\ell}{2} \right] \left(\frac{0}{0} \right) + m \left(\frac{0}{0} \right)$$

which is completely indeterminate. Applying L'Hospital's rule yields the result that

$$(D\text{-}3) \quad \lim_{K \to 0} I = I(0) + \frac{m\ell}{2} - \frac{m\ell}{2}\left\{\frac{1-e^{-K\ell}}{K\ell}\right\}$$

wherein the last term is still indeterminate. Reapplication of L'Hospital's rule leads directly to the result that

$$(D\text{-}4) \quad \lim_{K \to 0} I = I(0) + \frac{m\ell}{2} - \frac{m\ell}{2} = I(0). \quad \text{Q. E. D.}$$

2. Limit as $K \to \infty$

Taking the limit as $K \to \infty$ of Equation D-1 yields

$$(D\text{-}5) \quad \lim_{K \to \infty} I = \left[I(0) + \frac{m\ell}{2}\right] \frac{1}{\infty} + m\left\{-\frac{\infty}{\infty}\right\}$$

wherein the first term is zero and the second is indeterminate. Applying L'Hospital's rule to the latter term yields that

$$(D\text{-}6) \quad \lim_{K \to \infty} I = 0 + \lim_{K \to \infty} \frac{m\ell}{2}\left\{\frac{1-e^{-K\ell}}{K\ell}\right\} = 0. \quad \text{Q. E. D.}$$

XV. APPENDIX E

A. The Assumption of Thermal J-population

Many factors affect the degree to which a given system approaches Maxwell-Boltzmann (M-B) behavior. It is beyond the scope of this report, and the scope of the author too, to discuss in great detail the ramifications of collision processes as they affect steady states and approach to equilibrium in a generalized plasma. The discussion which follows will therefore be strictly confined to the minimum necessary to justify Assumption E.

For discharges operating at reduced pressures, two principal factors affect the degree to which a given process in a plasma approaches M-B behavior.

(1) Particulate (atom, molecule, ion, electron) collision reactions must be the primary energy transfer mechanism operative in the plasma process considered. The principal competing mechanism for reduced pressure discharges is radiative energy transfer reactions. If the ratio

$$\frac{\text{collisional energy transfer}}{\text{radiative energy transfer}}$$

is large for the process in question, then that process may approach M-B behavior with respect to this first criterion.

(2) The potential energy transfer per inelastic collision required to populate the process in question must be within the ability of a

reasonable number of colliding particles to supply it. Hence, if the ratio

$$\frac{\text{most probable energy of bombarding particles}}{\text{energy required to excite target particle}}$$

is large, then the process may approach M-B behavior with respect to this second criterion.

It is germane to point out that many processes occur simultaneously in every discharge. Some of them may enjoy a close approach to M-B behavior; others may suffer distinct non-maxwellian behavior. A simple example will illustrate this. Consider the question of thermal equilibrium in a plasma. At pressures in excess of 10 atmospheres, it is in general true that electron temperature = excitation temperature = rotational temperature = translational temperature. The term temperature as used herein is restricted to systems of species which possess an M-B energy distribution, whereupon $\bar{E} = \frac{3}{2} kT$. As the pressure is decreased, the temperatures of the various species begin to diverge, but the species may still possess an M-B distribution within their own class. At this point, then, the plasma is composed of a number of species systems each of which may follow an M-B distribution, but the distributions are no longer the same. A steady state may then be said to exist amongst the various species classes. Upon again reducing the pressure further, the distribution of atomic and molecular excited states may begin to become non-maxwellian, whereupon it is no longer possible to

describe this species by the term excitation temperature. At increasingly lower pressures, the rotational energy distribution may begin to deviate from the M-B, followed in turn by the translational energy of the electrons. It is seen, therefore, that it is in principle quite possible for one species in a plasma to be described by an M-B distribution while the energy distribution of another species may be significantly non-maxwellian. Note furthermore that, other things being equal, the first species to deviate from the M-B is that requiring the greatest energy change per collision, in conformity with Criterion 2.

The example cited above considered classes of species, e. g., atomic excited states vs. molecular rotation states vs. atomic translational states, but the same effects are quite possible between different members of the same class. As a case in point, consider the distribution of excited states in helium with excitation potentials of 20-24 eV, under the action of the microwave-driven discharge. Departure of this distribution from the M-B is graphically demonstrated in Figure 27, which resulted from an attempt to measure the helium excitation temperature in the source as a function of pressure. It may be shown that the departure of the curves from linearity is proportional to the departure of the distribution from the M-B. It is interesting to note that the three transitions comprising the curves are members of the same configurational system $n^3D \rightarrow 2^3P^\circ$, and that the $5^3S \rightarrow 2^3P^\circ$ transition is consistently displaced down from the former. Although the evidence is admittedly sketchy, this may

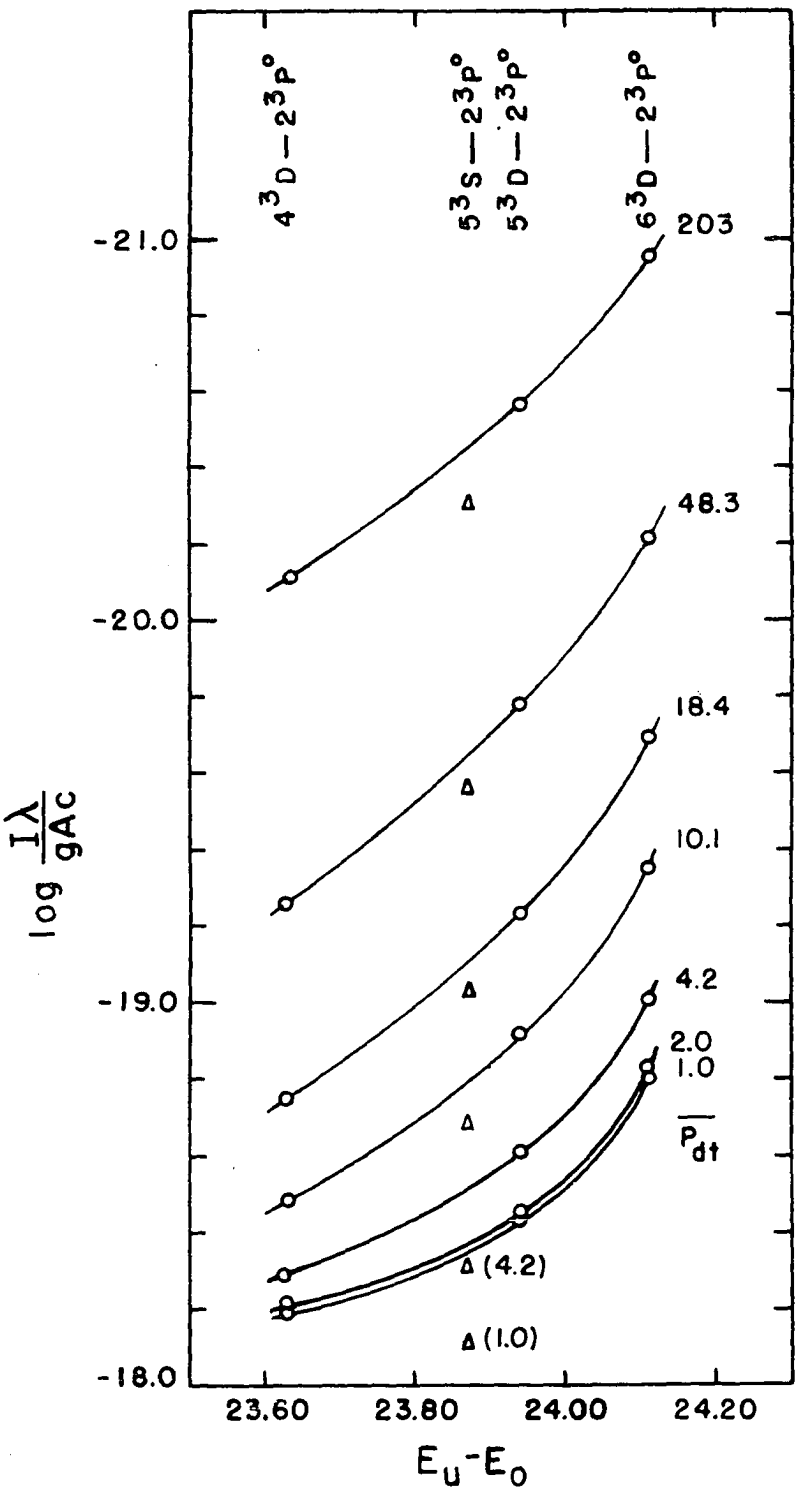

Figure 27. Departure of the helium plasma from thermal equilibrium

indicate that a steady state exists between the $n^3S \rightarrow 2^3P^\circ$ and the $n^3D \rightarrow 2^3P^\circ$ distributions. But whether this be true or not, lack of intra-configurational equilibrium is strongly indicated by the increasing curvature of the plots with decrease in pressure.

It is not surprising that the helium excited state distribution is non-maxwellian, since the Criterion 2 ratio must be a rather small number, having as it does a denominator of 20 eV. If the ratio were even as great as unity, the temperature of the bombarding particles would have to be in excess of 230,000 °K to satisfy Criterion 2. Contrast this, now, with the energy required to thermalize the N 3s ^2P state (0.01 eV), the N 2p $^2D^\circ$ state (0.001 eV), and the N 2p $^2P^\circ$ state (0.000 eV). For the same bombarding particle temperature, the Criterion 2 ratio is respectively 2000-fold, 20,000-fold, and ca. 100,000-fold greater. Indeed, energies of these magnitudes are readily supplied by collisions with atoms at room temperature. If, then, the helium excited states be still reasonably maxwellian at 200 torr, is it unreasonable to expect the J-distribution to be still reasonably maxwellian at 2 torr?

Consider now Criterion 1. Helium is the matrix gas. Its resonance line is He 584 Å, and a 584 Å photon carries with it 21.13 eV of energy. The resonance line is generally the strongest line in the spectrum of any species. Self-absorption effects are maximal when the species exists normally in the discharge as ground state atoms, as is the case with helium. Hence, there are many λ 584 Å photons, they are strongly self-absorbed, and each absorption process transfers

21.13 eV of energy. The radiative energy transfer mechanism is thus strongly operative for the helium excitation process, yielding a large denominator for the Criterion 1 ratio.

Coupled with this is the fact that as discharge pressure decreases, the collision frequency decreases, and collisional energy transfer thus also decreases --other things being equal. Hence the Criterion 1 numerator decreases with decrease in pressure. The sum total of all these effects is to make the Criterion 1 ratio marginally small at moderate pressures, and continuously smaller with decreasing pressure.

Consider now the J radiative energy transfer mechanism. First, the intensity of the $J_u \rightarrow J_\ell$ transition is very low because of the Einstein (frequency)^4 factor; second, the concentration of J_ℓ states is small by comparison to the helium ground state concentration; and third, the energy transfer per radiative event is 0.001 eV or less. Radiative energy transfer in this process is thus insignificant by comparison to the helium process, with the result that the Criterion 1 ratio is considerably larger for the J-equilibrium process than it is for the helium excitation process. In view of the moderate rate of departure from the M-B with decreasing pressure exhibited by the helium species, is it reasonable to expect that the Criterion 1 ratio for the J-equilibrium process becomes even marginal at 2 torr?

XVI. APPENDIX F

A. Calculation of the Theoretical Doublet Ratios $R_{12}^t(0)$ and $R_{34}^t(0)$

The technique to be used for the calculation of the relative intensities of spectral lines within a multiplet has been firmly established by many eminent workers on both classical and quantum-mechanical bases. The procedure used below parallels that reported by White (15). It requires that Assumption F be made -- that Russell-Saunders coupling is operative in the nitrogen atom -- which is highly probable.

The intensity ratio of two spectral lines may be written in the form

$$\text{(F-1)} \qquad \frac{I_i}{I_j} = \frac{P_i \ \nu_i^4 (N_i/g_i)}{P_j \ \nu_j^4 (N_j/g_j)}$$

wherein N_i/g_i is the concentration of atoms in any one of of the g degenerate states of the upper level of the transition i, ν_i^4 is the Einstein ν^4 - factor, and I_i is the unabsorbed transition intensity. P_i is a nameless quantity which is related to the probability that a transition will occur from a given upper state J-level to a given lower state J-level. The defining formulae for P_i describing all possible cases involving L-S coupling are given in Table 17, wherein A and B are constants of proportionality, and the other quantities have their usual meaning.

Table 17. Defining formulae for the quantity P_i

	For transitions L-1 → L	
(F-2a)	J-1 → J	$I = \frac{B(L+J+S+1)(L+J+S)(L+J-S)(L+J-S-1)}{J}$
(F-2b)	J → J	$I = -\frac{B(L+J+S+1)(L+J-S)(L-J+S)(L-J-S-1)(2J+1)}{J(J+1)}$
(F-2c)	J+1 → J	$I = \frac{B(L-J+S)(L-J+S-1)(L-J-S-1)(L-J-S-2)}{J+1}$
	For transitions L → L	
(F-3a)	J-1 → J	$I = -\frac{A(L+J+S+1)(L+J-S)(L-J+S+1)(L-J-S)}{J}$
(F-3b)	J → J	$I = \frac{A[\,L(L+1)+J(J+1)-S(S+1)\,]^2(2J+1)}{J(J+1)}$
(F-3c)	J+1 → J	$I = -\frac{A(L+J+S+2)(L+J-S+1)(L-J+S)(L-J-S-1)}{J+1}$

1. Calculation of P_1/P_2 and P_3/P_4

The P_i for transitions a-g of Figure 9 follow directly from insertion of the proper values of L, J, and S into the formulae F-2 and F-3. The data are presented in Table 18. Since intensities are additive, and P_i is proportional to intensity, we have that

(F-4a) $P_1 = P_a + P_b = 32A,$

(F-4b) $P_2 = P_c + P_d = 16A,$

(F-4c) $P_3 = P_e + P_f = 160B,$

Table 18. Calculation of the P_i

Transition	L	S	J	Defining Equation	P_i
a	1	1/2	3/2	F-3b	80A/3
b	1	1/2	1/2	F-3c	16A/3
c	1	1/2	3/2	F-3a	16A/3
d	1	1/2	1/2	F-3b	32A/3
e	2	1/2	5/2	F-2a	144B
f	2	1/2	3/2	F-2b	16B
g	2	1/2	3/2	F-2a	80B

(F-4d) $P_4 = P_g = 80B,$

whence it follows that

(F-5) $P_1/P_2 = 2; \quad P_3/P_4 = 2.$

2. Evaluation of $(N_i/g_i)/(N_j/g_j)$

The quantity N_i/g_i is given, for the Maxwell-Boltzmann distribution, by

(F-6) $N_i/g_i = N_o \exp[-E_i/kT].$

Hence,

(F-7) $$\frac{N_i/g_i}{N_j/g_j} = \exp[(E_j - E_i)/kT].$$

Now, to account for the copious excitation occuring in the source of helium lines with excitation potentials in excess of 20 eV, kT must be > 5 eV. But since $E_2 - E_1 = 0.01$ eV for the N 3s ^2P state, it follows that

$$(F\text{-}8) \quad 0.990 < \frac{N_1/g_1}{N_2/g_2} < 1.000$$

3. Evaluation of $R^t_{12}(0)$ and $R^t_{34}(0)$

The Einstein ν^4-factors for these transitions have the values

$$(F\text{-}9) \quad (\nu_1/\nu_2)^4 = (\lambda_2/\lambda_1)^4 = 1.005\ 801;$$

$$(\nu_3/\nu_4)^4 = (\lambda_4/\lambda_3)^4 = 1.005\ 233.$$

Insertion of Equations F-5, F-8, and F-9 into Equation F-1 yields

$$(F\text{-}10) \quad 1.9915 < R^t_{12}(0) < 2.0116,$$

$$(F\text{-}11) \quad 1.9904 < R^t_{34}(0) < 2.0105.$$

The best precision attainable in the experimental measurement of doublet ratios is on the order of ± 1% relative, as shown in Appendix J. Since the minimum experimental error exceeds the range of the theoretical ratios, the effect of the source excitation temperature on the doublet ratio is seen to be insignificant provided thermal J-population exists. It is therefore justifiable to assign the values

(F-12) $R^{t}_{12}(0) = R^{t}_{34}(0) = 2.00$

for this study, since the permissable deviation of the theoretical ratios from this value is less than the experimental error.

XVII. APPENDIX G

A. Calculation of A_{12}/A_{34} from Related Multiplet Considerations

Two multiplets are related if their upper states both arise from the same initial electron configuration, and their lower states both belong to the same final electron configuration. Consider the nitrogen system shown in Figure 9. The electron configuration for the upper state is $1s^2, 2s^2, 2p^2, 3s$; that for both lower states is $1s^2, 2s^2, 2p^3$. Thus we see that both the N 1743, 5 and N 1493, 5 Å multiplets arise from the same $3s \rightarrow 2p$ electron transition. Rules have been derived, and are reported by White (15), relating the relative intensities of such multiplets providing they arise from one-electron jumps in atoms obeying the L-S coupling scheme. Both of these conditions are satisfied for the case under consideration here.

The prescribed procedure is quite simple. Let L_o denote the Z-component of the orbital angular momentum of the parent electron shell, l the orbital quantum number of the jumping electron, and L their resultant. These quantities couple together in the same fashion as S, L, and J, and it may be shown that they lead to the same formulae presented in Equations F-2 and F-3. These latter formulae may be applied to related multiplet intensities if the following substitutions be made: L_o for S, l for L, and L for J. As in Appendix F, these formulae yield P-values, but we shall denote them here as Q-values to distinguish them from the former. Note that Q-values correspond to the total intensity of

all lines of the multiplet, whence it follows that

(G-1) $$Q_{12} = Q_1 + Q_2, \qquad Q_{34} = Q_3 + Q_4,$$

wherein Q_{12} is the total Q-value for both lines of the doublet λ_1, λ_2. The calculations are outlined in Table 19, and yield $Q_{12}/Q_{34} = 3/5$.

Table 19. Calculation of Q_{12} and Q_{34}

Transition	$l(\rightarrow L)$	$L_o(\rightarrow S)$	$L(\rightarrow J)$	Defining Equation	Q_{ij}
$3s\ ^2P \rightarrow 2p\ ^2P^\circ$	1	1	1	F-2b	12 B
$3s\ ^2P \rightarrow 2p\ ^2D^\circ$	1	1	2	F-2a	20 B

It remains now to establish the relationship between A and Q. To do this, we note that the intensity of a spectral line was given by Equation 3-26 as

(3-26) $$I_i = K_i A_i \nu_i N_i$$

wherein K was defined as an instrumental light-sampling parameter, and the other quantities have their usual significance. However, from Equation F-1 we have also that

(G-2) $$I_i = K_i Q_i \nu_i^4 N_i/g_i.$$

Equating Equations 3-26 and G-2 yields

(G-3) $$K_i A_i \nu_i N_i = K_i Q_i \nu_i^4 N_i/g_i.$$

whence it follows that

(G-4) $$A_i = Q_i \nu_i^3 /g_i.$$

Consider now transition 2 of Figure 9. For this transition Equation G-4 may be written

(G-5) $$A_{12} = Q_2/\lambda_2^3 g_2.$$

Similarly, for transition 4 we have that

(G-6) $$A_{34} = Q_4/\lambda_4^3 g_4.$$

Noting that $g_2 = g_4$ since the upper state is the same for both transitions, it follows that the quotient Equation G-5/Equation G-6 yields

(G-7) $$\frac{A_{12}}{A_{34}} = \frac{Q_2 \lambda_4^3}{Q_4 \lambda_2^3}$$

No value of Q_2 or Q_4 exists in Table 19 since the related multiplet intensity formulae yield only the sums Q_{12} and Q_{34}. But the distribution of the total intensity within each multiplet is known from Appendix F. Hence we have that

(G-8) $$Q_2 = Q_{12}\left(\frac{P_2}{P_1+P_2}\right); \quad Q_4 = Q_{34}\left(\frac{P_4}{P_3+P_4}\right).$$

With these relations Equation G-7 may be written

(G-9) $$\frac{A_{12}}{A_{34}} = \frac{Q_{12}\, P_2\, (P_3+P_4)\, \lambda_4^3}{Q_{34}\, P_4\, (P_1+P_2)\, \lambda_2^3}\,.$$

Inserting the known values of these quantities from Tables 18 and 19 provides the result that

(G-10) $$A_{12}/A_{34} = 0.376\,895.$$

It is pertinent to note that the assumption of thermal J-population was required to evaluate the P_i in Appendix F. Hence, it was necessary to make this assumption in order to calculate the value of A_{12}/A_{34}. But A_{12}/A_{34} is an atomic constant which, once it has been evaluated via an equilibrium experiment, is true thereafter also for non-equilibrium experiments. Hence Equation G-10 is valid irrespective of whether or not equilibrium exists in the experimental plasma.

XVIII. APPENDIX H

A. The Magnitude of m(0)/I(0) at λ1743, 5 Å

To deduce m(0)/I(0) from m(K)/I(K), it is necessary to obtain relations between the corresponding quantities. It was shown in Appendix C that, experimentally,

(C-3) $I(K, h) = m(K)\, h + b(K)$.

Thus, m(K) is seen to be given by

(H-1) $m(K) = \partial I(K, h) / \partial h$.

But the corresponding derivative of Equation 4-104 yields

(H-2) $$\partial I(K, h)/\partial h = \frac{1 - \exp[-K\ell]}{K\ell}\, m(0).$$

Hence,

(H-3) $$m(K) = \frac{1 - \exp[-K\ell]}{K\ell}\, m(0).$$

If this result be now divided by Equation 4-104 one obtains

(H-4) $$\frac{m(K)}{I(K)} = \frac{m(0)}{I(0)} \left\{ \frac{1}{1 + \delta\left[(1/K\ell - (1/2)\coth(K\ell/2)\right]} \right\}.$$

It will prove convenient to define the following nomenclature:

(H-5) $\delta(0) \equiv m(0)\,\ell/I(0), \qquad \delta(K) \equiv m(K)\,\ell/I(K),$

(H-6) $V \equiv (1/K_1\ell) - (1/2)\coth(K_1\ell/2),$

$W \equiv (1/K_2\ell) - (1/2)\coth(K_2\ell/2).$

Thus, Equation H-4 becomes for λ_1 and λ_2 respectively

(H-7) $\delta_1(K) = \delta_1(0)\,[1+V\,\delta_1(0)]^{-1}$

$\delta_2(K) = \delta_2(0)\,[1+W\,\delta_2(0)]^{-1}$

Algebraic manipulation then provides the results

(H-8) $\delta_1(0) = \delta_1(K)/1-V\,\delta_1(K), \qquad \delta_2(0) = \delta_2(K)/1-W\,\delta_2(K).$

Now, $\delta_1(K)$ and $\delta_2(K)$ are experimental measurables, but V and W are not known since they are functions of $K\ell$ which is, as yet, not known. Let us therefore invoke Equation 5-29 in the form

(H-9) $$R_{12} = \frac{R_{12}(0)}{\alpha}\,\frac{(1-\exp[-\alpha K_2\ell])}{(1-\exp[-K_2\ell])}\left\{\frac{1+V\,\delta_1(0)}{1+W\,\delta_1(0)}\right\},$$

into which the relations H-8 may be substituted to yield

(H-10) $$R_{12} = \frac{R_{12}(0)}{\alpha}\,\frac{(1-\exp[-\alpha K_2\ell])}{(1-\exp[-K_2\ell])}\left\{\frac{1+W\,\delta_2(K)}{1+V\,\delta_1(K)}\right\}$$

This equation contains only one unknown, $K_2\ell$, whose value may thus be found.

For the study described in Appendix C there exists the following experimental data for the value h = 11.6 cm:

(H-11) $R_{12} = 1.766_3$, $m_1(K)/I_1(K) = -0.02377$, $\delta_1(K) = -0.156$,
$\ell = 6.55$ cm, $m_2(K)/I_2(K) = -0.02689$, $\delta_2(K) = -0.176$.

With this data, $K_2\ell$ is found by Equation H-10 to be 0.2751. Evaluating Equation H-8 with this value of $K_2\ell$ yields

(H-12) $m_1(0)/I_1(0) = -0.02394$, $\delta_1(0) = -0.156_8$,
$m_2(0)/I_2(0) = -0.02700$, $\delta_2(0) = -0.176_8$.

It is not necessary that these values be equal since they pertain to two different wavelengths. However, since the wavelength separation is only 2.5 Å, it is probable that their average, given by

(H-13) $m_{12}(0)/I_{12}(0) = -0.02547$,

is a better value than either one alone.

XIX. APPENDIX I

A. Precision of Measurement of the Doublet Ratio

The data below were derived from the λ1743, 5 Å h-variation study described in Appendix C. Table 20 treats the precision of measurement of the doublet ratio per single determination comprising four consecutive scans of the spectral doublet. Each value in the column headed R_{12} is the doublet ratio per single scan, and was obtained by ratioing the intensities presented in the third and sixth columns of Table 15. The arithmetic mean, denoted $\bar{R}_{12}$, is the doublet ratio per single determination. The average value of the percent average deviations per single determination is 1. 19 percent.

The precision of measurement per quadruplicate determination is shown in Table 21, wherein $\bar{\bar{R}}_{12}$ is the arithmetic mean of the $\bar{R}_{12}$. The average value of the percent average deviations per quadruplicate determination is 0. 87 percent.

Table 20: Precision of measurement of the doublet ratio R_{12} per single determination

h (cm)	Time (min.)	R_{12}	$\bar{R}_{12}$	% Average Deviation
8. 6	22. 5	1. 759 1. 746 1. 751 1. 796	1. 763	0. 94
8. 6	67	1. 729 1. 687	1. 729	1. 45

Table 20. (Continued)

h(cm)	Time (min.)	R_{12}	$\bar{R}_{12}$	% Average Deviation
		1.779		
		1.721		
8.6	107.5	1.788	1.756	1.74
		1.702		
		1.784		
		1.748		
8.6	148.5	1.756	1.754	0.44
		1.743		
		1.749		
		1.767		
11.6	11	1.786	1.770	1.10
		1.730		
		1.770		
		1.792		
11.6	33	1.785	1.777	1.22
		1.752		
		1.812		
		1.758		
11.6	56	1.802	1.772	0.97
		1.738		
		1.775		
		1.774		
11.6	77.5	1.735	1.739	1.39
		1.788		
		1.696		
		1.738		
11.6	97.5	1.783	1.787	0.94
		1.781		
		1.821		
		1.764		
11.6	117	1.759	1.751	1.30
		1.710		
		1.747		
		1.789		

Table 20. (Continued)

h(cm)	Time (min.)	R_{12}	$\bar{R}_{12}$	% Average Deviation
11.6	138	1.757 1.745 1.740 1.770	1.753	0.60
11.6	158	1.775 1.745 1.747 1.761	1.757	0.63
11.6	178	1.820 1.777 1.815 1.825	1.809	0.90
11.6	198.5	1.735 1.744 1.795 1.774	1.762	1.28
11.6	218	1.763 1.777 1.744 1.749	1.758	0.67
15.6	0	1.779 1.809 1.762 1.750	1.775	1.07
15.6	43.5	1.731 1.802 1.777 1.722	1.758	1.79
15.6	88	1.791 1.727 1.840 1.750	1.777	2.17
15.6	127.5	1.788 1.845	1.811	2.43

Table 20. (Continued)

h(cm)	Time (min.)	R_{12}	$\bar{R}_{12}$	% Average Deviation
		1.865		
		1.746		
15.6	208	1.779	1.766	0.74
		1.758		
		1.747		
		1.778		

Table 21: Precision of measurement of the doublet ratio R_{12} per quadruplicate determination

h(cm)	Time (min.)	$\bar{R}_{12}$	$\bar{\bar{R}}_{12}$	% Average Deviation
8.6	22.5	1.763	1.751	0.60
8.6	67	1.729		
8.6	107.5	1.756		
8.6	148.5	1.754		
11.6	11	1.770	1.765	0.71
11.6	33	1.777		
11.6	56	1.772		
11.6	77.5	1.739		
11.6	97.5	1.787	1.762	0.71
11.6	117	1.751		
11.6	138	1.753		
11.6	158	1.757		
11.6	158	1.757	1.772	1.07
11.6	178	1.809		
11.6	198.5	1.762		
11.6	218	1.758		
15.6	0	1.775	1.769	0.40
15.6	43.5	1.758		
15.6	88	1.777		
15.6	208	1.766		

XX. APPENDIX J

A. The Experimental Doublet Ratio Data

For the helium-500 vpm nitrogen matrix, the experimental data are presented in Table 22, whereas the doublet ratio data derived from the argon-500 vpm nitrogen matrix is presented in Table 23. Since the data are so extensive, only the four-scan averages, $\bar{R}_{ij}$, and their arithmetic mean, $\bar{\bar{R}}_{ij}$, are given.

Table 22. Experimental doublet ratios for the helium matrix

Run No.	P_{dt} [a]	$\bar{R}_{12}$ [b]	$\bar{\bar{R}}_{12}$ [c]	$\bar{R}_{34}$ [b]	$\bar{\bar{R}}_{34}$ [c]
D	9.00	1.556	1.5545	1.650	1.6530
		1.546		1.663	
		1.563		1.654	
		1.554		1.645	
D	0.90	1.890	1.8927	1.712	1.7152
		1.881		1.718	
		1.899		1.726	
		1.901		1.704	
D	5.25	1.636	1.6321	1.564	1.5566
		1.627		1.560	
		1.636		1.552	
		1.629		1.551	
D	7.90	1.575	1.5718	1.609	1.6192
		1.572		1.622	

[a] Discharge tube pressure in torr.

[b] Ratio per four-scan determination.

[c] Ratio per sixteen scans.

Table 22 (Continued)

Run No.	P_{dt}	$\bar{R}_{12}$	$\bar{\bar{R}}_{12}$	$\bar{R}_{34}$	$\bar{\bar{R}}_{34}$
		1.569		1.621	
		1.571		1.625	
D	16.00	1.500	1.4990	1.741	1.7407
		1.500		1.748	
		1.498		1.720	
		1.497		1.754	
D+35	117.5	1.258	1.2505	1.711	1.7190
		1.257		1.700	
		1.243		1.745	
		1.245		1.720	
D+35	87.8	1.254	1.2565	1.772	1.7718
		1.254		1.768	
		1.260		1.775	
		1.257		1.773	
D+35	74.0	1.281	1.2794	1.783	1.7861
		1.279		1.783	
		1.278		1.790	
		1.280		1.788	
D+35	66.5	1.302	1.2975	1.789	1.7878
		1.298		1.782	
		1.297		1.788	
		1.293		1.792	
D+35	58.2	1.316	1.3151	1.800	1.7935
		1.312		1.794	
		1.317		1.780	
		1.315		1.800	
D+35	49.00	1.356	1.3518	1.805	1.7971
		1.352		1.796	
		1.351		1.787	
		1.349		1.801	
D+36	220.9	1.271	1.2689	1.616	1.6154
		1.272		1.610	

Table 22. (Continued)

Run No.	P_{dt}	$\bar{R}_{12}$	$\bar{\bar{R}}_{12}$	$\bar{R}_{34}$	$\bar{\bar{R}}_{34}$
		1.266		1.600	
		1.264		1.636	
		1.272		1.615	
D+36	209.3	1.273	1.2632	1.632	1.6273
		1.268		1.639	
		1.259		1.630	
		1.258		1.614	
		1.258		1.622	
D+36	198.0	1.262	1.2568	1.635	1.6383
		1.253		1.651	
		1.255		1.640	
		1.257		1.628	
D+36	183.7	1.257	1.2465	1.663	1.6594
		1.240		1.660	
		1.248		1.654	
		1.240		1.654	
		1.248		1.665	
D+36	170.6	1.245	1.2471	1.676	1.6643
		1.242		1.652	
		1.245		1.680	
		1.257		1.649	
D+36	157.3	1.242	1.2443	1.672	1.6746
		1.245		1.682	
		1.247		1.658	
		1.243		1.686	
D+36	145.6	1.242	1.2461	1.696	1.6914
		1.246		1.677	
		1.249		1.693	
		1.248		1.701	
D+36	134.8	1.241	1.2382	1.687	1.6944
		1.240		1.699	
		1.231		1.694	
		1.241		1.696	

Table 22. (Continued)

Run No.	P_{dt}	$\bar{R}_{12}$	$\bar{\bar{R}}_{12}$	$\bar{R}_{34}$	$\bar{\bar{R}}_{34}$
D+36	122.4	1.242	1.2412	1.720	1.7149
		1.239		1.707	
		1.248		1.719	
		1.235		1.714	
D+39	151.5	1.237	1.2360	1.695	1.6906
		1.236		1.686	
		1.235		1.693	
		1.237		1.688	
		1.235		1.690	
D+39	142.6	1.240	1.2387	1.690	1.6883
		1.238		1.675	
		1.238		1.689	
		1.239		1.690	
		1.239		1.697	
D+39	132.7	1.243	1.2368	1.708	1.7002
		1.238		1.702	
		1.230		1.700	
		1.238		1.699	
		1.235		1.692	
D+39	121.9	1.238	1.2385	1.723	1.7190
		1.236		1.724	
		1.246		1.716	
		1.239		1.708	
		1.233		1.724	
D+39	111.6	1.249	1.2422	1.737	1.7295
		1.242		1.717	
		1.236		1.736	
		1.247		1.732	
		1.237		1.726	
D+39	101.4	1.248	1.2520	1.754	1.7399
		1.254		1.734	
		1.254		1.737	
		1.249		1.740	
		1.254		1.735	

Table 22. (Continued)

Run No.	P_{dt}	$\bar{R}_{12}$	$\bar{\bar{R}}_{12}$	$\bar{R}_{34}$	$\bar{\bar{R}}_{34}$
D+39	94.1	1.260	1.2556	1.758	1.7577
		1.254		1.754	
		1.260		1.758	
		1.250		1.761	
D+39	82.1	1.271	1.2702	1.764	1.7674
		1.268		1.780	
		1.273		1.766	
		1.269		1.759	
D+39	72.2	1.284	1.2860	1.764	1.7690
		1.283		1.772	
		1.290		1.777	
		1.287		1.764	
D+39	63.0	1.310	1.3118	1.776	1.7802
		1.306		1.786	
		1.307		1.778	
		1.330		1.778	
		1.316		1.782	
		1.316		1.782	
D+41	185.8	1.248	1.2516	1.652	1.6474
		1.252		1.652	
		1.256		1.644	
		1.250		1.642	
D+41	169.8	1.249	1.2489	1.670	1.6746
		1.245		1.671	
		1.253		1.684	
		1.249		1.674	
D+41	158.0	1.244	1.2438	1.682	1.6820
		1.245		1.680	
		1.240		1.688	
		1.248		1.678	
D+41	135.0	1.246	1.2394	1.703	1.7053
		1.241		1.719	
		1.234		1.702	
		1.238		1.697	

Table 22. (Continued)

Run No.	P_{dt}	$\bar{R}_{12}$	$\bar{\bar{R}}_{12}$	$\bar{R}_{34}$	$\bar{\bar{R}}_{34}$
D+41	114.3	1.245	1.2468	1.726	1.7294
		1.246		1.728	
		1.246		1.732	
		1.250		1.733	
D+41	80.0	1.278	1.2803	1.786	1.7758
		1.276		1.774	
		1.284		1.772	
		1.282		1.772	
D+41	56.6	1.338	1.3385	1.793	1.7969
		1.333		1.802	
		1.342		1.806	
		1.340		1.788	
D+41	42.05	1.385	1.3837	1.782	1.7905
		1.385		1.787	
		1.385		1.798	
		1.380		1.796	
D+43	95.6	1.240	1.2449	1.757	1.7655
		1.244		1.781	
		1.249		1.766	
		1.246		1.757	
D+43	70.0	1.278	1.2770	1.785	1.7962
		1.277		1.800	
		1.275		1.795	
		1.278		1.804	
D+43	49.90	1.339	1.3444	1.798	1.8020
		1.352		1.806	
		1.344		1.805	
		1.343		1.799	
D+43	34.50	1.419	1.4137	1.790	1.8020
		1.408		1.808	
		1.415		1.808	
		1.414		1.802	
D+43	20.50	1.496	1.4967	1.766	1.7654
		1.499		1.770	

Table 22. (Continued)

Run No.	P_{dt}	$\bar{R}_{12}$	$\bar{\bar{R}}_{12}$	$\bar{R}_{34}$	$\bar{\bar{R}}_{34}$
		1.494		1.759	
		1.499		1.763	
		1.496		1.770	
D+43	10.87	1.550	1.5471	1.681	1.6803
		1.542		1.672	
		1.556		1.673	
		1.545		1.682	
		1.544		1.692	
D+46	2.80	1.745	1.7450	1.541	1.5390
		1.743		1.544	
		1.748		1.534	
		1.744		1.537	
D+46	4.40	1.652	1.6472	1.534	1.5409
		1.649		1.544	
		1.649		1.548	
		1.638		1.538	
D+46	7.30	1.571	1.5692	1.637	1.6250
		1.569		1.625	
		1.567		1.626	
		1.570		1.612	
D+46	11.65	1.536	1.5362	1.712	1.7058
		1.537		1.700	
		1.543		1.702	
		1.529		1.710	
D+46	15.05	1.512	1.5134	1.741	1.7431
		1.514		1.741	
		1.512		1.744	
		1.517		1.747	
D+49	0.90	1.895	1.9016	1.709	1.7058
		1.894		1.702	
		1.910		1.703	
		1.907		1.709	
D+49	1.70	1.833	1.8318	1.601	1.5959
		1.825		1.592	

Table 22. (Continued)

Run No.	P_{dt}	$\bar{R}_{12}$	$\bar{\bar{R}}_{12}$	$\bar{R}_{34}$	$\bar{\bar{R}}_{34}$
		1.832		1.596	
		1.837		1.594	
D+49	1.95	1.818	1.8188	1.560	1.5682
		1.825		1.569	
		1.812		1.576	
		1.820		1.568	
D+49	2.60	1.741	1.7476	1.532	1.5325
		1.754		1.527	
		1.747		1.540	
		1.749		1.531	
D+49	3.25	1.701	1.6891	1.524	1.5292
		1.680		1.532	
		1.682		1.530	
		1.694		1.531	
D+49	4.05	1.642	1.6469	1.540	1.5389
		1.645		1.548	
		1.644		1.544	
		1.657		1.524	
D+49	4.70	1.634	1.6294	1.554	1.5515
		1.626		1.560	
		1.629		1.547	
		1.628		1.545	
D+49	5.55	1.599	1.6005	1.578	1.5742
		1.600		1.581	
		1.604		1.569	
		1.598		1.568	
D+49	7.00	1.590	1.5802	1.607	1.6100
		1.582		1.616	
		1.578		1.616	
		1.570		1.602	
D+49	9.45	1.556	1.5500	1.658	1.6582
		1.556		1.658	
		1.547		1.651	
		1.541		1.666	

Table 22. (Continued)

Run No.	P_{dt}	$\bar{R}_{12}$	$\bar{\bar{R}}_{12}$	$\bar{R}_{34}$	$\bar{\bar{R}}_{34}$
D+49	13.60	1.532 1.527 1.538 1.530	1.5320	1.721 1.712 1.730 1.726	1.7220
D+49	23.45	1.478 1.478 1.490 1.476	1.4805	1.779 1.787 1.780 1.768	1.7786
D+49	3.60	1.674 1.674 1.666 1.670	1.6709	1.526 1.526 1.554 1.538	1.5315
D+49	3.00	-- [d]	--	1.524 1.526 1.524 1.540	1.5286
D+49	2.60	--	--	1.528 1.539 1.529 1.533	1.5322

[d] A dash indicates that measurements were not made for the doublet in question.

Table 23. Experimental doublet ratios for the argon matrix

Run No.	P_{dt}	$\bar{R}_{12}$	$\bar{\bar{R}}_{12}$	$\bar{R}_{34}$	$\bar{\bar{R}}_{34}$
D+14	0.70	1.9498 1.9700 1.9665 1.9795	1.9664	1.772 1.754 1.733 1.705	1.7414
D+14	0.35	2.0223 2.0038 1.9940 1.9770	1.9992	1.807 1.756 1.749 1.767	1.7698
D+14	0.20	1.9648 2.0732 1.9823 1.9748	1.9988	--	--
D+19	0.40	--	--	1.785 1.723 1.797 1.793 1.748	1.7692
D+19	0.20	--	--	1.827 1.798 1.805 1.819 1.801	1.8100
D+19	0.20	--	--	1.786 1.813 1.777 1.790 1.764	1.7859
D+19	31.20	--	--	1.808 1.779 1.788 1.792 1.800 1.790	1.7927
D+54	2.50	1.789 1.790	1.7976	1.785 1.783	1.7872

Table 23. (Continued)

Run No.	P_{dt}	$\bar{R}_{12}$	$\bar{\bar{R}}_{12}$	$\bar{R}_{34}$	$\bar{\bar{R}}_{34}$
		1.814		1.785	
		1.797		1.796	
D+54	2.90	1.782	1.7921	1.809	1.7951
		1.788		1.811	
		1.800		1.776	
		1.798		1.784	
D+54	3.45	1.746	1.7472	1.806	1.8033
		1.758		1.794	
		1.746		1.816	
		1.738		1.798	
D+54	4.55	1.718	1.7186	1.816	1.8155
		1.728		1.820	
		1.701		1.824	
		1.728		1.801	
D+54	6.45	1.679	1.6855	1.834	1.8176
		1.680		1.808	
		1.690		1.818	
		1.693		1.810	
D+54	11.65	1.598	1.5882	1.826	1.8320
		1.573		1.820	
		1.590		1.842	
		1.592		1.840	
D+54	14.95	1.544	1.5430	1.831	1.8285
		1.533		1.825	
		1.546		1.832	
		1.548		1.826	
D+54	18.85	1.507	1.5004	1.812	1.8220
		1.507		1.824	
		1.497		1.844	
		1.491		1.809	
D+54	23.30	1.456	1.4506	1.812	1.8178
		1.444		1.816	
		1.450		1.824	
		1.453		1.820	

Table 23. (Continued)

Run No.	P_{dt}	$\bar{R}_{12}$	$\bar{\bar{R}}_{12}$	$\bar{R}_{34}$	$\bar{\bar{R}}_{34}$
D+54	29.00	1.436	1.4270	1.803	1.8084
		1.431		1.810	
		1.412		1.800	
		1.430		1.821	
D+54	35.50	1.372	1.3728	1.782	1.7756
		1.374		1.783	
		1.373		1.773	
		1.373		1.764	
D+54	36.55	1.394	1.3778	1.776	1.7786
		1.372		1.785	
		1.368		1.777	
		1.377		1.776	
D+54	43.30	1.348	1.3462	1.752	1.7498
		1.343		1.751	
		1.351		1.743	
		1.342		1.754	
D+55	1.35	1.882	1.8834	1.745	1.7704
		1.879		1.774	
		1.866		1.766	
		1.840		1.774	
D+55	2.70	1.796	1.7924	1.794	1.7927
		1.796		1.798	
		1.790		1.785	
		1.787		1.794	
D+55	5.65	1.700	1.6942	1.836	1.8288
		1.696		1.816	
		1.694		1.832	
		1.687		1.831	
D+55	7.50	1.669	1.6590	1.858	1.8384
		1.653		1.822	
		1.659		1.836	
		1.655		1.838	
D+55	9.50	1.623	1.6210	1.828	1.8342
		1.611		1.843	

Table 23. (Continued)

Run No.	$\sim P_{dt}$	$\bar{R}_{12}$	$\bar{\bar{R}}_{12}$	$\bar{R}_{34}$	$\bar{\bar{R}}_{34}$
		1.621		1.843	
		1.629		1.823	

XXI. APPENDIX K

A. Influence of the Exit and Entrance Slit Widths on the Doublet Ratio

There is presented in Table 24 the results of a study made to determine whether there exist optimum values of the spectrometer slit widths for doublet ratio measurements. This data was collected from a discharge operating in the argon - 500 vpm nitrogen matrix at a pressure of 30.85 torr. The data collection was as follows:

(1) With the entrance slit set at 3.2 microns, one four-scan was made for each of the two doublets for each listed exit slit width in sequence.

(2) A duplicate run was prosecuted sequentially varying the exit slit in the same order.

(3) Steps 1 and 2 were repeated with the entrance slit set at 5.5 microns.

(4) Step 1 only was repeated with the entrance slit set at 10.5 microns, but the 80 micron exit width was not run.†

Thus the 3.2 and 5.5 micron doublet ratio values are averages of eight doublet scans, whereas the 10.5 micron values are averages of only four scans. For the R_{12} doublet, none of the data save the 3.2-20 entrance-exit combination varied from the arithmetic mean by greater

† More measurements could not be made for lack of time on this day.

Table 24. Dependence of doublet ratio on spectrometer slit widths

Doublet	exit width (microns)	entrance slit width (microns) 3.2	5.5	10.5	Average per exit width	Arithmetic Mean
R_{12}	10	1.430	1.425	1.444	1.433	1.4337
	20	1.414	1.434	1.434	1.427	
	30	1.423	1.438	1.440	1.434	
	40	1.424	1.438	1.442	1.435	
	50	1.428	1.440	1.439	1.436	
	80	1.436	1.438	--	1.437	
R_{34}	10	1.783	1.771	1.790	1.781	1.7814
	20	1.784	1.776	1.784	1.781	
	30	1.784	1.774	1.784	1.781	
	40	1.788	1.791	1.782	1.787	
	50	1.784	1.778	1.770	1.777	
	80	1.737	1.716	--	1.726	

than one percent. For the R_{34} doublet, however, the 80 micron exit width yielded values significantly lower than the mean. It is clear that, for entrance slit widths between 3.2 and 10.5 microns, the exit slit width may take any value between 10 and 50 microns without significantly affecting the value of the doublet ratio.